2009

Development of a Focused Broadband Ultrasonic Transducer for High Resolution Fundamental and Harmonic Intravascular Imaging

Chaitanya K. Chandrana
Cleveland State University

DEVELOPMENT OF A FOCUSED BROADBAND ULTRASONIC TRANSDUCER FOR HIGH RESOLUTION FUNDAMENTAL AND HARMONIC INTRAVASCULAR IMAGING

CHAITANYA CHANDRANA

Bachelor of Engineering in Electrical Engineering

Andhra University, Vizag, India

August, 2000

Master of Science in Electrical and Computer Engineering

South Dakota School of Mines and Technology

December, 2002

Submitted in partial fulfillment of requirements for the degree

DOCTOR OF ENGINEERING

at the

CLEVELAND STATE UNIVERSITY

September, 2008

This dissertation has been approved
for the Department of Chemical and Biomedical Engineering
and the College of Graduate Studies by

_____
Dissertation Chairperson, Aaron J. Fleischman, Ph.D.,
Department of Chemical and Biomedical Engineering

_____
Date

_____
Shuvo Roy, Ph.D.
Department of Chemical and Biomedical Engineering

_____
Date

_____
George Chatzimavroudis, Ph.D.
Department of Chemical and Biomedical Engineering

_____
Date

_____
Randolph Setser, Ph.D.
Department of Chemical and Biomedical Engineering

_____
Date

_____
Miron Kaufman, Ph.D.
Department of Physics

_____
Date

Dedicated to my parents, brother and my beloved wife

ACKNOWLEDGEMENTS

I would like to express my sincere appreciation and gratitude to my advisor Dr. Aaron Fleischman for his guidance and support throughout my graduate study.

I would like to thank my committee members Dr. Shuvo roy, Dr. George Chatzimavroudis, Dr. Randolph Setser, and Dr. Miron kaufman for their helpful ideas and suggestions. I specially thank Dr. Tao Pan for his directions.

A special recognition to my friends and colleagues for their scientific discussions, surprise parties, and for making my life in Cleveland worthwhile.

Most importantly, I acknowledge my parents, brother and sister-in-law for their love and blessings and also for giving me the opportunity to study abroad. I also thank my in-laws for their being there for me.

This acknowledgement will hardly justify my gratefulness to my wife, Vishnu Priya Koneru, who through friendship to marriage has endured the doctoral activities as part of our life. It is your love that has propelled me this far and further.

DEVELOPMENT OF A FOCUSED BROADBAND ULTRASONIC TRANSDUCER FOR HIGH RESOLUTION FUNDAMENTAL AND HARMONIC INTRAVASCULAR IMAGING

CHAITANYA CHANDRANA

ABSTRACT

Intravascular ultrasound (IVUS) is increasingly employed for detection and evaluation of coronary artery diseases. Tissue Harmonic Imaging provides different tissue information that could additionally be used to improve diagnostic accuracy. However, current IVUS systems, with their unfocussed transducers, may not be capable of operating in harmonic imaging mode. Thus, there is a need to develop suitable transducers and appropriate techniques to allow imaging in multi modes for complementary diagnostic information.

Focused PVDF TrFE transducers were developed using MEMS (Micro-Electro-Mechanical-Systems) compatible protocols. The transducers were characterized using pulse-echo techniques and exhibited broad bandwidth (110% at -6dB) with axial resolutions of <19 micron. These transducers were demonstrated to be suitable for harmonic imaging in IVUS. Improvements in lateral resolution for harmonic signals were investigated. A method was developed to present five modes of images (standard 40 MHz, fundamental 20

MHz (F20), fundamental 40 MHz (F40), harmonic 40 MHz (H40) and harmonic 80 MHz (H80)) using a single transducer.. *Ex vivo* human aorta and coronary ostium were imaged using PVDF TrFE transducers and compared to corresponding images from commercial systems. PVDF TrFE transducers demonstrated improved image quality and showed better definition of the calcific area in the coronary ostium when compared to the corresponding images from current IVUS systems. Standard mode40 MHz images of the human cadaveric aorta were obtained using PVDF TrFE transducers and compared to histology. The images demonstrated near histologic resolution and identified the loose connective tissue and focal necrotic area in the aorta.

Such promising results suggest that focused, broadband PVDF TrFE transducers have opened up the potential to incorporate harmonic imaging modality in IVUS and also improve the image quality. In addition, the transducer's multimodality imaging capability, not possible with the current systems, could enhance the functionality and thereby the clinical use of IVUS.

TABLE OF CONTENTS

LIST OF TABLES

LIST OF FIGURES

CHAPTER I

INTRODUCTION

High frequency (>30 MHz) ultrasound imaging, with its microscopic resolution, has opened up new areas of medical study in the fields of ophthalmology, dermatology and intravascular imaging (IVUS) [1, 2]. IVUS is an imaging technology capable of providing real-time, cross-sectional images of the arteries and is being used by interventional cardiologists for the clinical investigation of atherosclerosis [3]. IVUS is increasingly employed to assist in selecting and evaluating therapeutic intervention for coronary artery diseases. Ultrasound backscatter analysis has shown that IVUS has the potential to characterize specific lesions and identify plaques such as thin-cap fibroatheroma (TCFA) that lead to various clinical syndromes [4]. Identifying vulnerable plaque is a challenging task. The Virmani group has defined plaque vulnerability based on the actual cap thickness of fixed autopsy

specimens [5]. They found that in rupture, 95% of the caps measured less than 64 μm within a limit of only 2 standard deviations; and the mean cap thickness was 23 ± 19 μm. Hence, axial resolutions of <23 μm are required to detect TCFA. For better lateral visual quality, especially in cases where IVUS is being applied to evaluate the implantation of drug-eluting stents, resolutions <100 μm are required to better visualize the stent (which have thickness' around 100 μm) placed inside the arteries. It is therefore, not surprising that the 40 MHz IVUS systems with expected lateral and axial resolutions of 200-250 μm and 60 - 80 μm, respectively, are not capable of providing clear definition of the images [1]. Current IVUS systems are made from ceramic-based lead zirconium titanate (PZT) and are unfocussed. The low lateral and axial resolutions could be attributed mainly due to the unfocused nature and narrow bandwidths of the PZT transducers. Lateral resolution could be improved by shaping the transducer into a spherical section to produce focused ultrasound beams. Axial resolution could be improved by using a broad bandwidth material. Piezoelectric polymers such as PVDF (Poly (vinylidene difluoride)) and its co-polymer PVDF-TrFE (copolymer with trifluroethylene (TrFE)) offer the required benefits to produce a high resolution transducer. PVDF and its copolymer can be shaped easily to spherical sections to produce focused beams thereby improving lateral resolution. Comparison between the relevant piezo electric materials (PVDF, PVDF TrFE and PZT) was provided by Foster et al [6] and is listed in Table 1.1 below.

Table 1.1 Electromechanical properties for various piezoelectric materials.

Comparison of Electromechanical properties for PVDF, PVDF TrFE and PZT 5A

Parameter	PVDF	PVDF TrFE	PZT5A
Speed of Sound (m/s)	2200	2400	4350
Density (g/cm^3)	1.78	1.88	7.75
Z (Mrayl)	3.9	4.5	33.7
Relative dielectric permitivity	6	5	1200
Mechanical Q	10	25	75
Mechanical Flexibility	Satisfactory	Satisfactory	Poor

The difference in efficiencies between the PZT and the polymer materials can be perceived from the above table. PZT has high electromechanical coupling and high mechanical Q, However, its high acoustic mismatch to tissue and low bandwidth are limitations to its use in high frequency imaging. For a 40 MHz transducer, the thickness required for the PZT is only a few times thicker than the grain size of the ceramic. This causes a decrease in coupling factor and unwanted increase in electromechanical losses [7] [8]. Moreover, the brittle structure of PZT makes it extremely difficult to shape into a spherically shaped miniature focused transducer. On the other hand, PVDF and its copolymers have good acoustic impedance matching with tissue, broad bandwidths and therefore lend themselves as ideal choice for high frequency imaging. However, miniaturized polymer transducers have high output impedances and produce low SNR when connected to the standard 50-ohm transmission line. Consequently, for

obtaining higher SNR it requires that a preamplifier be placed close to the transducer [9].

Previous studies using polymer transducers have shown that piezoelectric film can be shaped into spherical sections and high resolutions can be obtained [10]. Focusing has been achieved by pressing the film against steel balls. Amplifier components were hand assembled. These transducers exhibited broad bandwidths (6dB bandwidth of 60-80%) and close to diffraction limited lateral resolutions. However, the transducer apertures in these studies are larger than the size of the catheter tip. Further miniaturization of the transducer is necessary if possible implementation in IVUS applications is desired. Secondly, in these studies, shaping of the film was done manually, electronics were hand assembled and placed close to the transducer. A more sophisticated fabrication procedure employing batch fabrication techniques could enable the development of miniature transducer at low costs. Such a device should meet the following criteria

1) Transducer - small enough for IVUS applications

2) Amplifier components- placed in close proximity,

3) Inexpensive – for single use procedures

A high-resolution ultrasonic device conforming to the above criteria can be achieved by using Micro-Electro-Mechanical Systems (MEMS) technology. MEMS technology has the ability to miniaturize functional components and integrate sensors, actuators, and electronics. Fortunately, PVDF and its copolymers are compatible with integrated circuit (IC) fabrication and lend themselves to MEMS implementation to provide transducers in close physical

proximity to electronics. A MEMS ultrasonic transducer chip with integrated electronics could be an ideal device for high-resolution ultrasonic imaging. This device will have the benefits of the

- Focused broad bandwidth polymer transducer –
    - High lateral and axial resolutions
- MEMS technology
    - Low cost, batch fabrication

The MEMS ultrasonic transducer chip benefiting from coupling the advantages of high-resolution images and the low cost, batch fabrication techniques, has the potential to deliver revolutionary improvements in performance and cost and represent a major advancement in IVUS imaging.

1.1 Existing transducer technologies

High frequency ultrasound technology is dominated by piezoelectric transducers. Another ultrasound technology, capacitive micromachined ultrasound transducers (CMUTs) [11] is recently emerging as an alternative with advantages such as wide bandwidth, ease of fabricating large arrays, and potential for integration with supporting electronic circuits. The advances in Micro-Electro-Mechanical Systems technology have made it possible to fabricate CMUT transducers competing in performance with the piezoelectric transducers. However, the resulting operating frequencies in the conventional and collapse regimes are only 8.5 MHz and 19 MHz, respectively [12] - much lower than the traditional IVUS frequencies. Moreover, concerns over limited output [13], and excitation of harmonics in transmission [14] need to be overcome.

Current state-of-the-art transducers use piezoelectric ceramics. The ceramics have high electromechanical coefficient and have higher sensitivities compared to piezoelectric polymers. However, as pointed out earlier, ceramic transducers produce lower resolutions due to their narrow bandwidth and poor acoustic match to tissue. Piezoelectric polymers are now emerging as a strong alternative because of their inherent characteristics such as broad bandwidth, good acoustic matching to tissue and ability to create focused transducers. Recent developments, by our group, in piezo micromachined ultrasound transducer (pMUT) include - development of focused polymer transducer for high resolution IVUS imaging and feasibility of harmonic imaging at high frequencies using focused polymer transducers. This unique approach of bringing the fabrication technology for developing polymer transducers has been successful in demonstrating high resolution fundamental and harmonic images in IVUS imaging. These results indicate the possible advent of new generation ultrasonic transducers for high frequency imaging.

1.2 Thesis overview

In this thesis, focused broadband transducers were created using MEMS compatible protocols for high resolution IVUS imaging. During this process, it was discovered that substrate capacitances of the microfabricated transducer degrade the performance of the transducer. The parasitic capacitances for these devices were identified, measured and evaluated. An alternate transducer model, with minimal parasitics, was suggested and a new minimal parasitic prototype device was developed and tested. The new model

showed significantly enhanced performance with ~ 21 dB improvement in insertion loss for a 1 mm transducer.

Another important aspect that will be addressed in this research will be application of these transducers beyond fundamental imaging techniques. Fundamental imaging mode is currently being used as a basis for diagnosis. Currently, IVUS systems operate only in this mode. Harmonic information obtained due to nonlinear ultrasound propagation provides different tissue information that could additionally be used to improve diagnostic accuracy. Unfortunately, conventional unfocused transducers with their narrow bandwidths may not be capable of operating in harmonic imaging mode. The need and desire to develop a transducer capable of operating in harmonic imaging mode has been addressed in this thesis. The feasibility of harmonic imaging modality in IVUS imaging has been investigated using the prototype PVDF TrFE transducers and appropriate harmonic imaging techniques. Additionally, the potential of PVDF TrFE transducers to generate multimodality (both fundamental and harmonic) ultrasonic images using a single transducer was also investigated. The complementary images could improve the diagnostic accuracy.

1.3 Specific Aims

The research goals can be categorized into the specific aims listed below.

SPECIFIC AIM 1: Develop miniature ultrasonic transducers suitable for IVUS applications using Micro-Electro-Mechanical Systems (MEMS) compatible protocols and subsequently characterize them. Prototype ultrasonic transducers with variable aperture and focus were developed using

MEMS compatible protocols to produce high-resolutions desirable for IVUS imaging. Piezoelectric Poly (vinylidene) difluoride (PVDF)/ PVDF TrFE were mechanically shaped on the substrate. The transducers were characterized experimentally.

Requirement: Resolutions less than 100 μm and perhaps as low as 30 μm are needed [1]

Hypothesis: PVDF/PVDF TrFE polymers with amplifier components in close proximity have the potential to produce high-resolution images.

SPECIFIC AIM 2: Improve the performance of the device by reducing substrate capacitance and characterize the improvement. The impact of the parasitic substrate capacitance on the performance of miniaturized ultrasonic transducers has been studied via modeling and experiments. A new transducer model with minimal parasitic capacitance was developed. The improvements in insertion loss due to the new model were characterized.

Requirement: A high quality ultrasonic image requires a high performance transducer with minimal insertion loss

Hypothesis: Eliminating the parasitic capacitor of the substrate could improve the sensitivity of 1 mm transducer by > 20 dB and thereby significantly improving the contrast range of the image.

SPECIFIC AIM 3: Investigate the feasibility of harmonic IVUS using focused PVDF TrFE transducers. The developed high-resolution PVDF

TrFE transducers are applied to nonlinear imaging techniques to investigate the feasibility of these transducers to harmonic IVUS. A method was developed for producing multimodality ultrasonic images using a single transducer.

Requirement: Harmonic images provide complementary information about the tissue required for enhanced diagnostic accuracy.

Hypothesis: A focused, broad bandwidth transducer could produce harmonic images of the arteries.

1.4 Significance of the current study

In this study, focused broad bandwidth PVDF TrFE transducers have been developed using MEMS compatible protocols for high-resolution IVUS fundamental and harmonic imaging applications. This work introduces PVDF TrFE transducers that demonstrate desirable resolutions for the detection of vulnerable plaques [10]. Such high resolutions were not possible with the current IVUS systems. This study presents transducers capable of near histologic resolutions that showed significantly better quality coronary ostium images when compared to the images from the state of the art commercial IVUS systems[15] .

In addition, this work establishes the feasibility of harmonic imaging in IVUS using focused PVDF TrFE transducers [16]. This demonstration opens up the potential to introduce harmonic imaging in IVUS. This study also initiated the multimodality ultrasonic imaging approach using a single PVDF TrFE transducer with pulse inversion technique [15]. Multi modality ultrasonic

images, not possible with the conventional systems, provide complementary information that could improve the diagnostic accuracy.

Finally, this work presenting 'high-resolution, multimodality capable, PVDF TrFE ultrasonic transducers' shows promise to vastly improve IVUS imaging and represents a potential advancement in the field of high frequency ultrasound imaging.

1.5 Brief Summary of other chapters

The second chapter gives the background for this study. Next, it gives a brief description of various vascular imaging techniques and explains IVUS imaging technology, its drawbacks and potential improvements in IVUS image quality.

The third chapter describes the fabrication and characterization of miniaturized high frequency focused polymer ultrasonic transducers. This study tested the sphericity of the transducer and showed that the fabricated transducers exhibited radiation patterns expected for perfectly spherical radiators. These transducers acted as a first step for the creation of a more sophisticated transducer.

The fourth chapter deals with improving the performance of the miniaturized transducer. This study identified, analyzed and rectified the performance of the miniature transducer. It then explored an alternate model with minimal parasitics that was developed and tested to show that the new model was more effective with improved insertion loss of ~ 30 dB for a 1mm transducer.

The fifth chapter proposes and verifies the significance of using focused, broadband transducers for harmonic imaging at IVUS frequencies via modeling and experimental results. It shows the feasibility of harmonic imaging in IVUS and demonstrates that focused transducers can be designed to generate significant harmonic information from desired regions of interest.

The sixth chapter presents the ultrasonic multimodality imaging capabilities using a single PVDF TrFE transducer with pulse inversion techniques. This study also compared the human coronary ostium images from the focused PVDF TrFE transducers with the commercial state of the art IVUS systems.

Finally, the seventh chapter concludes the work with general discussion and gives outlook for the work presented in this Thesis.

CHAPTER II

BACKGROUND

2.1 Heart and Coronary arteries

The heart, like any other organ, requires oxygen and nutrients. The heart does not receive any nourishment from the blood inside its chambers. Instead, it receives its own supply of blood from a network of arteries called the coronary arteries. There are two major coronary arteries – Right coronary artery (RCA) and left coronary artery (LCA). These arteries and their branches supply blood to all parts of the heart tissue. RCA originates above the right cusp of the aortic valve and supplies blood to the right atrium and right ventricle. LCA arises from the aorta above the left cusp of the aortic valve and then bifurcates into left anterior descending (LAD) artery and the left circumflex artery (LCX). Coronary arteries have lumen diameters in the 2 to 4 mm range. They have a tortuous, complex three-dimensional course.

The **intima** is the first layer of the artery wall from inside out and consists of endothelial cells that covers the artery's luminal surface, connective tissue (collagen and elastin), and a layer of compact elastic tissue called the internal elastic lamina (IEL). The intima serves as barrier and also keeps track of the pressure, flow and health of the artery. Further, endothelial cells secrete chemicals that adjust the function of the artery [17]

The **media** is the middle layer made up primarily of smooth muscle cells (SMCs). The muscle can contract and relax to control the blood pressure and flow in the artery. Elastic tissue and collagen in the media, along with elastic tissue in the IEL, increase the elasticity and strength of the wall of the artery, as the artery contracts and relaxes.

The **adventitia** is the outermost layer of connective tissue and cells (e.g., SMCs) that cover any organ, vessel or any structure.

2.1.1 Coronary artery diseases

Coronary artery disease (CAD), associated with the disease in the coronary arteries, is the single largest killer of both men and women in the United States. In 2006, it is predicted that as many as 700,000 people in the U.S. will have a new coronary attack (includes heart attack and fatal coronary disease) and about 500,000 will have a recurrent attack. More than half of the cardiovascular diseases are caused due to coronary heart disease. Estimated deaths worldwide due to coronary heart disease total 7.1 million per year. The estimated direct and indirect cost for Coronary heart disease in the United States for 2008 is $156.4 billion [18]. The major pathologic etiology causing coronary artery diseases is thought to be due to atherosclerosis.

2.1.2 Pathophysiology of coronary diseases-Atherosclerosis

Atherosclerosis is primarily an intimal disease, with secondary changes occurring in the media of the artery. It is the condition in which plaque builds up in the coronary arteries. Plaque is made up of low-density lipoprotein (LDL), macrophages, smooth muscle cells, platelets, and other substances. Progression of atherosclerosis narrows the lumen area and restricts the blood flow. Rupture of plaque can lead to the formation of thrombus and block blood flow that would eventually result in ischemic stroke or heart attack.

It is believed that the early atherosclerotic lesions, also called fatty streaks, are caused by endothelium (innermost layer) dysfunction. Once the endothelium is damaged, cholesterol is delivered into the intima by low-density lipoproteins (LDL) and fatty deposits start building up on the inside of the artery wall [19]. Monocytes, one type of white blood cells, also enter intima. Monocytes later change their characteristics to inflammatory cells called macrophages. The macrophages take up oxidised LDLs and give rise to foam cells. Foam cells eventually die and further propagate the inflammation. Over a period of time, the simple fatty streaks progress to complex vascular lesions called atheramatous plaques or atheramous with the accumulation of cellular debris, hemorrhage and the calcification of non viable components [20] [21]. Intracellular micro-calcification deposits are formed within vascular smooth muscle cells that, over period of time, lead to extracellular calcium deposits between the muscular wall and the outer portion of the atheromatous plaques as cells die. . The complex lesions expand into the artery wall [22]. Atheromas within the vessel wall are soft. As

atherosclerosis progresses, a thin (μm-range) fibrous cap is formed by new connective tissue (fibroatheromas) to separate the plaque from the lumen. Initially, these fibroatheromas do not restrict the lumen due to the outward remodeling of the vessel. However, in late stages, they expand into the lumen, narrowing the vessel (stenosis) and thereby reducing blood flow.

Atherosclerosis occurs in the low shear stress areas initially [22]. Quantitaive flow profile studies in carotid bifurcation suggest that flow separation, reduced flow rate and departures from unidirectional laminar flow may be important hemodynamic factors in plaque pathogenesis. The nature of atherosclerotic plaque plays an important role in the cause of coronary artery diseases.

2.1.3 Vulnerable plaque

The term, *vulnerable plaque*, has been used synonymously with the terms high-risk plaque, thrombosis-prone plaque, thin-cap fibroatheromas (TCFAs), unstable plaque and disrupted plaque and refers to a plaque at increased risk of causing thrombosis and lesion progression [23]

Cardiologists now believe that “vulnerable” plaque is the most important underlying cause of acute cardiovascular events like unstable angina pectoris (chest pain), Myocardium infarction (heart attack) and stroke. This vulnerable plaque refers to a plaque that is supposed to be unstable, prone to rupture, and is at an increased risk of causing severe stenosis, thrombosis and lesion progression. Pathologic studies of plaque rupture revealed that an eccentric thin-cap fibroatheroma (TCFA), characterized by a necrotic core with an overlying fibrous cap measuring < 65 μm containing rare

smooth muscle cells is assumed to be a vulnerable plaque [24]. The plaques become unstable due to biomechanical stresses developed in the thinnest part of the fibrous cap resulting in rupture of the cap. If the fibrous cap ruptures, fibroatheroma tissue fragments are exposed and released that promote clotting and thrombus is formed [25-28]. The thrombus produces an obstruction to arterial blood flow, depriving the tissue with blood resulting in myocardial ischemia or necrosis. Numerous clinical studies have confirmed the role of coronary thrombi in cases of acute Myocardial infarction, unstable angina, and sudden cardiac death [29-32]. Plaque buildup composed largely of cholesterol is far more dangerous than deposits composed of calcium or fiber. The lipids in cholesterol are more likely to break off and form a clot near the heart, which can lead to a heart attack. The fibrous and calcified blockages rarely carry such risks [33]. Hence, identification of vulnerable plaque before rupture is critical for treating atherosclerosis. Currently, cardiologists rely on diagnostic imaging modalities for evaluating and the progression of the disease. A wide variety of techniques that can image the artery lumen, and/or differentiate between different tissue and plaque components were developed or currently under investigation [3]

2.2 Vascular Imaging Modalities

The importance of detecting vulnerable plaques for the treatment of coronary artery diseases created considerable interest in the research efforts of existing as well as developing diagnostic imaging modalities. The imaging techniques improved rapidly with enhancements in real time imaging systems, image resolutions and image processing techniques making the images easily interpretable for physicians.

2.2.1 Non invasive techniques

2.2.1.1 Magnetic resonance imaging (MRI)

MRI is an imaging technique based on the magnetic property of an atom's nucleus. In this technique, the magnetic axis of hydrogen atoms is aligned with an external magnetic field. By perturbing this alignment using an electromagnetic field, different tissue types can be differentiated. In current practice, MRI has limited applicability to imaging atherosclerosis. A study by Yuan and Kerwin suggested that small coronary plaque structures and components could not be assessed with MRI [34]. A second study by de Feyter and Nieman showed that MRI acquisitions typically suffer from low signal intensities [35]. However, recent developments in receiver coils resulted in MR coronary images with in-plane spatial resolution of 0.46 x 0.46 mm, and a 2 to 5 mm slice thickness [36]. Kim et al showed an isotropic spatial resolution of 1.0 mm^3 in a three-dimensional coronary vessel wall [37]. Currently, more advanced intravascular MRI catheters are being investigated for performing high-resolution imaging of the vessel wall and atherosclerotic plaque invasively [38] [39]

2.2.1.2 Computed tomography (CT)

CT is an imaging technique based on X-ray attenuation differences between different tissues. Computed tomography (CT) scanners emit X-rays that pass through a patient and get absorbed at different levels. The diminished X-ray projection is detected by the scanner. Many one-dimensional projections are detected from various angles by allowing the scanner to rotate around the patient. Each projection is then backwards

reconstructed into a two dimensional image of the slice that was scanned. Modern CT scans –called multi slice CT (MSCT) - resulting in three-dimensional sets produce remarkably accurate imaging. This technique emerged as the most reliable noninvasive method for coronary arteries called Coronary CT angiography. Mollet et al reported the spatial resolution of the current MSCT scanners to be as low as 0.4 X 0.4 mm in the XY plane [40]. The spatial resolution in the z direction, determined by the minimum slice thickness, ranges from 0.5 to 0.75 mm. This makes it possible to depict the blockages in the coronary arteries. However, it cannot visualize the entire coronary tree. A recent study showed that only 71% of the important segments of the coronary arteries could be evaluated by MSCT scan [41], which means that if a blockage exists there is a 29% chance that MSCT will miss it

2.2.2 Invasive techniques

2.2.2.1 Angiography

Angiography is an imaging technique in which X-ray image is taken to visualize the inside of the blood vessel by administering the contrast agent at the region of interest. This imaging technique is performed to measure lumen diameters, cross-sectional areas of the arteries and has been the gold standard for the treatment of atherosclerosis. The percentage of stenosis deduced from this coronary angiogrpahy is used as a variable to quantify the disease [42]. The major drawback of this technique is that it is based on 2D projection of 3D asymmetric structures. This might result in misinterpretation of the actual stenosis as the arterial lumen at the stenotic site often includes

non-circular cross-sectional areas. As such, it could lead to over or under estimation of the disease depending on the angiographic view. Moreover, this technique cannot reveal vital information about the plaque delineation or its components

2.2.2.2 Optical Coherence Tomography (OCT)

OCT is a relatively new technique that can provide high-resolution cross-sectional images of the vessels using broad bandwidth light source. The intensity of light that is reflected from different depths is measured with interferometry. The resolution of OCT images is typically 10-20 μm [43]. Early in vitro experiments showed superior delineation of plaque details like thin caps and tissue proliferation with penetration depth of about 2 mm [44]. The major limitation with OCT is its inability to image through blood. Therefore, the application of this procedure requires that blood flow must be stopped and saline flushes be introduced at the imaging sight. The stopping of blood flow and subsequent ischemia could limit the clinical applicability of this technique. The other limitation with OCT is that the depth of penetration is only about 1 mm restricting OCT's applicability for positive remodeling studies where the visualization of the entire coronary depth is necessary.

2.2.2.3 Fiberoptic Angioscopy

Fiberoptic Angioscopy is an imaging modality that visualizes the surface of the vascular wall using a catheter-based optic fiber. Since blood is opaque to light, saline flushing is necessary to get the clear view of the artery wall. Angioscopy is useful for revealing the presence of thrombus [45, 46] and the surface of the lumen. However, it provides no information about the extent or

morphology of the plaque. The technique is also limited by its difficulty in performing the procedure.

2.2.2.4 Raman Spectroscopy

Raman Spectroscopy is a spectroscopic technique that allows characterization of the chemical composition of biologic tissue by measuring the shift in wavelength in the backscattered light. When laser light is incident on the sample, the molecules are excited to a virtual state. The backscattered light has undergone a wavelength shift [47]. The wavelength shift and the signal intensity are dependent on the chemical composition of the tissue sample. In vivo animal experiments by van de poll et al showed the powerful detection of cholesterol and calcified components with intravascular Raman spectroscopy. Limitations of this technique include limited depth of penetration (1 – 1.5 mm), lengthy acquisition times, inability to image through blood and lack of geometrical information.

2.2.2.5 Thermography

Thermography is a new technique that detects and produces thermal images of radiation in the infrared range of the electromagnetic spectrum. Intravascular thermography is based on the hypothesis that temperature increases in the vulnerable plaque due to the inflammatory process caused by macrophage infiltration. Currently, this technique employs one or more heat sensors with a contact surface area of 0.5 X 0.5 mm^2. Studied by Casscells et al showed that inflamed atherosclerotic plaques give off more heat than healthy vessel walls and that vulnerable plaques may be detected by measuring their temperature [48, 49]. Current limitations of this technique are

low signal to noise ratios, low spatial resolution, lack of information about the plaque composition and limited knowledge on the relationship between measured temperatures and pathologic temperatures of healthy and diseased arteries

2.2.2.6 Intravascular ultrasound (IVUS) imaging

IVUS is a diagnostic imaging technique used to visualize the artery from inside the lumen of the blood vessel by the transmission and detection of high frequency (> 30 MHz) ultrasound waves. More information that is detailed is given in the next section.

2.2.2.7 Elasticity imaging

2.2.2.7.1 Intravasular Elastography measures the stiffness or strain of the tissue using IVUS catheters to detect and classify tissue. The changing blood pressure produces relative deformation of the artery wall, which is detected by measuring the time shift of subsequent RF traces [50]. Stiff plaque components are deformed less than the soft plaque components. *In vitro* experiments on human arteries have demonstrated the potential of intravascular elastography to identify different plaque types based on their mechanical properties [51].

2.2.2.7.2 Palpography is a derivative of the elastography imaging technique in which the artery is deformed by high and low intraluminal pressures. Echograms are produced from ultrasound signals acquired at different pressures. Using cross-correlation analysis, strain information in the inner layer of the tissue is determined. This strain is color coded and plotted on the

IVUS echogram at the lumen-vessel boundary. [52]. Recent studies have shown that three-dimensional Palpography is feasible and allows scanning of coronary arteries in patients to identify and localize highly deformable regions [53].

2.3 IVUS Imaging

IVUS is a catheter-based technique which uses ultrasonic imaging to produce images of the coronary artery from inside the lumen of the artery. IVUS is capable of providing real-time high-resolution images allowing precise tomographic assessment of lumen area, plaque size, and composition of a coronary segment, and therefore provides new insights into the diagnosis and therapy of coronary disease. Currently, commercial IVUS systems are based on single element transducer or phased array transducer. In single-element IVUS catheters, the transducer is attached to the tip of the catheter and is continuously rotated at 30 rotations per second over 360 degrees. The center frequencies of these IVUS transducers are currently about 40 MHz. In the phased-array IVUS catheter, a 64-element transducer is folded around the tip of the catheter and is electronically steered to acquire cross-sectional images over 360 degrees. The center frequency of these catheters is 20 MHz. This thesis focuses on the development of single element transducers.

The IVUS imaging procedure using a single element and a phased array transducer is schematically explained in Figure 2.3-1.

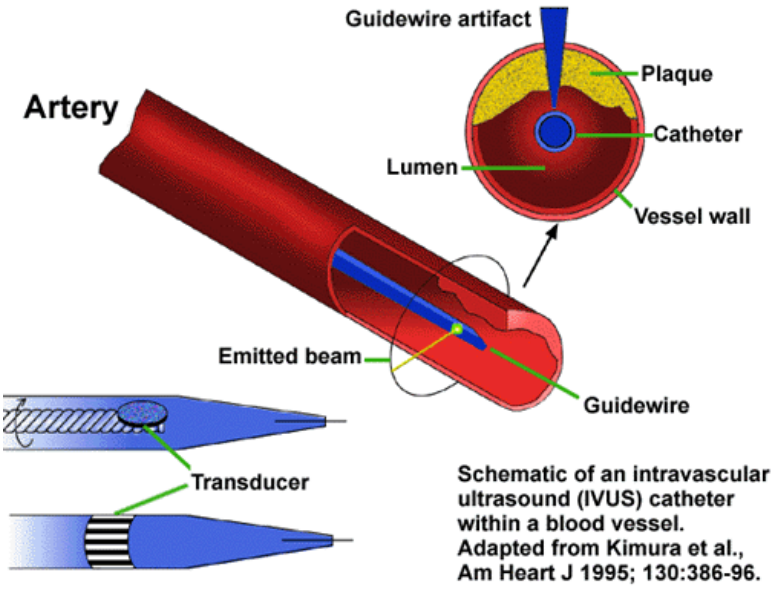

Figure 2.3-1: Schematic of the IVUS catheter, cross-sectional imaging plane with catheter inside the blood vessel and the resulting image [54].

A classic IVUS image as shown in Figure 2.3-2 consists of three layers around the lumen. The intima is a thin layer of endothelial cells supported by smooth muscle cells, fibroblasts and the internal elastic lamina; this layer thickens substantially, and usually eccentrically, in atherosclerosis. Outside the intimal layer a black ring represents the media, mostly composed of vascular smooth muscle cells bounded by the external elastic lamina. The capability of ultrasound to quantify the structure and geometry of normal and atherosclerotic coronary arteries will enable one to detect the vulnerable plaques.

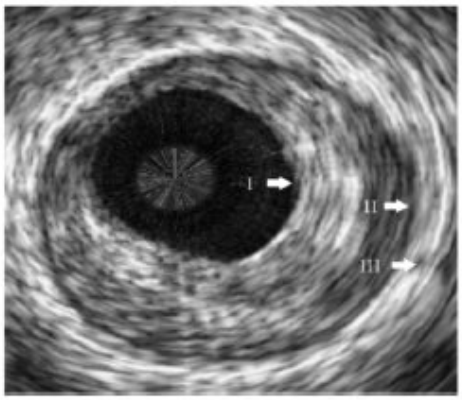

Figure 2.3-2: An IVUS image of an *ex vivo* coronary artery clearly portraying the three vessel wall structures. I-intima, II-media, III-adventitia [55].

Developments in IVUS imaging include 3D segmentation techniques, taking advantage of the similarity of borders between frames, for quantitative analysis [56-60]. Additional research into IVUS system development was done in areas such as display requirements [61], catheter materials[62] , electrical connections [63], angle effects [64], in vitro validation [65], phased-arrays [66], wall thickness measurement errors [67], calibration for quantitative use [68], IVUS image artifacts [69], transducer orientation [70, 71], focusing [71] and virtual histology [72]

2.3.1 Limitations with conventional IVUS

IVUS images indicate the overall composition of the large homogeneous regions. However, they are unreliable in differentiating adjacent smaller areas with heterogeneous composition, which is the characteristic of vulnerable plaque. The thickness of the intima ranges from 50 to 150 μm and the media is in the order of 200 to 300 μm. Systems with resolutions less than 100 μm and perhaps as low as 30 μm are needed [1]. Current resolutions of the IVUS

systems are in the order of 200-250 μm laterally and 80- 100 μm axially [1]. These resolutions are not sufficient to detect the vulnerable plaque. The low resolutions could be attributed to the inherent characteristics of the PZT transducer designs. The fundamental limitations due to conventional PZT transducer designs include narrow bandwidths and inability to focus the ultrasound beam at desired location and depths. Moreover, these devices are usually slivers of PZT that are chipped manually from large pieces. Since they are manually cut, there are wide variances in transducer performances and consequently the images. These drawbacks command the need for improvement in image quality of IVUS

2.3.2 Potential improvements in IVUS image quality

Improvement in IVUS image quality could be obtained by using a high resolution transducer. The transducer is the most important component in IVUS imaging that directly determines the image resolution, contrast and sensitivity. The inherent characteristics of the ultrasonic transducer dictate the quality of the IVUS image. The bandwidth of the transducer determines the axial resolution and as such a large bandwidth transducer material improves this resolution. Similarly, the transducer's radiation pattern defines lateral resolution which could be improved by focusing the transducer. Piezoelectric polymers such as PVDF (Poly(vinylidene difluoride)) and its co-polymer PVDF-TrFE (copolymer with trifluroethylene (TrFE)) offer many advantages over the conventionally used ceramic PZT materials. Ceramics are brittle and cannot be used to shape the transducer to produce focused ultrasound beam for improved lateral resolution. Ceramics also suffer from poor acoustic matching to tissue and therefore require additional acoustic matching layers

complicating the transducer design. In contrast, polymers can be easily shaped into spherical sections to form focused radiations and are acoustically well matched to tissue [6, 73]. In addition, polymers also have large bandwidths that translate to better axial resolution compared to ceramics. However, miniaturized polymer transducers have high output electrical impedances and produce low SNR when connected to the standard 50-ohm transmission line. Consequently, for obtaining higher SNR it requires that a preamplifier be placed close to the transducer. SNR can be further enhanced by using PVDF- TrFE, a copolymer of PVDF, which has a higher electromechanical coupling coefficient (0.30 as compared to 0.15-0.20 for PVDF) [6].

Previous studies have demonstrated the applicability of polymer based focused ultrasonic transducers for medical imaging [2, 74, 75]. In these studies, PVDF was manually shaped with precision steel balls. Amplifier components were hand assembled and planted close to the transducer inside the casing [2, 74, 75]. These transducers have broad bandwidth (6dB bandwidth of 60-80%) and have close to diffraction limited lateral resolution. However, this approach has limitations with respect to clinical implementation because of the high costs and sizes larger than the tip of the catheter. Further miniaturization of high resolution focused transducers should enable a clinically implementable device for IVUS applications.

2.4 Ultrasound nonlinear propagation

In conventional diagnostic ultrasound, the propagation media were assumed to be linear- the shape and amplitude of the acoustic wave is proportional to the input excitation. This assumption is a satisfactory way to

describe the low-amplitude ultrasound beams, as the linear theory applies to infinitesimal low acoustic pressures. However, recent studies indicated that the intensities associated with the propagation of diagnostic ultrasound pulses are large enough to take into consideration the nonlinear effects [76-78]. In nonlinear medium, the shape of the acoustic wave is not proportional to the input excitation. The pressure-density relationship is given by the series expansion 2.4.1-a:

$$P = C_0^2 \rho + \frac{1}{2}\frac{C_0^2}{\rho_0}\frac{B}{A}\rho^2 \qquad \text{(2.4.1-a)}$$

where *c0* is the infinitesimal sound speed (phase velocity), ρ is the static density, and *B/A* is the second order parameter of nonlinearity. At high intensities, a good approximation for the relationship between phase speed v_t, and particle velocity u_t on an acoustical waveform is given by 2.4.1-b [79]

$$v_t = c_0 + (1 + \frac{B}{2A})u_t \qquad \text{(2.4.1-b)}$$

Third and higher order effects are assumed negligible. The quantity (1 + B/2A) is referred to as the coefficient of nonlinearity β. This nonlinear coefficient is composed of two parts. The first is the convective component that denotes the linear acoustic propagation of the sound. In real situations, finite amplitudes are encountered and consequently the second component should be considered. The second component (B/2A) depends on the *B/A*-value, which is a property of the medium indicating its nonlinearity.

2.4.1 Tissue harmonic imaging in ultrasound diagnostics

Most ultrasonic diagnostic devices operate at high amplitudes capable of creating nonlinear distortion and hence harmonics need to be considered.

A strong potential for nonlinear effects in medical ultrasound was identified [80]. The harmonics are generated by the tissue because of the distal propagation of the fundamental beams. Low harmonic content in the near and far fields results in reduction of near and far field artifacts. The harmonic signals have a narrower beam because of twice the higher frequency and the side lobes are lower than the fundamental [81]. In addition, the harmonics are generated from the tissue, which means that the signals are aberrated only once, during the "receive", unlike the fundamental in which the signals are aberrated twice. As a result of these improvements, second harmonic imaging has made its way into commercial settings [82-84]. Clinicians favor the use of images using THI over those from the fundamental images [85].

2.4.2 High frequency harmonic imaging

So far, all of the research work in the field of nonlinear ultrasound has been directed towards the low frequency applications such as echocardiography. However, very little work has been done to see if the mechanisms of harmonic imaging can bring similar improvement in high frequency applications such as IVUS. . An initial study showed the feasibility of harmonic imaging with IVUS [86]. Another study showed experimental characterization of fundamental and second harmonic beams of a spherically focused, high-frequency, broad bandwidth transducer [87]. A third study showed the results of THI in IVUS application with a conventional rotating IVUS catheter in phantoms and *in vivo* [88]. Part of this work involved investigation of harmonic imaging in IVUS using focused broadband transducers suitable for harmonic IVUS. This work could dramatically enhance the image quality of IVUS and thereby the clinical use of IVUS.

2.5 Transducer development using Micro-Electro-Mechanical Systems

The goal of this thesis is to develop a sophisticated transducer that has the ability to produce high-resolution IVUS images and also has the capability to generate harmonic images of the arteries. Primary limitations in the development of such smart devices are difficulty in fabricating the miniature devices, integration with electronics and their incorporation into a coronary catheter.

2.5.1 Micro-Electro-Mechanical Systems (MEMS)

Micro-Electro-Mechanical Systems (MEMS), originating from microelectronics processing technology, has the ability to miniaturize functional components and integrate sensors, actuators, and electronics. MEMS fabrication involves micro photolithography, diffusion, wet chemical processing, reactive ion etching, surface modification and thin film deposition/removal. In addition, MEMS requires specialized processing technique, referred to as silicon micromachining, to create movable or 3D structures. Since there is a close relationship between silicon micromachining and IC processing, micromechanical structures can be fabricated at low unit cost on the same substrate as its control electronics. Commercially successful devices and systems that use MEMS technology include microsystems, microactuators and microsensors used in automobile and medical industry. All of these applications needed miniaturization, reliability and enhanced performance. Therefore, application of MEMS technology to develop

miniature, high-resolution, integrated ultrasonic transducers for IVUS imaging seems to be an ideal choice

Previous studies done towards creating miniature ultrasonic transducers include integration of polymer ultrasonic transducers with electronics [73]; micromachining of silicon (Si) to improve transducer performance [89]; and micromachining of dome shaped Si diaphragms for transducers [90]. CMOS compatibility of MEMS and its ability to miniaturize would allow for mounting transducers on IVUS catheters. Fortunately, PVDF and its copolymers are compatible with CMOS fabrication techniques. Moreover, PVDF and its copolymers can enable high frequency, large bandwidth, ultrasonic transducers that can be shaped into focused radiators for high-resolution images. The BioMEMS laboratory at the Cleveland Clinic developed a technique to produce focused polymer ultrasonic transducers that could be integrated with the preamplifier using MEMS technology [91]. This technique looks promising in producing high-resolution ultrasonic images for easier interpretation of IVUS studies. Further, it enables development of low cost effective device with additional benefit of transducer reproducibility

CHAPTER III

COMPONENTS FOR FOCUSED INTEGRATED pMUTS FOR HIGH-RESOLUTION MEDICAL IMAGING

Based on the publication "*Components for focused integrated pMUTs for high resolution medical imaging*" by Aaron J. Fleischman, Chaitanya Chandrana, Jin Fan, James Talman, Steve Garverick, Geoffrey Lockwood, and Shuvo Roy, Proceedings of the 2005 IEEE International Ultrasonics Symposium 2005, Vol 2. pp. 787-791. (2005).

3.1 Introduction

High frequency ultrasound imaging has many medical applications and has been demonstrated to provide high quality imaging of the anterior chamber of the eye, skin imaging, intravascular imaging, and endoluminal imaging [6]. Image resolution is primarily determined by properties of the transducer such as bandwidth, focusing and pulse length. High-resolution images can be obtained by using broad bandwidth materials and focusing the ultrasonic transducer. Though higher frequency transducers produce higher resolution

images, it is at the cost of reduced penetration [92]. This trade-off has limited the applicability of high frequency ultrasonic transducers to areas of interest that require small amounts of penetration. However intravascular ultrasound (IVUS) and endoluminal imaging applications have not benefited from the increased lateral resolution that can be obtained by focusing of the transducer because of the difficulties associated with the fabrication of small lenses, mirrors or shaped transducers that can fit within a catheter profile.

Poly(vinylidene) difluoride (PVDF) and its copolymers can be shaped easily into spherically focused transducers and exhibit desirable properties for high frequency transducers such as broad bandwidth and acoustical impedance very close to tissue. However, miniaturized polymer transducers have reduced SNR due to loading the low impedance cable that attaches the transducer to the corresponding signal processing and imaging console and consequently require a high impedance preamplifier in close physical proximity [93]

Previous studies have demonstrated the applicability of polymer based focused ultrasonic transducers for medical imaging [2]. However, the design and fabrication of these devices have inadequacies that impede their implementation in clinical arena. Micro-Electro-Mechanical Systems (MEMS) technology has the ability to miniaturize functional components and integrate sensors, actuators, and electronics. Fortunately, PVDF and its copolymers are compatible with integrated circuit (IC) fabrication and lend themselves to MEMS implementation to provide transducers in close physical proximity to electronics. Previous studies done towards creating miniature ultrasonic transducers include integration of polymer ultrasonic transducers with

electronics [94] [89] micromachining of silicon (Si) to improve transducer performance [90] and micromachining of dome shaped Si diaphragms for transducers [95]. CMOS compatibility of MEMS and its ability to miniaturize would allow for mounting transducers on IVUS catheters.

This chapter describes the fabrication and characterization of micromachined high frequency focused polymer ultrasonic transducers. The fabrication techniques to produce these transducers are compatible with CMOS microelectronics and MEMS batch fabrication techniques and are capable of being manufactured on silicon wafers after the completion of CMOS electronics in order to create a monolithic transducer chip. We expect that this type of transducer chip will likely follow the path of other MEMS devices such as accelerometers, gene chips, and digital micromirror arrays, where batch production, high yields and economies of scale have lead to relatively low unit costs, potentially making this device inexpensive enough for single use procedures.

3.2 Methodology

Transducers are fabricated using the micromachining and membrane deflection techniques [96]. The substrate of the transducer is a 1 cm^2 Silicon (Si) die with has a laser drilled hole in the center. The diameter of the hole forms the aperture of the transducer. The Si die is also thermally oxidized to form a layer of Silicon dioxide along the circumference of the hole and both of the sides. A free standing 9 μm PVDF/PVDF TrFE polymer film with 200 nm thick gold coating on one side is used as the piezoelectric material for the transducer. 1 cm^2 Polyhmer film is laid flat on the Si substrate. The Polymer film and the Si substrate are clamped into a jiig against an O-ring forming an

air-tight seal. Air pressure is injected through the air inlet to deflect the PVDF film into a spherical section. Conductive epoxy is applied from the other end of the hole to retain the spherical shape of the transducer and act as a proper sound absorbing backing. A 30-gauge wire is potted inside the non cured epoxy to facilitate further electrical connections to the transducer. Air pressure is maintained until the time epoxy cures and the transducer is taken out of the jig. The fabrication process is illustrated in Figure 3.2-1

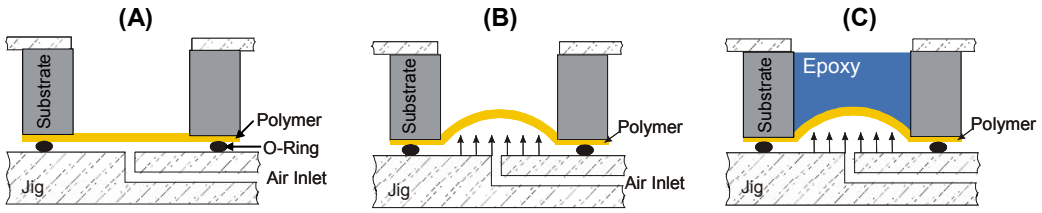

Figure 3.2-1: Development of focused polymer transducers using pressure deflection technique. (A) PVDF TrFE film is placed on the jig which has an air inlet. (B) Air is injected to shape the film into a spherical section. The differential pressure applied at the air inlet determines the deflection of the film and thereby the focal number of the transducer (C) The spherical shape is maintained by placing silver epoxy in the hole of the substrate. Silver epoxy also provides backside electrical contact and acts as sound absorbing backing.

The cross-sectional view of the transducer depicting the critical geometries is shown in Figure 3.2-2.

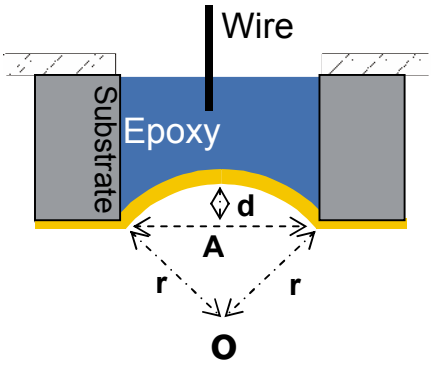

Figure 3.2-2: Crossectional view showing pertinent geometery of the focused transducer. The transducer has the ultrasound beam focused at a focal point 'O'. Transducer focus can be controlled by changing the deflection 'd' which can be controlled by varying the air presure during fabrication.

The f-number of these focused transducers is defined to be *r/A,* where *r* is the radius of curvature of the spherical section, and *A* is the diameter of the aperture. The focal point of the transducer is at point *O.* Any change in the center deflection of the membrane for a given aperture changes the radius of curvature *r,* and thereby the f-number of the transducer. Circular plates with clamped boundaries deform spherically under uniformly applied differential pressure [97]. However, for a large deflection there is some disagreement as to the exact shape [98] [99]. In this case, the deformation is close to spherical, especially away from the edges of the plate.

The center deflection is a function of membrane geometry, materials properties, and differential pressure, as described in equation (3.2-a) [100] :

$$P = \frac{C_1}{a^2}\sigma_o td + \frac{C_2 f(v)}{a^4}\frac{E}{1-v}td^3 \qquad (3.2\text{-a})$$

where P is differential pressure, a is radius of the aperture ($A/2$), E is the Young's modulus, v is the Poisson ratio, σ_o is the residual stress, d is the center deflection, $f(\nu)$ is a dimensionless function equal to 0.957-0.208 v for circular membranes, t is the membrane thickness, and C_1 and C_2 are geometrically dependant constants equal to 4.00 and 2.67, respectively for circular membranes. Thus, the f-number for arbitrarily sized apertures can be controlled by changing the differential pressure across the membrane.

Using this technique, transducers with apertures from 0.75 - 4.00 mm and f-numbers ranging between 1.9 and 4.0 were successfully fabricated using 9 μm free standing poled PVDF film on Si substrates. These transducers are later connected to high-input impedance pre-amplifier components mounted on a custom PC board. Figure 3.2-3 shows photographs of the transducer attached to a PCB and the amplifier components placed on the PCB that would be placed in close proximity to the transducer.

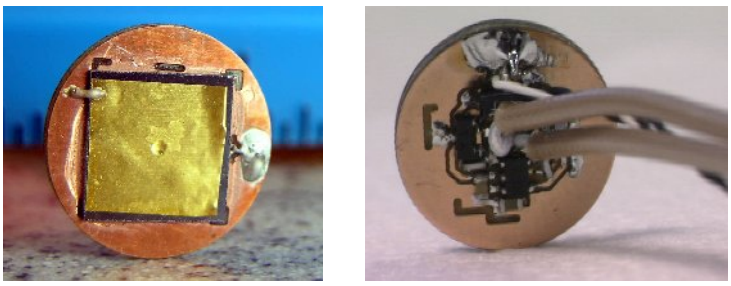

Figure 3.2-3: (a) Photograph of a focused 1 mm transducer on a 1 sq. cm silicon chip attached to a custom PC board. (b) Amplifier electronics along with input and output cables placed on the PC board that would be placed at the back of the transducer.

The transducer and its amplifier components placed on the PCB are fitted in an aluminum holder such that face of the transducer is outside. The aluminum holder prevents the water from seeping into the transducer while performing experiments. Figure 3.2-4 shows the photograph of a 4 mm aperture focused transducer fitted in an aluminum holder.

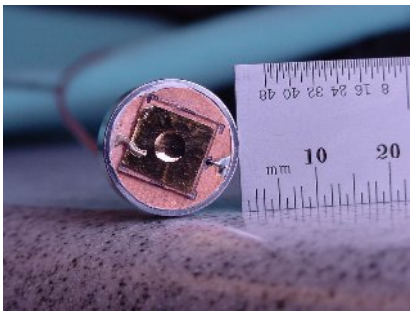

Figure 3.2-4: Photograph of the completed 4mm aperture transducer inside the alumunium holder.

The cross-sectional drawing of the input/output cables of the transducer placed inside an aluminum holder are shown in Figure 3.2-5

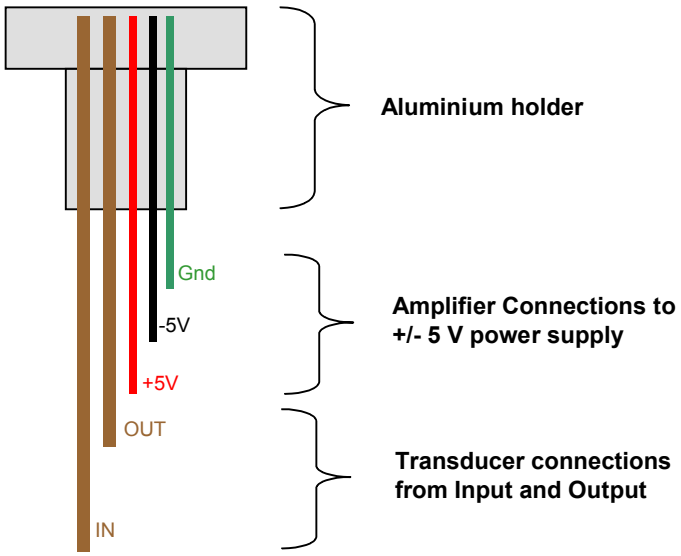

Figure 3.2-5: Drawing of power supply wires to preamplifer and input/output cables to transducer placed inside an aluminium holder.

3.3 Results

The ultrasonic experimental setup system consists of a pulser (Avtech AVB1–3-C monocycle generator, Avtech Electrosystems, Ogdensburg NY, USA) to excite the transducer through an expander. The received pulses from the transducer are collected by the digitizing oscilloscope (Agilent 54835A, Agilent Technologies, Englewood CO, USA) or a computer controlled A/D card (GaGe) through the limiter and a 30 dB amplifier (Miteq AU-1114, Miteq Corporation, Hauppauge NY, USA). The schematic of the ultrasonic testing setup is shown in Figure 3.3-1

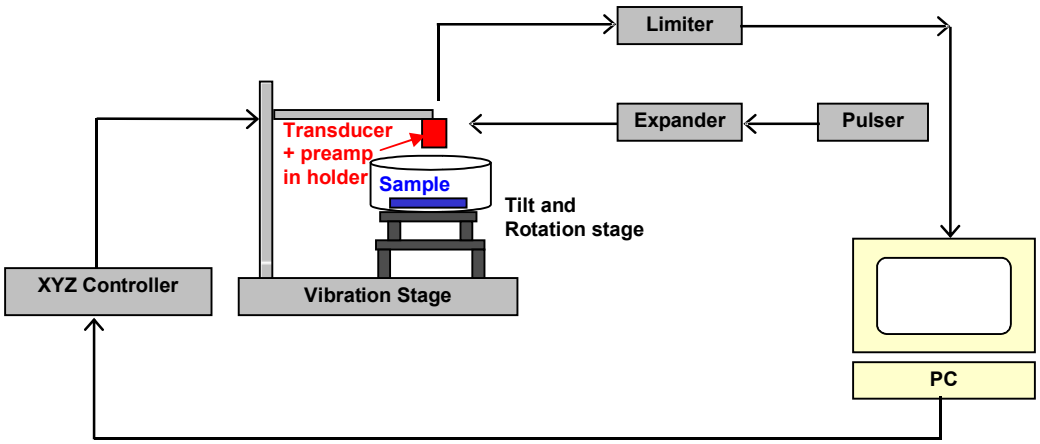

Figure 3.3-1: Schematic of the ultrasonic experimental setup.

The ultrasonic PVDF TrFE transducer was excited by 40 MHz, 50 V monocycle pulses at a 2 KHz repetition rate. The excitation pulse is shown in Figure 3.3-2

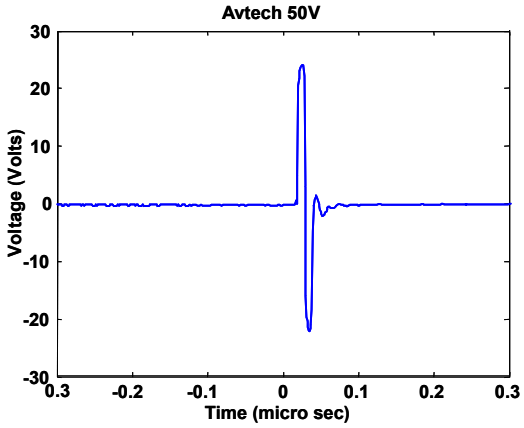

Figure 3.3-2: 40 MHz, 50 Vpp Pulse used for transducer excitation.

3.3.1 Transducer Characterization

The transducers were characterized using pulse-echo technique [91]. The PVDF TrFE transducers were mounted on a translational XYZ stage that can move with a precision of 1 μm. The transducer was excited with a 40 MHz, 50 V_{pp} monocyle pulse and was displaced vertically relative to a glass slide placed in a container having deionized (DI) water. The echoes were collected for each displacement and the peak-to-peak voltages were recorded. The data was collected without any external amplification to reduce the parasitic bandwidth effects. The echo with the maximum peak-to-peak voltage represents the pulse-echo of the transducer and the imaging plane constitutes the focal plane.

Pulse-echo response obtained from a 1 mm aperture transducer (f-number 2.08) is shown in Figure 3.3.1-1 (a). The pulse-echo exhibits minimal ringing, indicating large bandwidth. The axial resolution of the transducer was calculated from the full-width-at-half-maximum (FWHM) of the pulse-echo envelope. The FWHM has a value of 25 ns, and assuming the speed of sound

at 1500 m/s, the axial resolution was calculated to be 18.75 μm. The power spectral density of this pulse-echo is shown in Figure 3.3.1-1(b). The transducer has a center-frequency of ~30 MHz and has a -6 dB bandwidth of 120%. The transducers with such large bandwidths enable us to perform harmonic imaging.

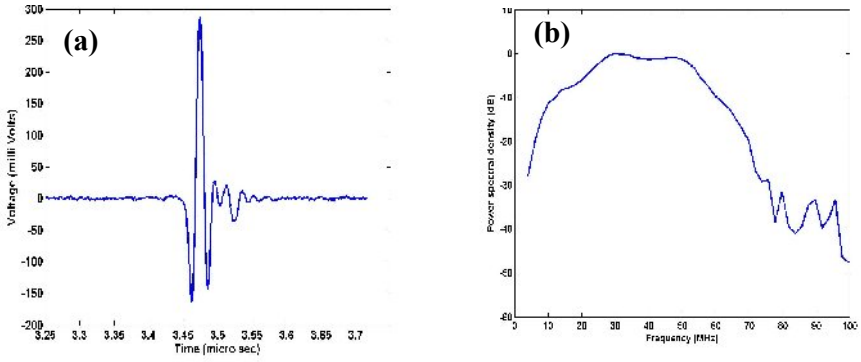

Figure 3.3.1-1: Figure showing (a) Pulse-echo of a 1 mm transducer with minimal ringing. (b) Power spectrum of the pulse-echo obtained via a fourier transform. The transducer shows a -6 dB bandwidth of 120%.

3.3.2 Radiation Patterns

3.3.2.1 Experimental

Transducer characterization experiments were performed in the pulse echo mode by exciting the transducers as described above. The radiation contours of the reflected pulses from the 60 μm stainless steel target wire were obtained by scanning the transducer laterally at different heights above the wire using a computer controlled XYZ stage with 1 μm resolution, coupled with a 500 MHz 8 bit A/D card. The measured radiation contours for a 2 mm aperture diameter transducer is shown in Figure 3.3.2.1-1.

3.3.2.2 Comparison of experimental and modeled radiation patterns

The radiation contours of focused transducers were modeled using a MATLAB program. The program assumes ideal spherical shape emitter for the given focal number and aperture diameter. It uses the analytic expression for impulse response, as described by Arditi et al [101], convolved with the emitted pulse to determine the field response. Comparison is made between the experimental and modeled radiation contours and it has been observed, as shown in Figure 3.3.2.2-1 that the experimental radiation contour agrees well with the modeled radiation contour.

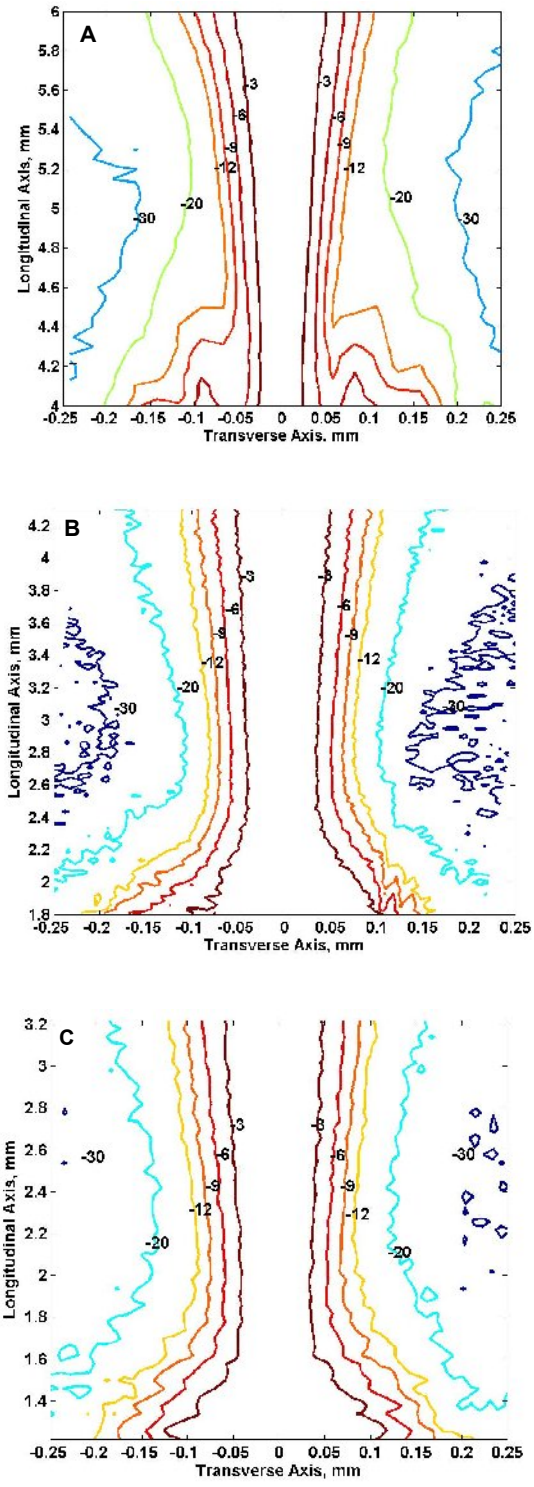

Figure 3.3.2.1-1: Experimental focused radiation patterns from three different aperture transducers (a) 2 mm; f-number 2.5 (b) 1 mm; f-number 3.1 (c) 0.75 mm; f-number 3.3.

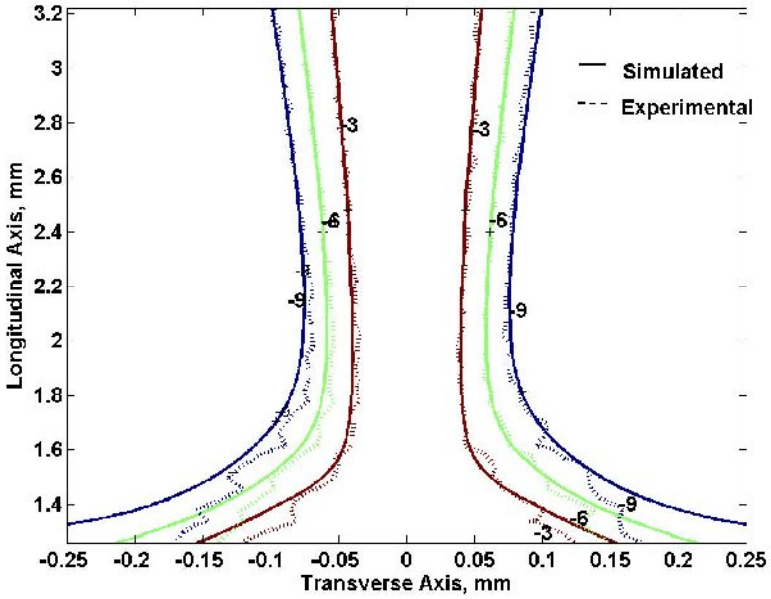

Figure 3.3.2.2-1: Comparison of experimental with simulated radiation patterns for a 0.75 mm aperture transducer (3.27 focal number) showing good agreement at 3 dB, 6 dB and 9 dB.

3.3.3 Transducer shape characterization

Continuous wave axial radiation pattern of a 2 mm diameter transducer with geometric focus at 7.1 mm was obtained by exciting the transducer with a gated sinusoidal pulse having 15 cycles and using a 20 μm stainless steel wire as a target. The continuous wave axial radiation pattern for an identical spherical transducer was simulated in MATLAB using the expressions given by H.T. O'Neil [102]. Figure 3.3.2-1 shows good agreement between the axial experimental and simulated radiation patterns with a Pearson correlation coefficient of 0.99, over the axial range from 5 mm to 10 mm indicating that the fabricated transducers are spherical. Deviations from the model are attributed primarily to the use of a wire reflector instead of a point.

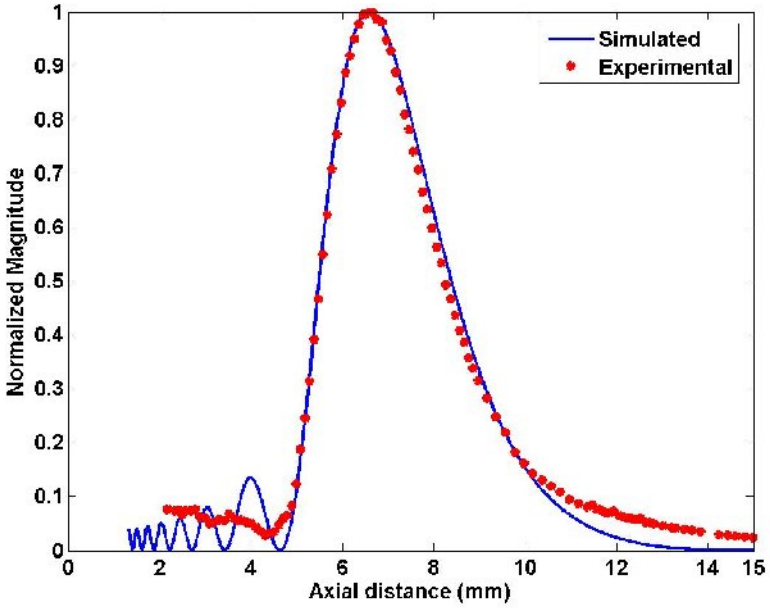

Figure 3.3.3-1: Comparison of experimental with simulated axial radiation patterns of a 2 mm aperture transducer (f-number 3.1) showing good agreement with a Pearson correlation of 0.99.

3.3.4 Tissue imaging

The capability of imaging tissue with micromachined transducers was tested on a human cadaveric aorta. As tissue is less echogenic than glass, a hybrid preamplifier circuit using an AD8001 was mounted in close proximity (< 1mm) from the transducer to reduce signal degradation [9] . A sample of human cadaveric aorta was pinned flat onto a paraffin base. The transducer was then scanned using a motorized stage in one direction in increments of 50 μm. The reflection at each position was sampled by the oscilloscope at 1 GSa/s and saved as a file to create one scan line. The scan lines were subsequently compiled and standard imaging software (MATLAB) was used to generate a 256 level gray scale image. Figure 3.3.4-1 shows the resulting ultrasound image.

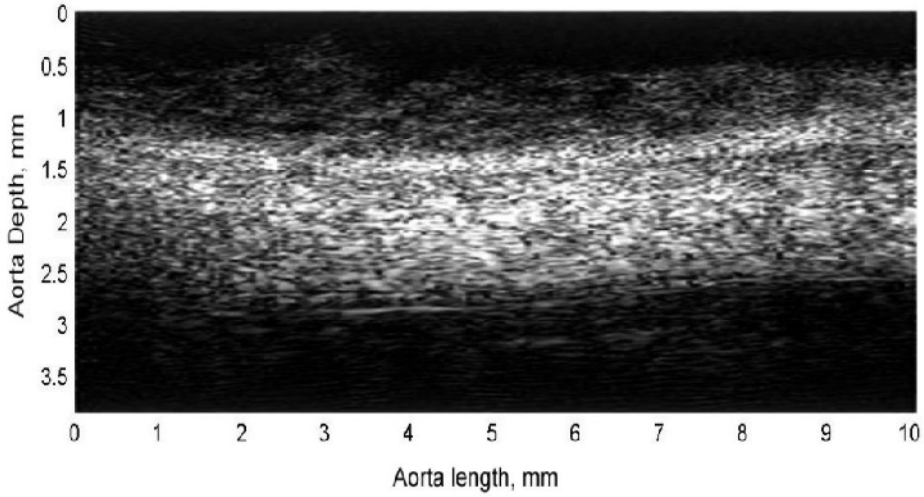

Figure 3.3.4-1: Ultrasonic image of a cadaveric aorta from a 2 mm aperture transducer.

3.3.5 Comparison to histology

Unfixed cadaveric human aorta was imaged using a PVDF TrFE transducer (2 mm, f-number 2.6) in standard IVUS imaging mode. After the completion of the imaging experiment, the tissue was fixed in 10% buffered formalin solution, subsequently processed with 50%, 75%, 95% and 100% ethyl alcohol. The dehydrated tissue is processed with the clearing reagent to remove the alcohol content and is embedded in paraffin. A series of sections each 5 μm thick were taken at locations 50 μm apart to get the closest tissue appearance of the imaging plane. These sections were mounted onto glass slides and underwent routine hematoxylin/eosin (HE) staining. The slides were observed using a microscope and the images were recorded for comparison with ultrasound images. The comparative images are shown in Figure 3.3.5-1. The 40 MHz ultrasonic image showed great resemblance to the histology. The ultrasonic image clearly showed the loose connective

tissue. Areas of focal necrosis with micro calcification can be identified as a typical shadow region in the ultrasound image.

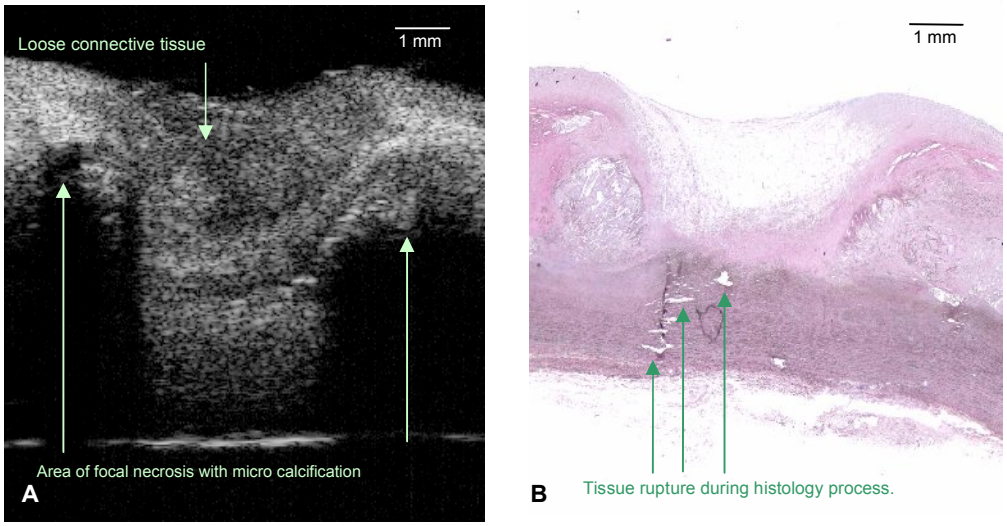

Figure 3.3.5-1: Comparison of (A) standard 40 MHz ultrasonic image of an unfixed human aorta obtained using PVDF TrFE transducer with (B) its histological image. The ultrasonic image clearly identified the loose connective tissue and showed good correlation with the histology. Micro calcified focal necrotic region can be identified as a typical shadow region in the ultrasound image.

3.4 Conclusion

This chapter describes the fabrication of focused ultrasound transducers with various aperture diameters and desired focal numbers using membrane deflection technique. These transducers were characterized using pulse echo technique and exhibited axial resolutions of <19 um. The beam profiles were measured and were shown to agree well with the predicted models. Tissue imaging experiments showed that PVDF TrFE transducers displayed high resolution. Tissue images obtained using PVDF TrFE

transducers were compared to histology images and showed great resemblance identifying various features observed in histology. The feasibility of the development of spherically focused high frequency ultrasound transducers compatible with CMOS microelectronics and MEMS batch fabrication process on a monolithic transducer chip for minimally invasive procedures was shown. Additional work on transducer design to eliminate parasitic issues could further improve the transducer performance in terms of insertion loss. A transducer with improved insertion loss is needed for harmonic imaging to capture harmonic echoes whose amplitudes are about 15 dB lower than the fundamental echoes. The next chapter deals with the development of a minimal parasitic capacitance transducer for improved insertion loss.

CHAPTER IV

ANALYSIS OF PARASITIC CAPACITANCE IN MINIATURIZED ULTRASONIC TRANSDUCERS FOR VASCULAR IMAGING

Based on the work “Effect of parasitic capacitance on MEMS based polymer ultrasonic transducers”, by Chaitanya Chandrana, Tao Pan, Shuvo Roy, Aaron J. Fleischman, *BMES*, Chicago, IL (2006).

4.1 Introduction

In the previous chapter, miniature high frequency focused PVDF transducers [96] were fabricated using techniques compatible with CMOS microelectronics and MEMS fabrication processes. These techniques were demonstrated to produce ultrasonic transducers capable of being integrated onto a monolithic chip. However, the insertion losses from these transducers are relatively higher which could translate to relatively poor performance in harmonic imaging conditions. Harmonics have very low amplitudes and hence

transducers with greater sensitivities are required. Further work needed to be done to improve the transducers insertion loss. A promising way of doing that is by reducing the parasitic capacitance

In this chapter, the effect of parasitic capacitance on the performance of MEMS based ultrasound transducers was investigated. Focused PVDF transducers using MEMS compatible protocols were developed and the parasitic capacitances for these devices were identified and measured. An improved transducer model with minimal parasitics was proposed and a prototype device was developed and tested. The effect of parasitic capacitances on the transducer's performance was evaluated. The minimal parasitic transducer showed significantly enhanced performance with ~ 21 dB improvement in insertion loss for a 1 mm transducer.

4.2 Device Development

Focused PVDF TrFE transducers were developed for minimally invasive procedures using pressure deflection and micromachining techniques [96]. The cross-sectional schematic of the miniaturized ultrasonic transducers is shown in Figure 4.2-1.

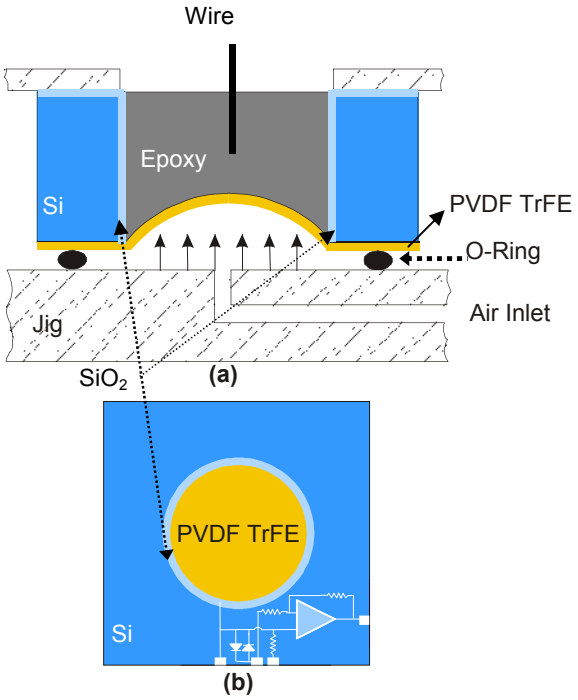

Figure 4.2-1: (a) Demonstration of deflection technique where focused transducers with desired focal numbers can be created by controlling the air pressure. (b) Plan schematic view of the integration of electronics with the transducer.

A piezoelectric PVDF film (with one side coated with Cr/Au for electrical contact) is placed on the silicon substrate that has a laser-trimmed opening in the center. There is layer of SiO_2 with a thickness of 1.5 μm along the inner circumference and on the top surface of the silicon substrate. The PVDF film with the substrate is firmly inverted onto a jig such that the non-metalized film is in contact with the silicon. Pressure is applied on the PVDF TrFE film exposed to the opening on the silicon substrate to render the polymer film into a concave shape. Later, silver epoxy is applied to the back of the opening to retain the shape and to form an electrical contact with the non-conducting PVDF side. The pressure is applied on the film for the duration of the epoxy

curing, typically 8 hours. After the epoxy is cured, the spherical shape of the transducer is fixed thereby forming a focused transducer. Thus, various focal number ultrasonic transducers can be created using the membrane deflection technique just by changing the air pressure during fabrication. These transducers are later connected to high-impedance pre-amplifier mounted on a custom PC board. A Schematic of the amplifier is given in Figure 4.2-2.

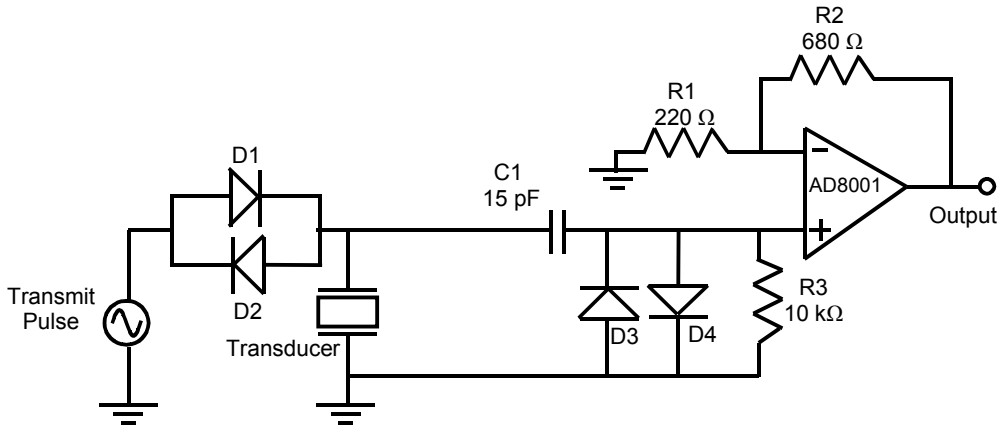

Figure 4.2-2: Schematic of the preamplifier circuit placed in close proximity to the transducers.

The diode pair D1 and D2, constituting the expander, suppresses the transmission of noise from the transmit pulse. The coupling capacitor C1 prevents excessive loading of the input pulse by the limiter. The diode pair D3 and D4, forming the limiter, protects the receive electronics from high voltage in transmit. The transducer is placed in close physical proximity to the amplifier components in order to maintain the SNR for the miniaturized high impedance PVDF TrFE transducers. The transducer and amplifier components are in Figure 3.2-3.

4.2.1 Identification of Parasitics

Cross-section schematic of the transducer attached to a printed circuit board is shown in Figure 4.2.1-1. It can be seen that there are three capacitors associated with this device.

1) Capacitance from the PVDF polymer film itself (labeled C_T in Figure 4.2.1-1). This is the inherent capacitance from the film and will always be present.

2) The capacitance due to 1.5 μm SiO_2 present along the inner circumference of the Silicon chip. SiO_2 acts as a cylindrical capacitor (C_C) between the conductive epoxy used as a backside electrode and silicon substrate.

3) The capacitance due to fringing fields in the dielectric of the substrate (C_f). C_f is considered much smaller than C_C.

The total parasitic capacitance, denoted C_p, is given by the sum of C_c and C_f. C_P forms a parallel impedance to the output and could significantly reduce the input to the preamplifier, thereby degrading the performance of the transducer.

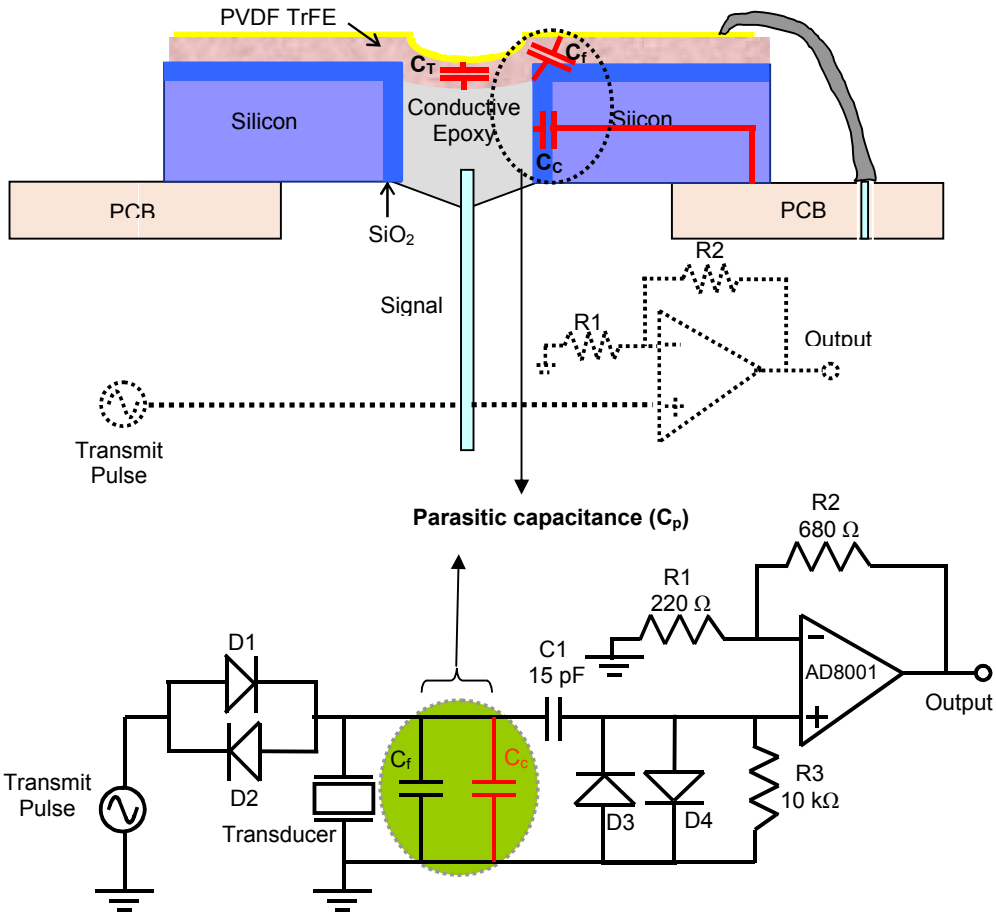

Figure 4.2.1-1: Cross-sectional diagram and schematic of the device showing the inherent transducer and parasitic capacitances associated with the device.

4.2.2 Analysis and Modeling

A simple model was developed to simulate and understand the effect of parasitic capacitance and is shown in Figure 4.2.2-1.

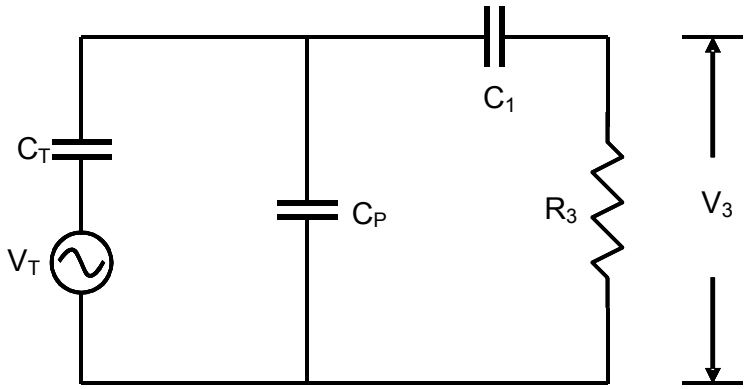

Figure 4.2.2-1: Circuit model to simulate the effect of parasitic capacitance.

The model considers the receive mode functions, when the transducer acts as a source. The source voltage is proportional to the voltage generated by the transducer due to the force on the PVDF film caused by the pressure wave. The model also shows the transducer capacitance C_T, Parasitic capacitance C_C, Coupling capacitance C_1, and the output resistance R_3. . R_3 provides a path for DC bias current to the amplifier. In the receiving mode, the transducer acts as a voltage source and generates an electric signal. Before the signal is picked up by the amplifier, the signal is attenuated by the parasitic capacitance. The effect of parasitic capacitance can be evaluated with the transfer function given below (4.2.2-a).

$$\frac{V_3}{V_T} = \frac{1}{1 + \dfrac{1}{2\pi \cdot f \cdot R_3 \left(\dfrac{1}{C_1} + \dfrac{1}{C_T} \right)} + \left(1 + \dfrac{1}{2\pi \cdot f \cdot R_3 C_1} \right) \dfrac{C_P}{C_T}} \qquad \text{(4.2.2-a)}$$

Since C_T and R_3 are inherent to the transducer and amplifier respectively and C_1 is part of the amplifier, it can be seen from the transfer function how parasitic capacitance C_P influences the response of the system. The equation

demonstrates that lower C_P has less impact on the overall system performance. Hence, it is important to reduce the C_P for improving the performance of the transducer.

4.3 Device with Minimal Parasitics

To evaluate the effect of parasitic capacitance experimentally, performance of the current device needs to be compared with the performance of a device that has minimum parasitic capacitance. For this purpose, prototype minimum parasitic capacitance transducers were built on polycarbonate substrate using same pressure deflection technique used to create transducers on silicon substrate. Although polycarbonate is not a semiconductor and therefore cannot be used in the MEMS fabrication process, it is employed here to clearly demonstrate the effects of removing the parasitic capacitance. Polycarbonate has a lower dielectric constant of 2.3, lower compared to the Silicon dioxide's dielectric constant of 11.6. The lower dielectric constant contributes towards lesser fringing capacitance, C_C. Polycarbonate transducers also do not have the second electrode that therefore, no cylindrical capacitance C_c. The schematic of this device is shown in Figure 4.3-1.

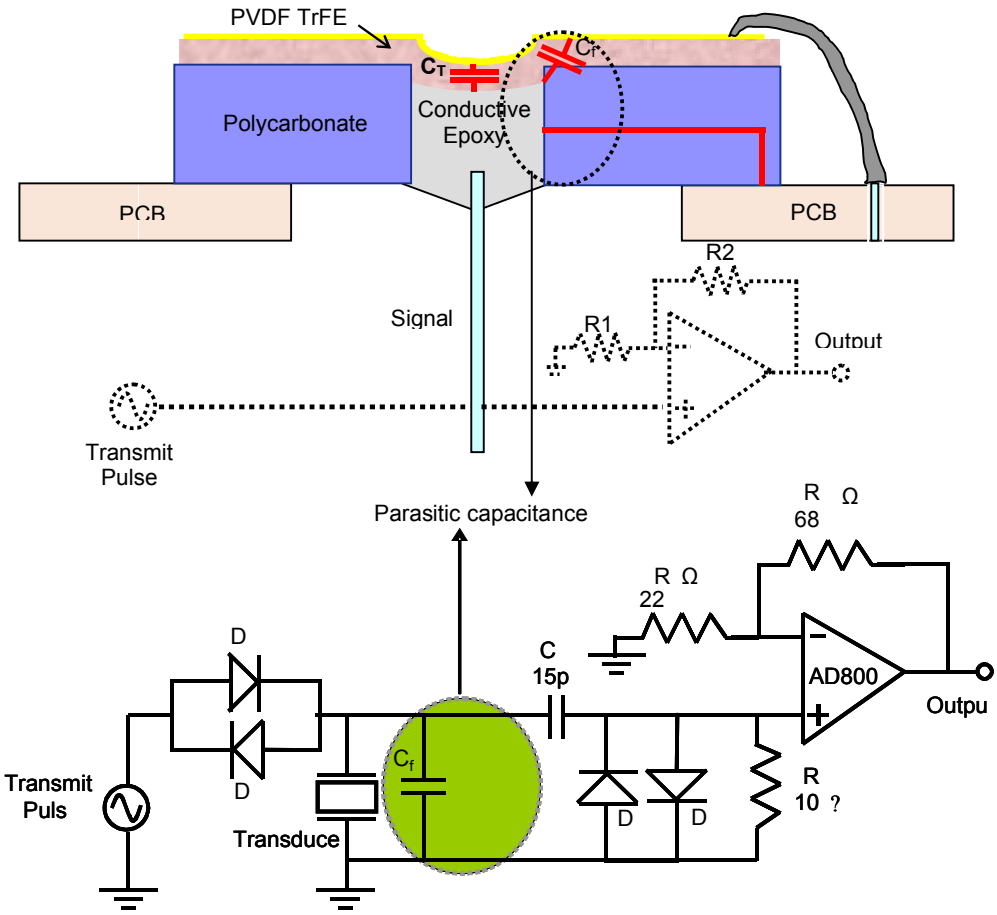

Figure 4.3-1: Cross-section and schematic of transducers with polycarbonate substrate (minimal parasitic devices) to study parasitic capacitance.

4.4 Parasitic Capacitance Measurement

Transducers with various apertures (1-mm, 2-mm and 4-mm) on silicon and polycarbonate substrates were fabricated using techniques described in previous sections. The substrate capacitances were measured using an impedance analyzer. The impedance analyzer was first calibrated to remove the parasitic contribution from the cables by connecting the open, short and 50Ω load cables. Next, the device was connected to the analyzer through the

cable. This gave the impedance measurement of the device (transducer + parasitic capacitances). In order to single out the parasitic capacitance from the device measurements, it was necessary to isolate the transducer capacitance. This was achieved by peeling off the section of the PVDF film that strictly contributes to the transducer capacitance (spherical section at the center of the chip). The remaining film was left unpeeled to make electric contact. The measurements from such devices yielded the required parasitic capacitance. The measured parasitic capacitance values for silicon substrate are significantly higher when compared to the corresponding measurements from polycarbonate substrates. Figure 4.4.1 shows the parasitic capacitance measurements for silicon and polycarbonate devices with various apertures. For silicon substrate transducers with 1, 2 and 4 mm apertures, the parasitic capacitance was measured to be 25, 38.2, and 89.3 pF, respectively. For polycarbonate substrate transducers with same apertures, the parasitic capacitance was measured to be 0.71, 0.95, and 1.1 pF respectively.

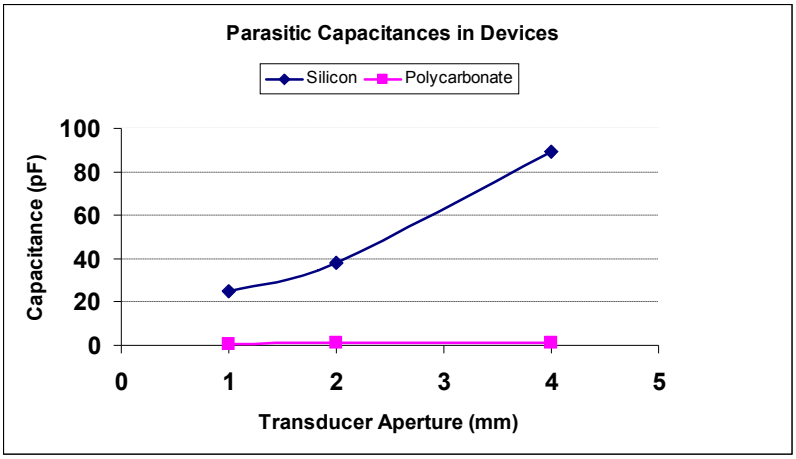

Figure 4.4.1: Measurements of parasitic capacitance with silicon and polycarbonate. It can be seen that silicon devices have higher capacitances compared to polycarbonate devices.

Transducer capacitance values were also obtained by subtracting the capacitance measured from the parasitic device (peeled PVDF device) from the capacitance measured from the entire device. The transducer capacitance for 1, 2 and 4 mm aperture silicon devices were measured to be 1.76, 11.7 and 53.3 pF respectively. As expected, these values were in good agreement with corresponding transducer capacitance values for polycarbonate substrate, which were measured to be 1.75, 11.8 and 49.5pF.

4.5 Analysis of Parasitic Effect

4.5.1 Simulation

The developed model as shown in Figure 4.2.2-1 was analyzed using electrical simulation software, PSPICE (Cadence, San Jose, CA) to predict the output voltage of transducers. The output voltage was simulated for silicon devices (parasitic); polycarbonate devices (minimal parasitic) and for devices with no parasitics. For the simulation measurements, an arbitrary input of 40MHz, 50mV monocycle was used as the driving voltage (pulse generated from the transducer). Measured transducer capacitance C_T values of 1.76, 11.7 and 53.3 pF were used for 1 mm, 2mm and 4 mm devices respectively. Parasitic capacitance C_P values obtained for silicon and polycarbonate devices (in previous section) were used in this model. For the device with no parasitics, no C_P was used. In other words, the parasitic capacitance was removed from the model. The output voltages for different devices with different parasitic capacitances were simulated and displayed relative to the transducers driving voltage. Figure 4.5.1-1 shows the voltage loss due to parasitic capacitance for various sized transducers at 40MHz.

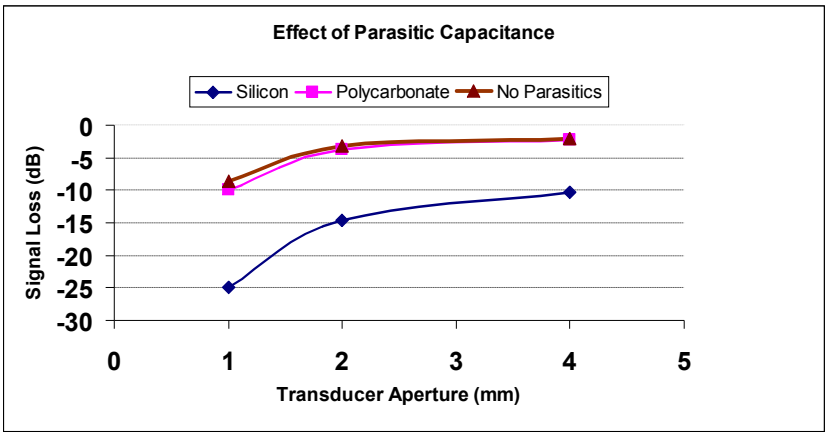

Figure 4.5.1-1: Effect of parasitic capacitance on signal loss for various aperture transducers. It can be seen that silicon devices have greater signals losses. Polycarbonate devices show lower signal loss compared to the silicon devices. Polycarbonate devices show similar signal loss with devices having no parasitic capacitances.

The results show that various diameter transducers (1 mm, 2 mm and 4 mm) with polycarbonate substrate have lower voltage losses (15 dB, 11 dB and 8 dB) than transducers with silicon substrate. The minimal parasitic polycarbonate transducers showed identical signal losses as the transducers with no parasitics. These results suggest that polycarbonate model can be approximated to be an ideal device.

For all the simulations, fixed driving voltage source (50 mV at 40MHz monocycle pulse) was used and hence the output results were displayed relative to the driving voltage. In this model, we did not take into consideration the exact signal generated by each transducer because of the inherent experimental limitations. A larger aperture transducer (4 mm) will generate a higher amplitude signal compared to a lower aperture transducer. However,

this model gives a good idea on the effect of parasitic capacitance for each aperture transducer.

4.5.2 Pulse-Echo Measurement

In order to obtain a realistic effect of the parasitic capacitance, insertion loss measurements using pulse echo techniques were taken both for silicon and polycarbonate transducers. **T**he experimental set up for these measurements is as described in Figure 3.3.1

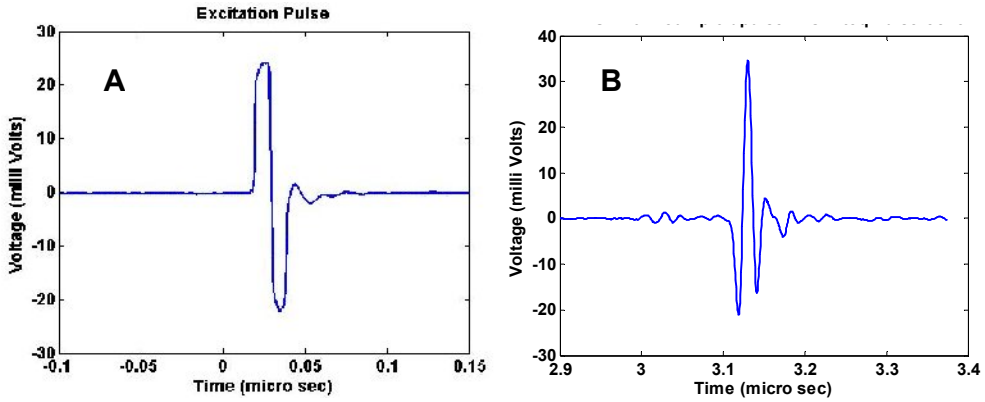

Figure 4.5.2-2: (a) Pulse-echo measurement driving signal and (b) typical transducer response.

During a pulse-echo measurement, the ultrasonic transducer is driven by a 40MHz, 50V pulse at a 2 KHz repetition rate through the expander. The transducer was mounted on an XYZ translational stage (Newport, Universal motion controller/driver, ESP 300) to move of the transducer in three axes with a precision of 1 μm. The reflected echoes captured by the transducer were passed through the limiter and saved in the PC. Expander and limiter are used as the protection circuit. No external amplification was used to minimize parasitic bandwidth components. The transducer was displaced

relative to the glass slide at the bottom of the beaker and the maximum peak-to-peak voltage was recorded. A 40-MHz monocycle driving signal and a typical pulse-echo from a 1-mm aperture transducer with f-number 2.3 are shown in Figure 4.5.2-2.

The pulse-echo measurements were performed on different aperture transducers made on silicon and polycarbonate substrate with or without the preamplifier. The insertion losses were calculated from the pulse-echo measurements as

$$\text{Insertion loss (dB)} = 20 \bullet \log_{10} \frac{Voltage_{pulse-echo}}{Voltage_{input}} \qquad \text{(4.5.2-a)}$$

The results indicated that polycarbonate transducers with preamplifier exhibit lower insertion losses compared to the silicon transducers with preamplifier, confirming the significant effect of parasitic capacitance on the transducer performance. The results are shown in Figure 4.5.2-3. For 1, 2 mm aperture transducers with preamplifiers, polycarbonate devices showed ~5 dB improvement and ~21 dB improvement, respectively compared to silicon devices. Better improvement in smaller transducers could be attributed to the proper impedance matching of the transducer with that of the amplifier.

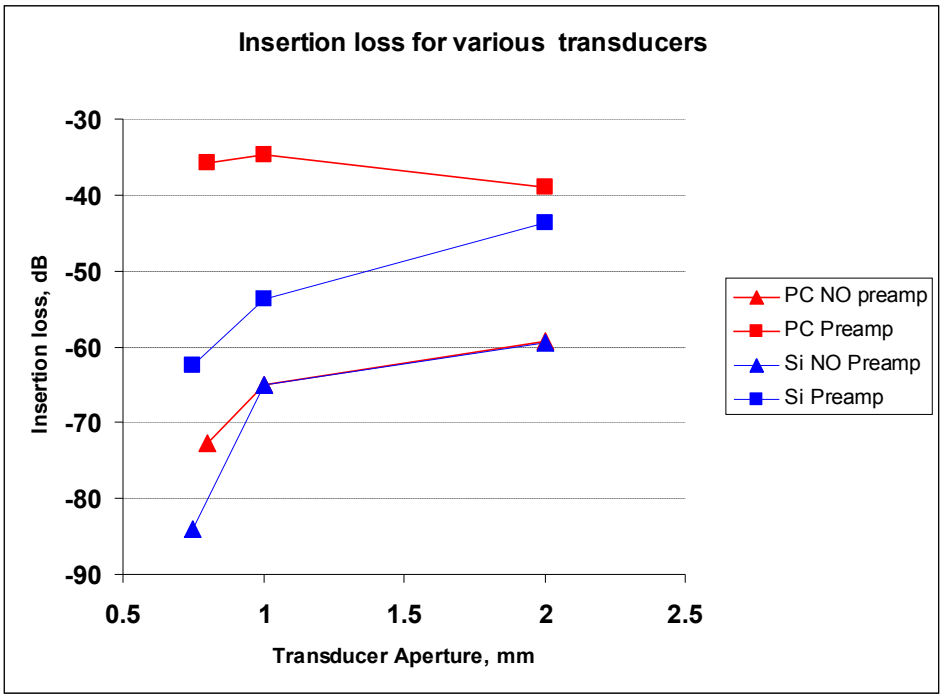

Figure 4.5.2-3: Pulse-echo measurement results of transducers with silicon and polycarbonate substrate.

The results indicated that transducers with polycarbonate substrate with minimal parasitic capacitance showed significantly lower insertion loss than silicon transducers.

4.6 Conclusion

The impact of parasitic capacitance on the performance of miniaturized ultrasonic transducers has been studied via modeling and experiments. Modeling and experimental results showed that parasitic capacitances significantly degrade the performance of the transducer. A new model with minimal parasitic capacitance was developed. The new model improved the insertion loss of the 1 mm transducer by ~ 21 dB. In order to eliminate the parasitic capacitance with silicon processing, one possible solution would be to use a non-conductive backing and connect the electrodes to the top and

bottom of the PVDF. This work demonstrates that parasitic capacitances must be accounted for in the development of integrated PVDF transducers for high-resolution medical imaging.

These high-resolution transducers with broadband characteristics could be explored to assess the potential benefits with harmonic imaging modality to high frequency ultrasound imaging.

CHAPTER V

APPLICATION OF FOCUSED BROADBAND MINIATURE ULTRASOUND TRANSDUCERS FOR HARMONIC IVUS

Based on the work "Micro-Electro-Mechanical Systems (MEMS) based focused ultrasound transducers for high resolution second harmonic imaging applications" by Chaitanya Chandrana, Nikolay A. Kharin, Geoff Vince, Shuvo Roy and Aaron J. Fleischman, Proceedings of 2006 IEEE *International Ultrasonics Symposium,* pp. 693-697, (2006).

5.1 Introduction

In diagnostic ultrasound, recent studies indicated that the intensities associated with the propagation of ultrasound pulses are large enough to generate nonlinear effects [76, 77, 103]. Subsequent studies extended the understanding of nonlinear propagation and development of harmonic

imaging techniques [104-107]. The properties of the nonlinear signals (harmonic echoes) such as narrow beam width and low side lobe levels provide improved lateral resolution and better contrast. The harmonics are generated by the tissue as a result of the distal propagation of the fundamental beams. Low harmonic content in the near and far fields results in reduction of near and far field artifacts. In addition, the harmonics are generated from the tissue, which means that the signals are aberrated only once during the "receive" mode, unlike the fundamental in which the signals are aberrated twice. As a result of these improvements, second harmonic imaging has made its way into commercial settings [82-84]. The image quality improvement using Tissue Harmonic Imaging (THI) has been demonstrated in precordial echocardiography and abdominal sonography, particularly in technically challenging patients [108].

The advent of THI has significantly improved image quality at lower frequencies. Clinicians favor the use of images using THI over those from the fundamental images [85]. However, very little work has been done to see if the mechanisms of harmonic imaging can bring similar improvement in high frequency IVUS. An initial study showed the feasibility of harmonic imaging with IVUS [86]. Another study showed experimental characterization of fundamental and second harmonic beams of a spherically focused, high-frequency, broad bandwidth transducer [87]. A third study showed the results of THI in IVUS application with a conventional rotating IVUS catheter in phantoms and *in vivo* [88]. These studies were carried out using conventional systems.

Unfortunately, existing commercial systems, with their narrow bandwidth and unfocused transducers have not been able to fully exploit the advantages associated with harmonic imaging. . For example, the -6 dB bandwidth of the Boston Scientific Atlantis 40 MHz catheter was measured to be ~34%; Boston Scientific Ultracross 40 MHz catheter has a bandwidth of about ~35% [109]; The disadvantage associated with using commercial catheters with such narrow bandwidth transducers is that the harmonic signal detection becomes difficult because the frequency of harmonic signal lies in the diminished frequency range of the transducer's bandwidth. Desired transducers should have broad bandwidths that allow harmonic frequencies to lie within the strong frequency range of the transducer. Another disadvantage with using commercial systems for harmonic IVUS applications is that the transducers are unfocused. Unfocused smaller aperture (≤ 1.0 mm) transducers have Rayleigh distances larger than the 2-4 mm range which is critical for IVUS applications. For eg; an unfocused transducer with aperture size 1.0 mm, operating at a fundamental frequency of 20 MHz has a Rayleigh distance (lo = $ka^2/2$) of 10.5 mm. In this situation, the harmonic pressures from the desired 2- 4 mm regions are weak. The weak harmonic content from the region of interest translates into low SNR of harmonic acquisitions making the unfocused transducer unsuitable for high frequency harmonic imaging applications. In one of the harmonic IVUS studies, Frijlink et al reported no significant reduction of stent artifacts using an unfocused transducer [110]. This situation could be improved by using focused transducers with broad bandwidths.

Focused transducers are capable of producing peak harmonic pressures at specific depth and range and also produce better resolutions compared to unfocused transducers. Broad bandwidth materials are required to capture the harmonic signal and also for improved axial resolutions. Focused transducers with broad bandwidth could be an ideal choice for harmonic IVUS because of their ability to quickly build up harmonic pressures within the region of interest and also capture harmonic signals within the transducers frequency bandwidth. Although, focused transducers have relatively diminished lateral resolutions beyond the focal point, the lateral resolutions achieved by the focused transducers are better than unfocused transducers. These high resolution transducers with harmonic imaging capabilities could open up the potential for a new dimension in high frequency ultrasound imaging.

This chapter proposes and demonstrates the significance of using focused broadband transducers for harmonic IVUS modality. Such transducers were developed using PVDF TrFE film. Modeling results showed the peak harmonic pressures could be controlled by using focused transducers. These results were verified by experimental harmonic axial radiation patterns, which confirmed that peak harmonic pressures occur as a function of focal number of the transducer. The improvements in image resolution due to nonlinearity were investigated. Finally, *ex vivo* human aorta images were presented in fundamental and harmonic imaging modes.

5.2 Significance of using focused transducers for harmonic IVUS

Analytical solutions for moderately nonlinear (nonlinear effects and absorption of same order, Goldberg number =1) second harmonic focused and unfocused beams have been derived from the Khokhlov-Zabolotskaya-Kuznetsov (KZK) equation [111, 112]. The equations were based on continuous wave input. The pressure amplitude of the unfocused second harmonic beam is given by the expression 5.2-a:

$$p_2 = \frac{j\beta\omega_2 p_0^2}{2\rho_0 c_0^3 (1 - jz/l_0)} \exp\left[-\frac{z}{l_a} - \frac{2r^2}{a^2(1 - jz/l_0)}\right] \times \int_0^z \frac{\exp(z'/l_a)}{1 - jz'/l_0} dz' \qquad (5.2\text{-a})$$

where, j=√-1 (time convention e^{jwt}), β is the coefficient of nonlinearity, ω_2 *is* angular second harmonic frequency *(ω_2=2ω_0,* where ω_0 is angular fundamental frequency), p_0 = pressure on face of the transducer; ρ_o = equilibrium value of density, c_0 = speed of sound, z is axial distance, l_o = $ka^2/2$; where k is the wave-number at fundamental frequency, a is radius of transducer, l_a= *1/*α, α is a combined coefficient of absorption at fundamental and harmonic frequencies. r= radial distance ($r^2=x^2+y^2$); Primed coordinates correspond to locations of source points in the same way as it has been reported in published literature [113].

Similar pressure amplitude expression for the focused beam is given by the lossless solutions to KZK associated with second-harmonic generation [114]. This approximation is valid as we measured axial radiation patterns in water, where absorption is small in comparison with the tissue.

$$p_2 = \frac{jP_0}{1 - jG} \frac{\ln\left[1 - \left(1 + jG^{-1}\right) z/R\right]}{1 - \left(1 + jG^{-1}\right) z/R} \exp\left[-\frac{2(1 - jG)(r/a)^2}{1 - \left(1 + jG^{-1}\right) z/R}\right] \qquad (5.2\text{-b})$$

$$P_o = (\beta\omega_0^2 p_o^2 a^2) * (4\rho_0 c_0^4)^{-1}$$

where, , R is the radius of the curvature (focal length) and $G = ka^2/2R$.

Using the expressions (5.2-a) and (5.2-b), harmonic axial radiation patterns were modeled using a continuous 40 MHz wave input for 1 mm aperture diameter transducer for unfocused and various focused (f-numbers 2, 3, 4, 5) sources. The modeled results are shown in Figure 5.2-1.

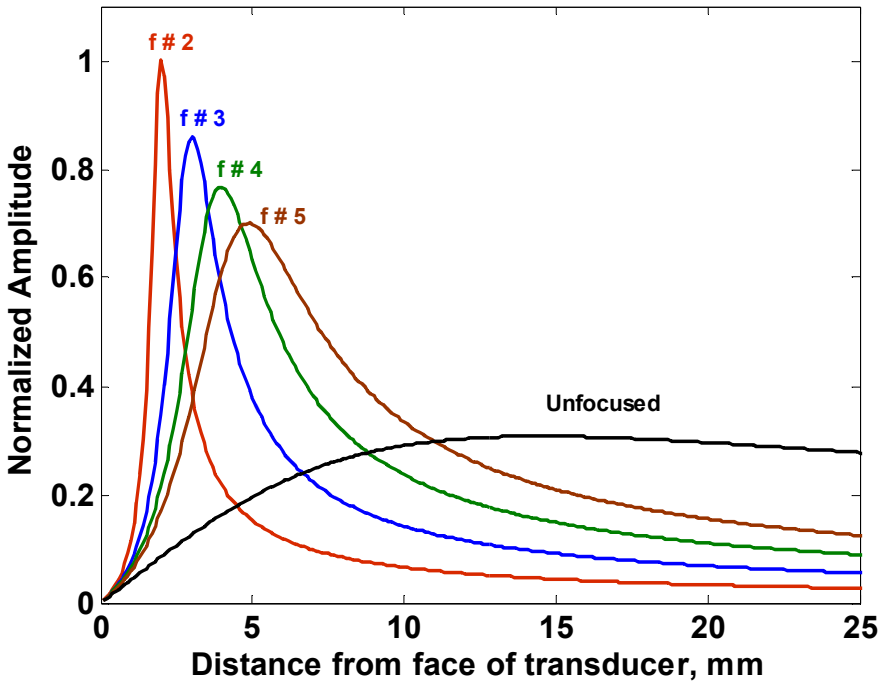

Figure 5.2-1: Theoretical 40 MHz harmonic pressures for 1 mm aperture transducers with unfocused and focused sources. It can be seen that focused transducers have their peak harmonic pressures corresponding to their focal length where as the peak pressures for an unfocused transducer occur far off from the face of the transducer. High harmonic peak pressures due to focusing can also be observed.

These results show that the unfocused transducer has its peak pressure amplitude at 12 mm from the face of the transducer. The harmonic pressures from the region of interest (2-4 mm range) are 15-20 dB lower than the peak harmonic pressures at 12 mm. In such cases, the signal-to-noise ratio of the harmonic signals from these regions is low. On the other hand, focused transducers showed that the peak harmonic pressures occurred corresponding to the focal length of the transducer; which means peak harmonic pressure amplitudes can be made to occur from the desired regions by choosing an the corresponding f-number transducer. This scenario would result in significantly higher SNR of the harmonic content. In addition, focused transducers have stronger harmonic pressures compared to the unfocused transducers. Development of focused broadband transducers is a key step for IVUS imaging as it has the potential to open up harmonic imaging modality.

5.3 Materials and Methods

5.3.1 Focused transducer fabrication

Focused, broadband, high frequency (35-45 MHz) ultrasonic transducers suitable for harmonic IVUS have been developed using a 9 μm thick Polyvinylidene fluoride-trifluoroethylene (PVDF TrFE) film (Ktech Corp, Albuquerque, NM, USA). The technique used to develop these focused transducers was described in section 3.2 Methodology of Chapter 3.

5.3.2 Experimental setup

The experimental setup for high frequency harmonic imaging is shown in Figure 5.3.2-1.

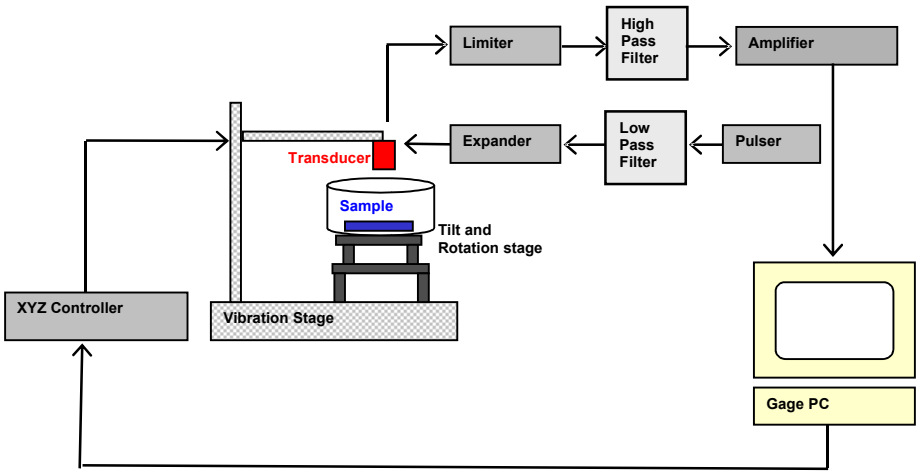

Figure 5.3.2-1: Experimental setup for harmonic imaging.

It consists of a pulser (Avtech AVB2–TB-C-CCA monocycle generator, Avtech Electrosystems, Ogdensburg NY, USA) to excite the transducer through an expander and a low pass filter. The low pass filter (3 dB @ 33 MHz, Butterworth) was used in the transmit side to filter out the unwanted high frequency components generated by the pulser that might interfere with the harmonic echoes generated by the sample. The received echoes from the sample were collected by the digitizing oscilloscope (Agilent 54835A, Agilent Technologies, Englewood CO, USA) through the limiter, a high pass filter and a 30 dB amplifier (Miteq AU-1114, Miteq Corporation, Hauppauge NY, USA). A high pass filter (3 dB @ 35 MHz, Butterworth) was used in the receive side to filter out the fundamental components from the received echo. The expander and limiter constitute the protection circuitry [115]. The custom developed low pass and high pass filters were characterized using a Network analyzer (Hewlett Packard, 4395A). The characteristics of the filters are shown in Figure 5.3.2-2

The transducer was mounted on to an XYZ translational stage (Newport, Universal motion controller/driver, ESP 300). The stage moves with a resolution of 1 μm in the three axes. The transducer was moved in different axes with various step sizes depending on the experiment. Data was collected in three ultrasonic imaging modalities- Fundamental 20 MHz (F20), Harmonic 40 MHz (H40) and Fundamental 40 MHz (F40). Following parameters were used for each imaging mode.

1. Fundamental 20 MHz (F20): Transmitting at 20 MHz and receiving at 20 MHz. Low pass filter (33 MHz - 3dB) was used in the transmit side.
2. Harmonic 40 MHz (H40): Transmitting at 20 MHz and receiving at 40 MHz (H40). Low pass filter in the transmit side and high pass filter in the receive side were used.
3. Fundamental 40 MHz (F40): Transmitting at 40 MHz and receiving at 40 MHz (F40). No Filters were used.

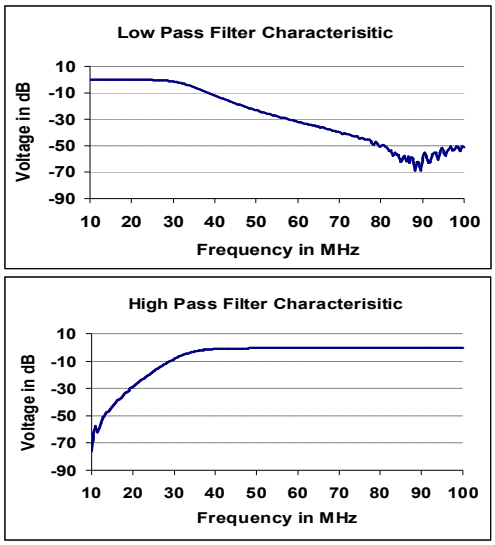

Figure 5.3.2-2: Characteristics of 33 MHz Low pass filter and 35 MHz High pass filter. The low pass filter was designed for use in the transmit side to block the high freuqency components from the pulser. High pass filter was used to filter out the fundamental frequencies and pass the harmonic frequencies for processing. These filters also reduce the noise level outside the frequency range of interest.

5.4 Results

5.4.1 Peak harmonics as a function of f-number

Experimental harmonic axial radiation patterns were obtained for various f-number transducers at 40 MHz and compared to the theoretical model. Radiation patterns were obtained for 4 mm aperture transducers with f-numbers 2.3 and 2.9. The measurements were done in H40 mode as described in section III. The transducer was moved vertically relative to the glass plate in a beaker containing de-ionized (DI) water in steps of 50 μm. The echoes at each position were recorded and the peak voltages were

calculated. The peak voltages from each point were plotted to generate the axial radiation pattern. The experimental harmonic axial radiation patterns demonstrated that the peak harmonics occurred corresponding to the focal length of the respective transducers. Harmonic axial radiation patterns for identical transducers were modeled using the equation (2). The modeled results were compared to the experimental results and are as shown in Figure 5.4.1-1.

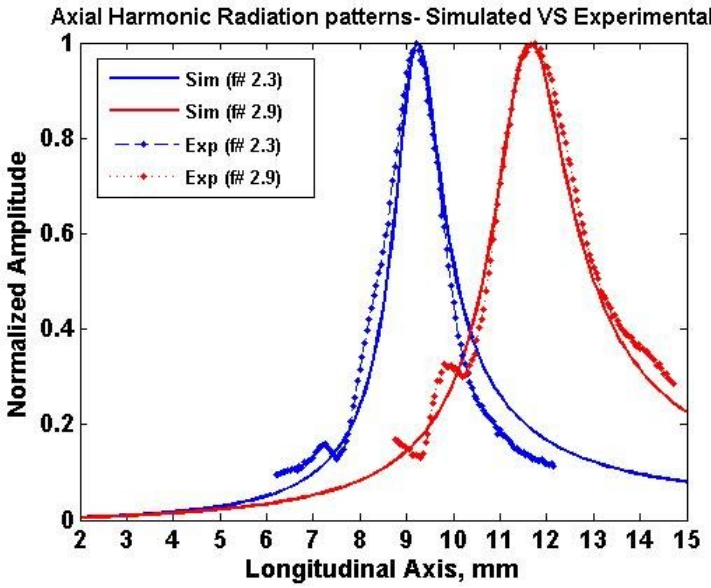

Figure 5.4.1-1: Comparison of simulated (dashed line) and experimental (dotted line) harmonic axial radiation patterns for 4 mm transducers with various f-numbers. It can be clearly seen that the experimental results show good agreement with the modeled results.

It can be seen that the experimental results compared favorably to the modeled results. This demonstration leads to the conclusion that the peak harmonics can be adjusted to occur at desired locations by changing the f-number of the transducers.

5.4.2 Lateral resolution improvement

Improvement in lateral resolution due to nonlinearity was investigated. Lateral resolution measurements were performed in DI water in the three imaging modes – F20, H40 and F40. A 60 μm-diameter stainless steel wire was used as the target. A 1 mm aperture transducer with f-number 3.2 was used to scan across the wire in the focal plane. The transducer was excited with 20 MHz 50V monocycle pulse to generate the F20 data. H40 data was obtained by applying appropriate filters as described in the experimental setup section. The transducer was excited with a 50V 40MHz monocycle pulse to generate the F40 data. In all the three imaging modes, the transducer was placed such that the wire is in the focal plane of the transducer. The transducer was moved transversely across the wire with a step size of 5 μm. The reflections at each point were recorded and the peak-to-peak voltages were plotted as shown in Figure 5.4.2-1. The lateral resolution is given by the beam width, which occurs at half of the peak voltage. The lateral resolutions in F20, F40, H40 modes were measured to be 162 μm, 123 μm and 124 μm, respectively.

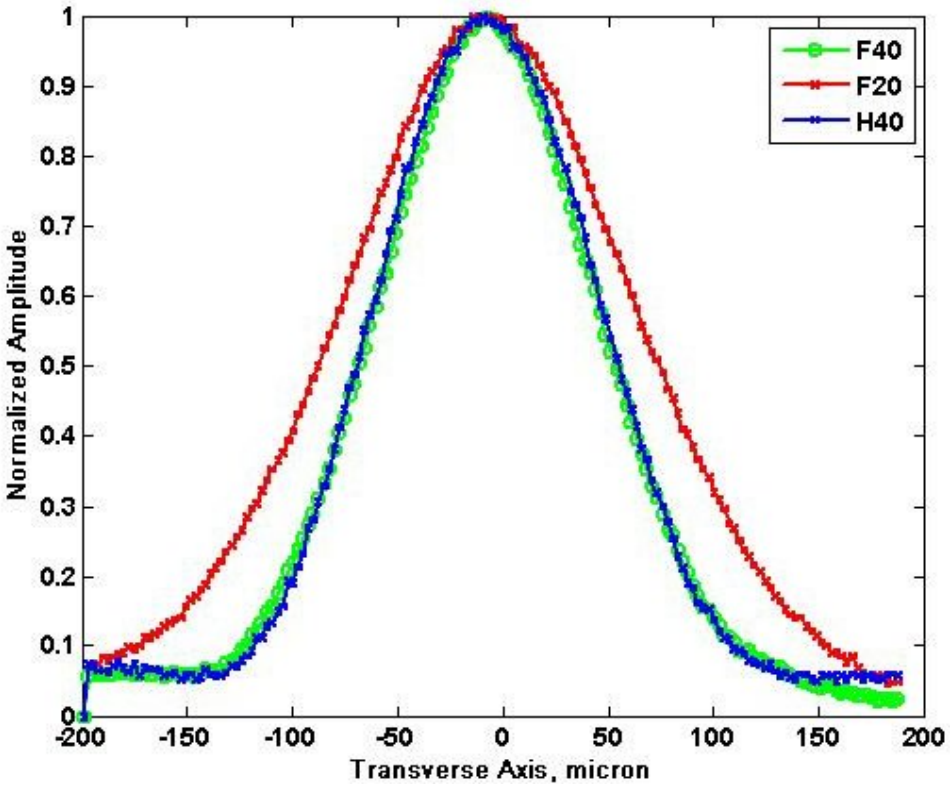

Figure 5.4.2-1: Measured lateral beam profiles of the focused transducers in both fundamental (F20 and F40) and harmonic (H40) modes. The profiles are normalized to the maximum signal at focus.

The experimental values were compared with the theoretical values. Theoretical lateral resolutions for both the fundamental modes (F20 and F40) were obtained using the following equations [2].

$$F_{resolution} = \lambda * f - number \qquad (5.4.2\ a)$$

$$\lambda = \frac{c}{f} \qquad (5.4.2\text{-}b)$$

Where λ is the wavelength, *c* is the speed of sound in water (assumed as 1500 m/s) and *f* is the center frequency. The wavelengths of F20 and F40 beams were determined to be approximately 55 μm and 37 μm respectively. Using these values, the lateral resolutions in F20 and F40 modes for the 1

mm aperture transducer with f-number 3.2 were calculated to be 175 μm and 120 μm, respectively. The theoretical harmonic resolution is given by the expression [116]

$$H_{resolution} = \frac{1}{\sqrt{2}} * F_{resolution} \qquad (5.4.2\text{-c})$$

Using the above expression the H40 resolution was calculated to be 124 μm. It was observed that the experimental resolutions agree pretty well with the theoretical resolutions with less than 8% error. Table 5.4.2-1 provides the theoretical and measured lateral resolutions of the three imaging modes.

Table 5.4.2-1: Theoretical and measured and lateral resolutions for F20, H40 and F40 imaging modes for a 1 mm transducer with f-number 3.2.

THEORETICAL AND MEASURED LATERAL RESOLUTIONS FOR VARIOUS IMAGING MODES

Imaging Mode	Theoretical (μm)	Measured (μm)
F20	163	175
H40	123	120
F40	124	124

The lateral resolution improvement due to harmonics was better presented using respective scans from a micromachined silicon phantom wafer. The phantom wafer consists of fixed beams and spaces alternately with widths ranging from 20 μm to 160 μm. A photograph of the phantom wafer is shown in Figure 5.4.2-2.

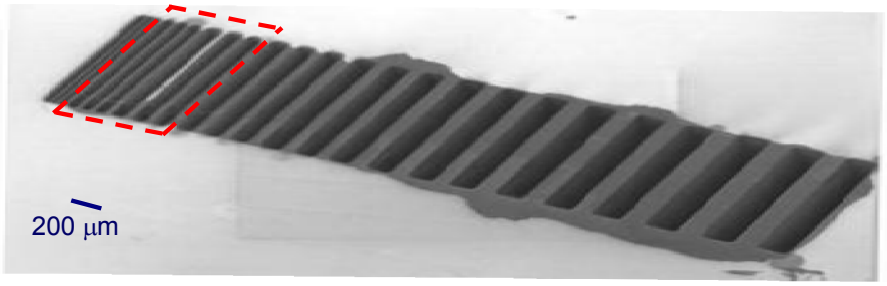

Figure 5.4.2-2: Figure showing the photograph and schematic of the silicon phantom wafer used for lateral resolution characterization.

A 1 mm aperture transducer (f-number 1.7) was used to scan the phantom wafer with a step size of 1 μm. Experiments was done in the three imaging modes - F20, H40 and F40 as described in section III. For the F20 and F40 imaging modes, the transducer was excited with 50 V_{pp} 20 MHz monocycle pulse. For the F40 imaging mode, the transducer was excited with 50 Vpp, 40 MHz monocycle pulse. The reflections at each point were recorded and the peak-to-peak voltages were measured. Figure 8 shows the normalized amplitude response of the F20, H40 and F40 signals across 60 μm and 80 μm bars and spaces of the phantom wafer. The signals were normalized with respect to the maximum value at focus in their respective modes. It was observed, and shown in Figure 5.4.2-3, that the H40, in comparison to the F20, showed comparatively higher dynamic range for the 40 μm and 60 μm beams with increased signal strength of ~4 dB and ~7 dB, respectively.

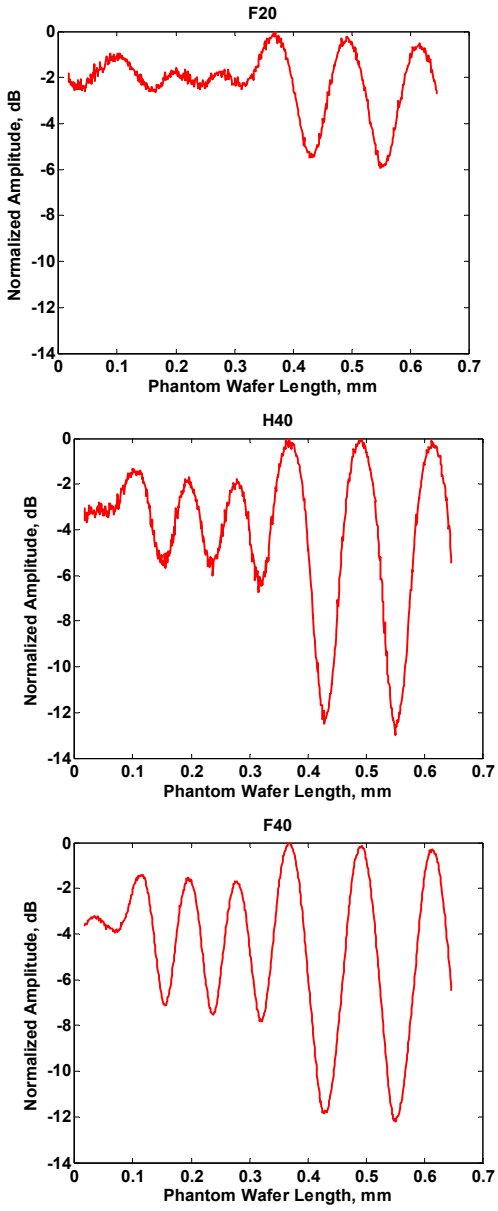

Figure 5.4.2-3: Figure showing the signal strength across the 40 and 60 μm beams in the three imaging modes. It can be seen that H40 shows better lateral resolution compared to F20 for the 40 μm beams (first three peaks) and 60 μm beams (last three peaks).

5.4.3 Tissue Harmonic Imaging

The PVDF TrFE transducers were used to image tissue in three imaging modes -F20, H40 and F40. Human cadaveric aorta was placed on a paraffin bed covered with DI water. A transducer with aperture size 2 mm and f-number 2.5 was used to scan the tissue laterally in increments of 50 μm. The reflections at each point were sampled at 1 GHz and standard imaging software –MATLAB (The Mathworks, Inc. MA, USA) was used to process the data. Figure 5.4.3-1 shows the images of the tissue imaged in F20, H40 and F40. H40 demonstrates the feasibility of harmonic IVUS using the focused PVDF TrFE transducer. Harmonic image, unlike the fundamental image, is obtained due to the nonlinear propagation and shows different information about the tissue. It can be expected that the additional diagnostic information about the tissue could be used for better diagnosis and also tissue characterization [117].

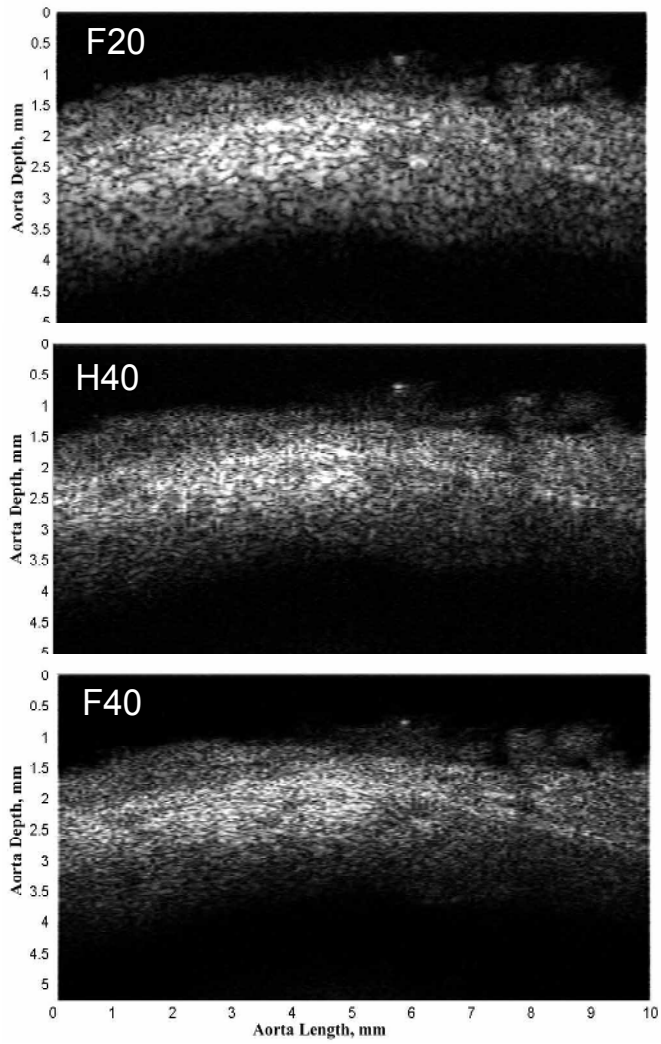

Figure 5.4.3-1: Cadaveric aorta images acquired using the broadband focused PVDF TrFE transducer in both fundamental (F20 and F40) and harmonic (H40) modes. The images are individually normalized to the maximum signal in each image.

5.5 Conclusion

In this chapter, significance of using focused broadband transducers for harmonic imaging at IVUS frequencies has been proposed and verified via modeling and experimental results. Such transducers were built and

characterized to exhibit broad bandwidth (100% at -6 dB) with axial resolutions of about 20 μm. The transducers, in H40 mode, demonstrated better lateral resolution compared to F20. Modeled and experimental results have shown that focused transducers have the capability to generate significant harmonic pressures from regions of interest relevant to IVUS. These transducers have shown the feasibility of harmonic imaging. Once fully integrated, these transducers would have sizes small enough to fit the catheter profile, available at low cost and are clinically implementable. Such devices with high resolutions and harmonic imaging capabilities could open the potential for harmonic imaging in IVUS and could enhance the functionality of IVUS. Future work could include the incorporation of Pulse inversion techniques for harmonic IVUS.

CHAPTER VI

HIGH RESOLUTION FUNDAMENTAL AND HARMONIC INTRAVASCULAR IMAGING USING FOCUSED PVDF TRFE TRANSDUCERS AND PULSE INVERSION TECHNIQUES

Based on the work "High resolution intravascular fundamental and harmonic imaging using a MEMS fabricated focused ultrasonic transducer" by Chaitanya Chandrana, Nikolay Kharin, Anuja Nair, Kendall R. Waters, Geoffrey D. Vince, Barry Kuban, Geoffrey Lockwood, Shuvo Roy and Aaron J. Fleischman. IEEE International Ultrasonics Symposium 2007, pp.1183 - 1187, (2007).

6.1 Introduction

In the previous chapter, the benefit of using focused PVDF TrFE transducers for harmonic IVUS has been proposed and verified. That study showed the potential for THI at high frequencies for IVUS by using a technique, which uses high pass and low pass filters to separate the

harmonic. Nonetheless, this technique imposes a limitation to the benefits that could be obtained with harmonic imaging because low intensity, high frequency linear echoes will overlap with the important tissue harmonic signal [118]. Figure showing the overlap between the transmit and receive bands is shown in Figure 6.1-1 The filtering technique cannot filter out the tissue harmonic signal alone, and hence, detection of pure harmonic echoes is not possible. To reduce the overlap between the high frequency linear echoes and the harmonic echoes, transmit and receive bands must be narrower. However, this is not an ideal solution because it degrades axial resolution.

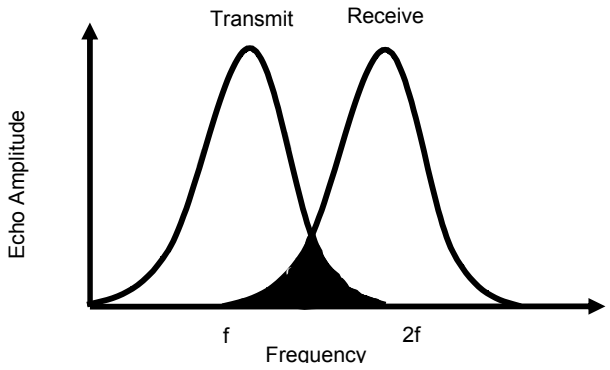

Figure 6.1-1: Schematic illustrating the drawbacks of harmonic imaging using filtering approach. The overlap between the transmit and receive bands results in an unwanted linear echo in the harmonic mode [119].

A promising alternative to extract the tissue harmonic signal is the pulse inversion technique [118, 120, 121]. In this method, two ultrasound wideband pulses that differ by 180^0 in phase are transmitted. When the received signals are summed together, the linear echoes are cancelled and the non-linear echoes are doubled. Thus, a better cancellation of the linear echoes and improved detection of harmonic echoes can be expected with this technique. As a result, the pulse inversion technique overcomes the limitation imposed

by the filtering technique. Another advantage of using pulse inversion technique relative to the filtering approach is that the pulse inversion imaging is controlled completely electronically. For clinical implementation, Pulse inversion could be implemented in the commercial settings by just changing the input pulse sequence and without the need for additional hardware unlike the filtering approach. Another benefit of using Pulse inversion imaging is that both fundamental and harmonic data are obtained with one excitation sequence potentially decreasing motion artifacts.

In this chapter, it is proposed and verified that focused broadband transducers, when applied with pulse-inversion techniques, can bring about dramatic improvements in the image quality of IVUS. A method was developed to enable ultrasonic multimodality imaging where a single transducer is used to obtain images in five different modes - standard 40 MHz IVUS, fundamental 20 MHz (F20), harmonic 40 MHz (H40), fundamental 40 MHz (F40) and harmonic 80 MHz (H80); by simply changing the excitation signal and applying appropriate post processing techniques. Multimodality images obtained by the focused broadband PVDF TrFE transducers, not possible with the conventional systems, can provide more diagnostic information, which, in turn, could lead to better tissue characterization. The improvement in lateral resolution due to second harmonics were investigated. Multimodality ultrasonic images of the human cadaveric coronary ostium using a 1 mm-diameter focused PVDF TrFE transducer are presented. High-resolution human cadaveric tissue images were obtained in the standard 40 MHz mode using PVDF TrFE transducers and compared to the commercial systems, and also with corresponding histology.

6.2 Methods

In this Chapter, various experiments are conducted. Pulse-echo response experiments are done to characterize the resolution parameters of the focused transducer. Lateral resolution experiments are performed to characterize the improvement in lateral resolution due to nonlinearity. Human aorta and coronary ostium images are obtained to show the feasibility of high resolution fundamental and harmonic imaging using focused transducers. Different transducers are used for different experiments and are specified at the description of each experiment. The transducers are excited with 40 MHz monocycle pulses for maximum axial resolution to generate the standard 40 MHz images. The transducers are excited with 20 MHz Gaussian pulses to generate F20 and H40 images and also with 40 MHz Gaussian pulses to generate the F40 and H80 images. Additional description on the transducers and the imaging procedures are given in the subsequent sections of the chapter.

6.2.1 Focused PVDF TrFE tranducer

The crucial component for the proposed ultrasonic multimodality imaging is the transducer. More specifically, the transducer should have broad bandwidth to capture harmonic signals. In addition, the transducer needs to be focused to develop significant harmonic content at specified depth and range within the dimensions of the coronary geometry [16]. Such miniature transducers were developed [10] as detailed in the previous chapters. The miniaturized PVDF TrFE transducers exhibit high output impedances. Hence, in order to maintain the SNR, the transducers were placed on a printed circuit

board in close proximity to high impedance preamplifier components having a gain of 12 dB [96].

6.2.2 Ultrasonic multimodality imaging setup

The experimental method, constructed to obtain multiple imaging modes (standard 40 MHz, F20, H40, F40, H80) using a single transducer, is shown in Figure 6.2..2-1. Standard 40 MHz imaging mode was obtained by exciting the transducer with a 40 MHz Monopulse using a pulser (Avtech AVB2–TB-C-CCA monocycle generator, Avtech Electrosystems, Ogdensburg NY, USA) and processing the echo data. The other imaging modes - a pair of fundamental and harmonic (F20, H40) and a second pair (F40, H80) imaging modes were obtained by exciting the transducer with Gaussian 20 and 40 MHz pulses, respectively and applying pulse inversion techniques.

For the fundamental and harmonic imaging modes, the transducer was excited with a pulse sequence containing two waveforms. The two waveforms (two Gaussian pulses with initial phases 0^{o} and 180^{o} and separated by 15 μs) were created as txt files using MATLAB (The Mathworks, Inc, MA, USA). The waveforms were then configured through a arbitrary waveform generator card CG 4300 (Gage applied technologies, Lockport, IL, USA). The output waveforms from the CG 4300 were amplified using a 53 dB power amplifier (3200L broadband power amplifier, Electronics & Innovation Ltd., Rochester, NY, USA). The amplified signals were used to drive the 40 MHz focused transducers through an expander circuit. The received pulses were amplified by 12 dB by a preamplifier circuit placed at the back of the transducer. These pre-amplified pulses pass through a limiter circuit and a 30dB external

amplifier (Miteq AU-1114, Miteq Corporation, Hauppauge NY, USA). Overall, there is a system gain of 42 dB the receive side. The echoes were sampled at 1 GHz with an 8-bit digitizing oscilloscope (Agilent 54835A, Agilent Technologies, Englewood, CO, USA).

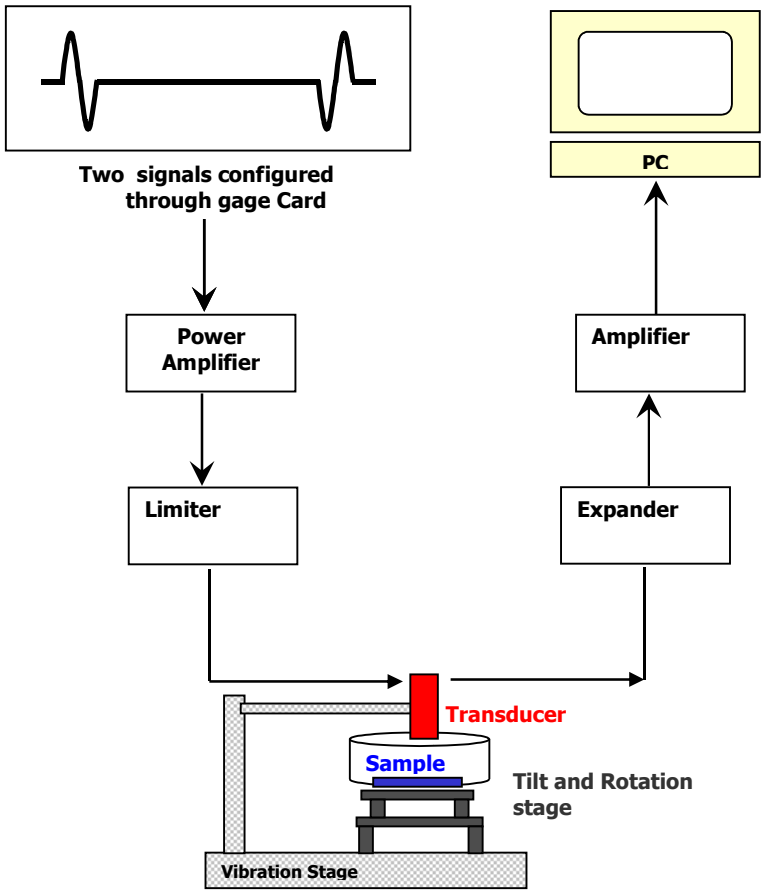

Figure 6.2.2-1: Schematic diagram of the custom method for multiple modality imaging. Using this method, a single broadband focused transducer, can produce 4 imaging modalities from the same sample by just changing the input pulse once.

The transducers were mounted on a XYZ translational stage (Newport, Universal motion controller/driver, ESP 300). The stage can be controlled via a motion controller with a precision of 1 μm in all the three axes. For radial

imaging experiments, the transducer was mounted on a rotational stage, which can rotate with a precision of 0.1 μm.

6.2.3 Transmit waveform bandwidths

Harmonic signal at a particular imaging depth consists of two components. One is the harmonic echo due to the finite amplitude propagation of ultrasound and the other is the harmonic leakage produced by the system prior to propagation. The harmonic leakage signal may mask the vital harmonic echo signal that reveals different information of the tissue. Transmit waveforms with large bandwidths are a source of harmonic leakage as they may have frequency components outside of the fundamental bandwidth. A narrow bandwidth waveform cannot be used as it reduces the image quality. Hence, the transmit waveform bandwidth needs to be optimized to offset the tradeoff.

Pairs of Gaussian shaped transmit waveforms were created (as described in the earlier section) with varying bandwidths ranging from 10% to 100 %. For instance, one pair consisted of a 20 MHz Gaussian pulse with 10 % bandwidth and its inverse. A second pair consisted of 20 MHz Gaussian pulse with 20 % bandwidth. Figure 6.2.3-1 (a) and (b) show 20 MHz Gaussian pulse with 60 % bandwidth and its inverse. These pulses are used for majority of the experiments in this thesis.

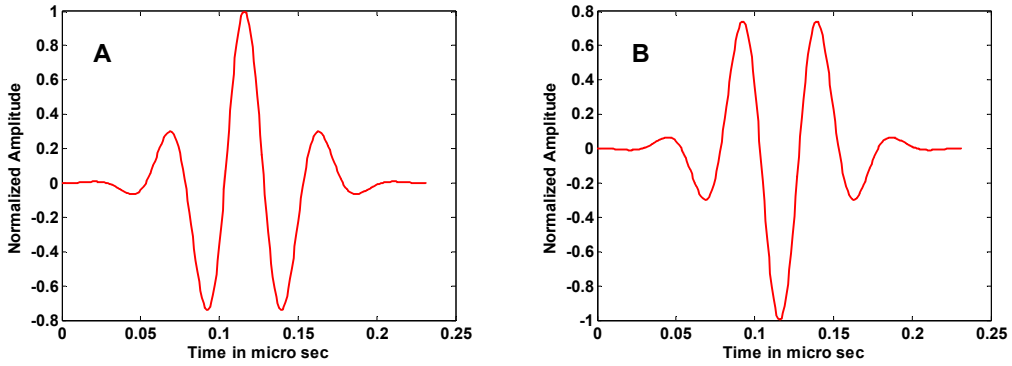

Figure 6.2.3-1: Figure (A) - 20 MHz Gaussian pulse with 60 % bandwidth. Figure (B) - Inverse of figure (A). Both pulses separated by 20 μs form a pair of pulses for pulse inversion imaging.

The pulse-pairs were used to excite a 1 mm aperture transducer (focal number 2.5). The pulse-echoes were captured and the fundamental and harmonic signals were derived using pulse inversion techniques. The power spectral densities of the fundamental and harmonic echoes were analyzed. Figure 6.2.3-2 shows the power spectra of the fundamental and harmonic echoes for various transmit Gaussian bandwidths. It can be seen that as the bandwidth of the excitation pulse pair increases, the high frequency portion of the fundamental signal enters into the bandwidth of the second harmonic, causing harmonic leakage.

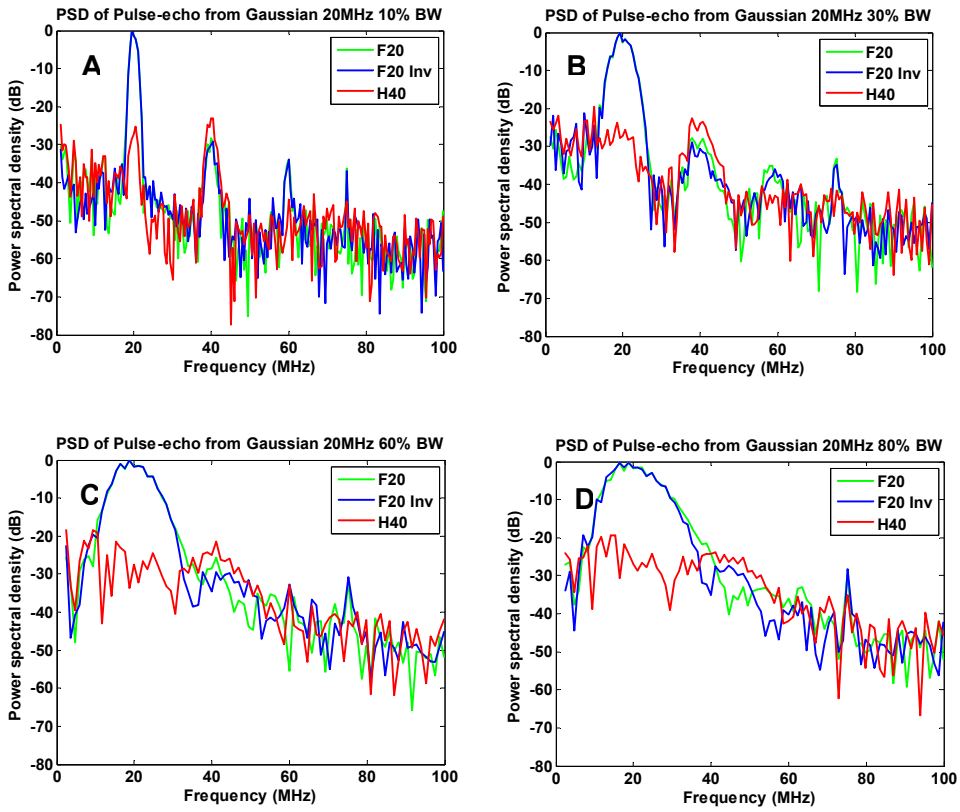

Figure 6.2.3-2: Figures A, B, C, D showing the power spectral densities of the fundamental and harmonic echoes for excitation pulse pairs with bandwidths 10%, 30%, 60% and 80% respectively. It can be seen that as the bandwidth of the excitation signal increases, high frequency fundamental echoes overlap with the bandwidth of the harmonic signal. For the narrow bandwidth (10%, Figure A) Gaussian excitation, there is no overlap. However, the narrow bandwidth of the harmonic signal degrades the image quality.

6.2.4 Multimodality imaging description

When the transducer was excited with 20 MHz Gaussian alternate waveforms, differing by 180^0 phase, the echoes constitute F20 (corresponding to excitation waveform with 0^0 phase) and F20 inverse (corresponding to

excitation waveform with 180^0 phase) data. The transducer was moved in the lateral/radial direction using the translational/rotational stage depending on the experiment. The data acquisition was repeated at each position. For each position, multiple scanlines were collected and averaged to reduce the noise in the system and improve the signal to noise ratio. For tissue imaging experiments, 1024 scanlines were averaged to reduce the noise. Temporal averaging on commercial IVUS systems is limited in part because of tissue motion under clinical conditions. For the pulse-echo and lateral resolution experiments, 16 scanlines were averaged. After averaging, the two data sets- F20 and F20 inverse, were added to cancel the fundamental components and enhance the harmonic components (H40). Additionally, finite impulse response (FIR) equiripple high pass digital filter designed in MATLAB (Stop band frequency - 25 MHz; Pass band frequency - 35 MHz; Stop band attenuation - 0.0001) was used to remove the residual fundamental components in the sum echo. In this way, the transducer excited by 20 MHz positive and negative Gaussian pulses produces F20 and H40 data. Similarly the same transducer, when excited with 40 MHz Gaussian positive and negative pulses, and using similar pulse inversion techniques, generates F40 and H80 data. For the H80 data, a MATLAB generated FIR equiripple high pass digital filter (Stop band frequency - 55 MHz; Pass band frequency - 65 MHz; Stop band attenuation - 0.0001) was used to remove the residual fundamental components in the sum echo. In this way, a single PVDF TrFE broadband transducer with the multimodality imaging approach was able to produce four modes of images by electronically changing the input pulse sequence once.

6.3 Results and Discussion

6.3.1 Enhancement of Harmonics

The results in this section demonstrate that fundamental components are effectively cancelled, and the harmonics are enhanced when pulse inversion techniques were applied to the PVDF TrFE transducers. The transducers were excited with a pulse sequence containing two 20 MHz Gaussian waves (15% bandwidth) separated by 180^0 phase difference. The pulse-echo responses from these transducers were captured as detailed in the previous section. Figure 6.3.1-1 compares the power spectral densities of the received echoes before and after the application of pulse inversion technique. It was found that the odd-order harmonics were effectively cancelled, whereas the even-order harmonics were doubled. For example, the amplitude of fundamental component was reduced by nearly 30 dB and the second harmonic component was enhanced by 6 dB.

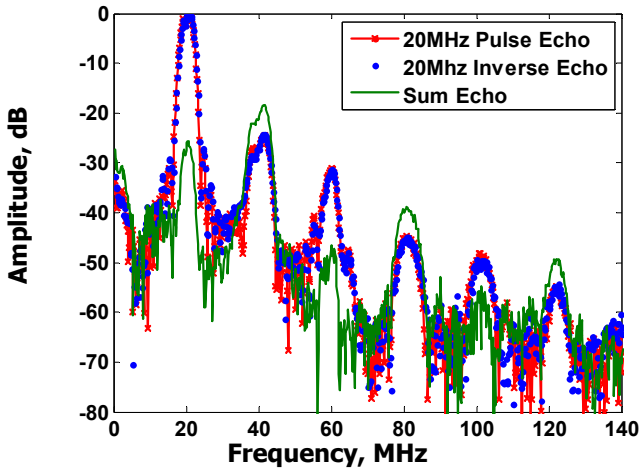

Figure 6.3.1-1: Figure showing the enhancement of even-order harmonics by 6dB and effective cancellation of the odd- order harmonics for broad band transducers using pulse inversion technique.

6.3.2 Lateral resolution improvement

Lateral resolutions of the transducer were measured in multiple imaging modes (F20, H40, F40, H80). The four modes were generated as described in the 6.2.2 and 6.2.3 sections. A 2 mm PVDF TrFE focused transducer with f-number 2.1 was used. The transducer was excited with Gaussian pulses (70 V, 60% bandwidth) separated by 15 μs. The excited transducer was used to scan across a 20 μm stainless steel wire in the focal plane with a step size of 5 μm. The maximum amplitudes from the target wire at each step were calculated and plotted as shown in Figure 6.3.2-1.

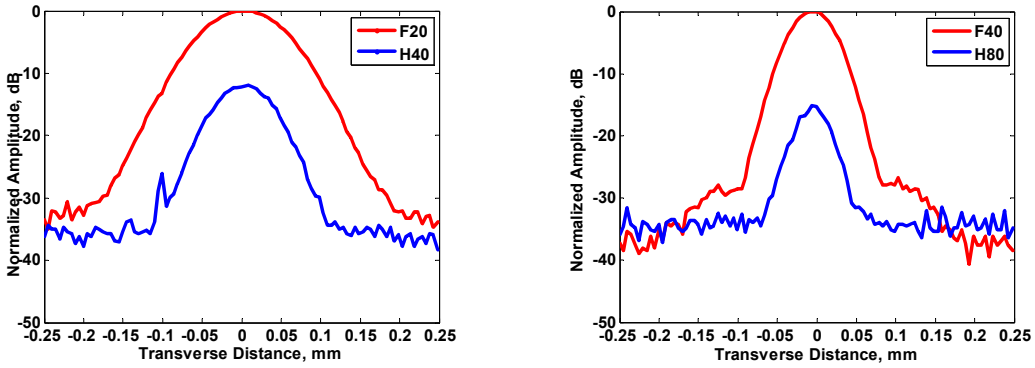

Figure 6.3.2-1: Figure showing the lateral resolutions in the focal plane for the four imaging modes- F20, H40, F40 and H80.

The experimental lateral resolutions were given by the width of the beam at -6 dB . The theoretical lateral resolutions in fundamental mode are given by equation 5.4.2-a .The theoretical lateral resolutions in harmonic mode were derived from the fundamental resoltuions using the formula 5.4.2-b [116].

Table 6.3.2-1 provides the experimental and theoretical lateral resolutions in the four imaging modes. The experimental resolutions in all the

imaging modes matched well with the theoretically calculated resolutions with <10 % pecentage error. The experimental results showed slightly better compared to the theoretical results. This could be attributed to the following reasons. A 20 μm wire was used for measuring experimental resolutions to replicate a point souce. Secondly, there could be < 10% error in the calculated focal number. The sound of speed in water could be different than the assumed speed of 1500 m/s.

Table 6.3.2-1: Theorectical and measured and lateral resolutions for F20, H40, F40 and H80 imaging modes for 2 mm transducer with f-number 2.1.

THEORETICAL AND MEASURED LATERAL RESOLUTIONS FOR VARIOUS IMAGING MODES

Imaging Mode	Theoretical (μm)	Measured (μm)
F20	156	142
H40	106	100
F40	82	77
H80	58	57

In order to graphically show the lateral resolution in diffrerent modes, a micromachined silicon phantom wafer consisting of beams and gaps ramging from 20 μm to 160 μm was used. A 1 mm aperture transducer (f-number 2.6) was used to the scan the phantom wafer with a stepsize of 2 μm. The peak harmonics of H40 and H80 signals were observed to be 17 dB and 28 dB lower than their fundamental F20 and F40 signals, respectively. The data obtained along the lateral direction of the phantom was displayed with 4 dB contrast for better visual representation. Figure 6.3.2-2 shows the response of the phantom wafer in multiple imaging modes. It can be seen that the harmonic data (H40), in comparison to fundamental data (F20) showed better

resolution of the 100. μm beams. In the same way, H80 showed better resolution compared to the F40. It can be seen that H80 resolves the 60 μm beams more clearly compared to the F40.

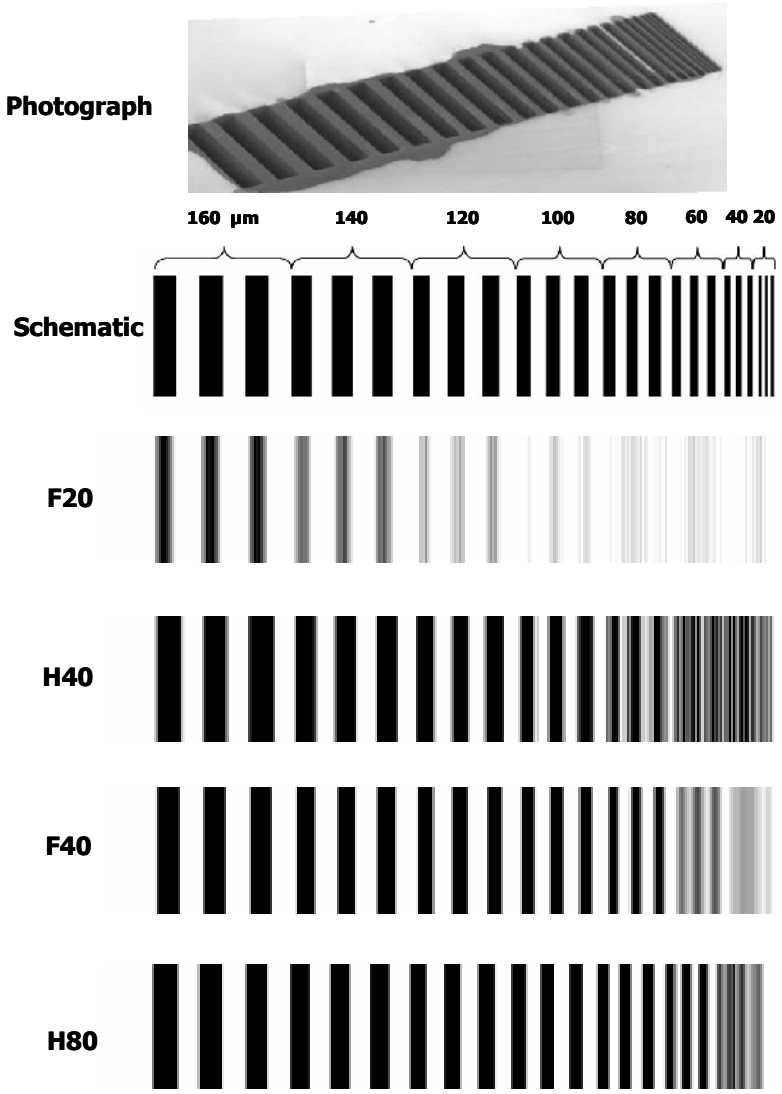

Figure 6.3.2-2: Figure showing the photograph and schematic of the Silicon phantom wafer used for resolution characterization. H40 shows better resolution of the 100 μm beams compared to F20. H80 was better able to resolve 60 μm beams and even 40 μm beams compared to the F40.

Lateral resolution improvement quantification in four imaging modes was done by comparing the amplitude of the echoes across the 80 μm beams and gaps in the corresponding modes. The response of the reflected echoes in fundamental and harmonic modes normalized to their maximum amplitudes is shown in Figure 6.3.2-3. It was observed that H40 showed better dynamic range with increased signal strength of 8 dB compared to F20. Similarly, H80 showed improved dynamic range with better signal strength of ~ 15 dB compared to F40.

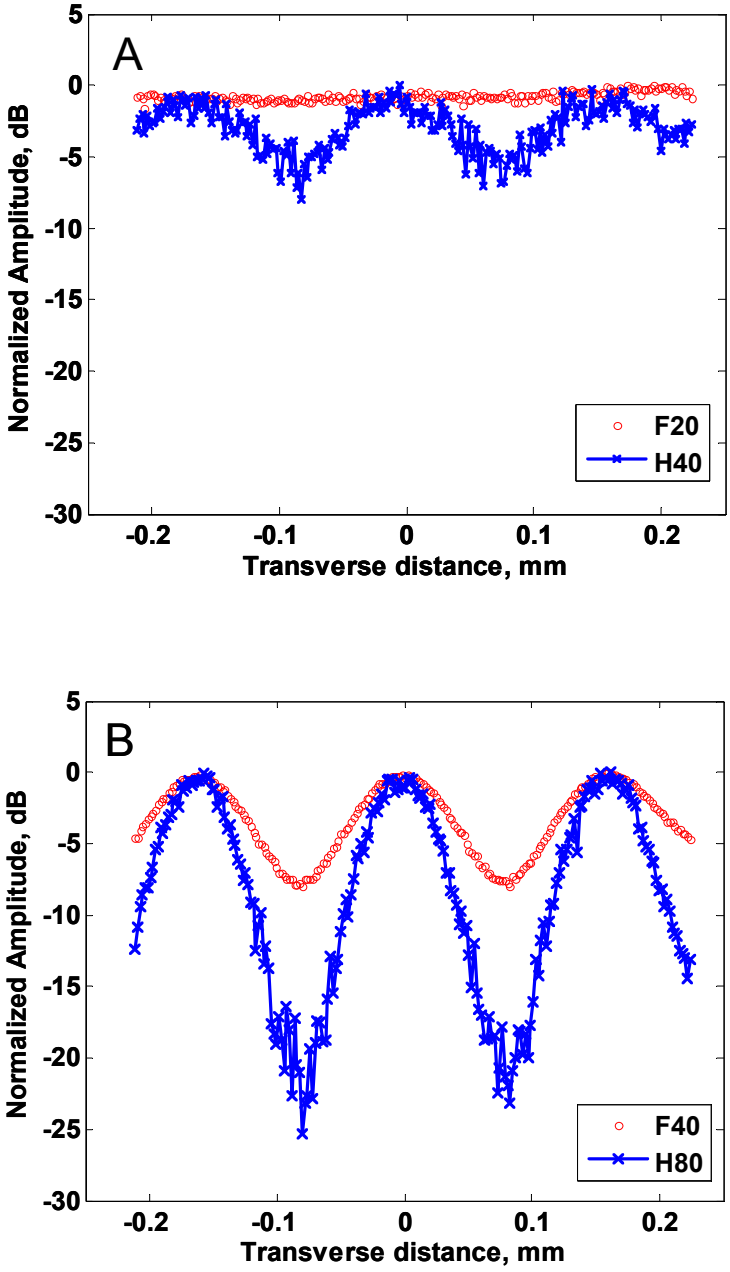

Figure 6.3.2-3: Figure demonstrating the improved signal amplitude for harmonic echoes along the lateral direction of the three 80 μm beams and gaps of the Silicon phantom wafer. 'A' shows H40 displaying 7.5 dB improved signal strength compared to F20. 'B' displays improved signal strength of ~ 14 dB for H80 compared to F40.

6.3.3. Ultrasonic multimodality tissue imaging

A sample of human cadaveric aorta was pinned flat onto a paraffin base, and covered with de-ionized (DI) water. A section of aorta was scanned using a 2 mm aperture PVDF TrFE transducer with f-number 2.1. The transducer was attached to the front of a custom PC board which has the preamplifier circuit mounted on its back. The transducer was focused to obtain the maximum pulse-echo response from the aorta. The transducer was then moved in 50 μm increments in one direction using a motorized translational stage. The reflections from the sample at each step were sampled at 1 GSamples/s and saved as a scanline. A total of 200 scanlines were recorded to cover the tissue lateral length of 10 mm. Using the ultrasonic multimodality imaging techniques described in the previpus sections, with a single PVDF TrFE transducer two fundamental (F20 and F40) and two harmonic modes (H40 and H80) of tissue data were obtained by simply changing the input excitation pulse sequence. Images of the aorta in the four modes are shown in Figure 6.3.3-1.

The harmonic images (H40 and H80) do not show the tissue as deeply as in the fundamental images (F20 and F40) because the harmonic peaks are lower and have a narrow dynamic range. However, H40 and H80 represent the harmonic information obtained from the nonlinear interactions between the tissue and the ultrasound waves. As such, these images represent tissue properties different from those obtained in the fundamental imaging mode [122]. Therefore, harmonic imaging could provide new and complimentary information about the tissue that could be used for better tissue characterization [117].

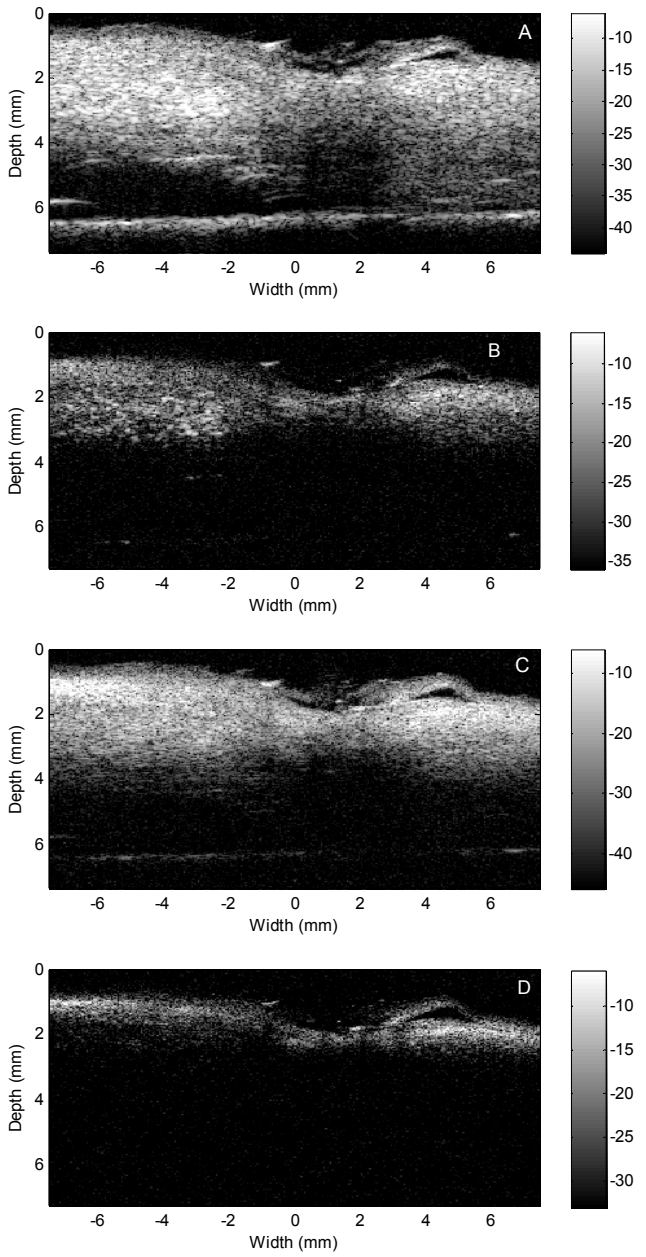

Figure 6.3.3-1: Figures showing four modes of human aorta images. 'A'- fundamental 20 MHz, 'B' - harmonic 40 MHz, 'C' - fundamental 40 MHz and 'D' - harmonic 80 MHz. Fundamental images provide linear information about the tissue. Harmonic images provide additional (nonlinear) information about the tissue. Such information could be used for better tissue or plaque characterization.

6.3.4 Intravascular tissue harmonic imaging

The sample of human coronary ostium was pinned such that it was vertical onto a paraffin base containing DI water. The *ex vivo* circumferential imaging setup of the human coronary ostium with PVDF TrFE transducers having amplifier components in close proximity is shown in Figure 6.3.4-1. A 1 mm aperture PVDF TrFE transducer with an f-number 2.7 was used. The transducer was rotated using a motorized rotational stage to scan the sample in increments of 0.5 degrees to generate 720 scanlines.. Each scanline was recorded with a sampling rate of 1 GHz. Pulse inversion techniques were employed and the images in four modes- F20, H40, F40 and H80 were generated.

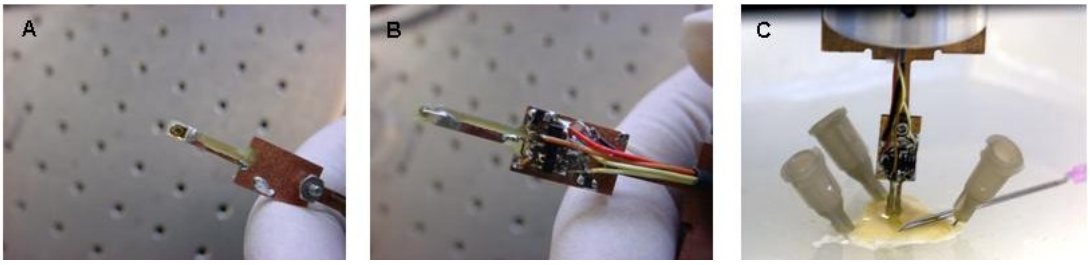

Figure 6.3.4-1: Figure showing (A) 1 mm focused broadband ultrasound transducer on the tip of the PC board, (B) Amplifier components mounted on the other side of PC board and in close proximity to the transducer (C). Imaging setup to obtain ex-vivo ecircumferntial tomographic images of the arteries. The transducer is placed inside the lumen of the ostium and rotated using a motorized rotational stage. An 18 gauge needle is shown for size reference.

High-resolution fundamental and harmonic images obtained with focused PVDF TrFE transducers are shown in Figure 6.3.4-2. As expected, the harmonic images do not show as good penetration as the fundamental.

However, they demonstrate the feasibility of obtaining nonlinear information from the coronary geometry at specified depth and range using focused transducers, which is not possible with the commercial systems.

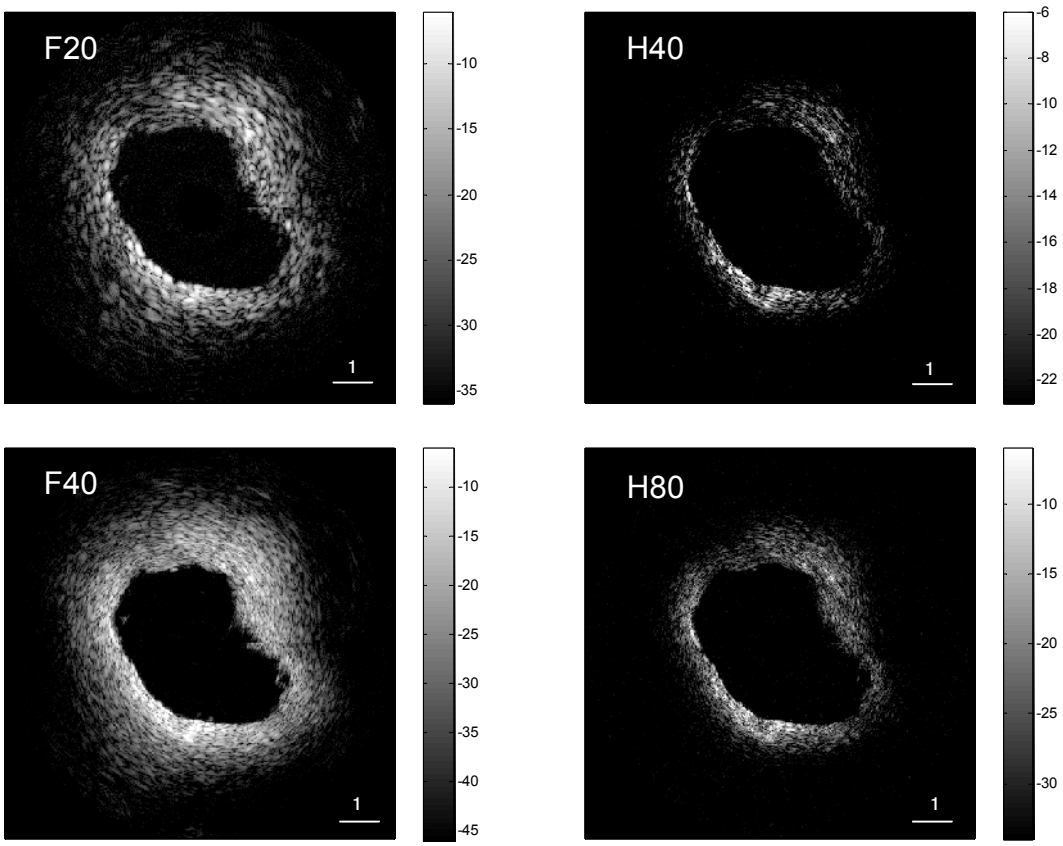

Figure 6.3.4-2: Ultrasonic images of human coronary ostium using a PVDF TrFE transducer (Aperure 1 mm; f-number 2.7) in four modes- fundamental 20 MHz (F20), harmonic 40 MHz (H40), fundamental 40 MHz (F40) and harmonic 80 MHz (H80). The harmonic images demonstrate the feasibility of obtaining nonlinear information from specified depth and range of a coronary ostium using focused transducers.

6.3.5 Comparison to commercial IVUS systems

For qualitative image comparison, a section of ostium was imaged using focused PVDF TrFE transducer and compared to the images from commercially-available Volcano InVision Gold IVUS system. Two types of catheters were employed: (1) Volcano Eagle Eye^{TM} *Gold* 20 MHz array catheter and (2) Volcano Revolution^{TM} 45 MHz single element rotational catheter. For the images from PVDF TrFE transducer, a 1 mm transducer with f-number 2.7 was used. The transducer was excited with 40 MHz monopulse for better axial resolution and the scanlines were acquired. For each acquisition, 1024 scanlines were collected and averaged to reduce the inherent noise in the system. The PVDF TrFE transducer did not have any catheter sheath as would be present in the commercial IVUS system. The standard 40 MHz image was generated using standard image processing software (MATLAB, The Mathworks, Natwick, MA, USA). Corresponding images of the Ostium from almost the same exact region were generated using the two Volcano IVUS Catheters. An issue that prohibits the precise co-registration of the three images for a more direct comparison is the uncertainty in aligning the transducers in the exact imaging plane orientation and location. As such, comparative images are used to asses the image quality and identify different features in the relative locations. The comparative images are shown in Figure 6.3.5-1. Eagle Eye^{TM} *Gold* is lower in frequency (20 MHz) and hence the lowest resolution. Overall, the PVDF TrFE image displayed better axial and lateral resolution than the other two commercially available systems and this is obvious from the visible media delineation in the PVDF TrFE image that is not visible clearly in the other two images

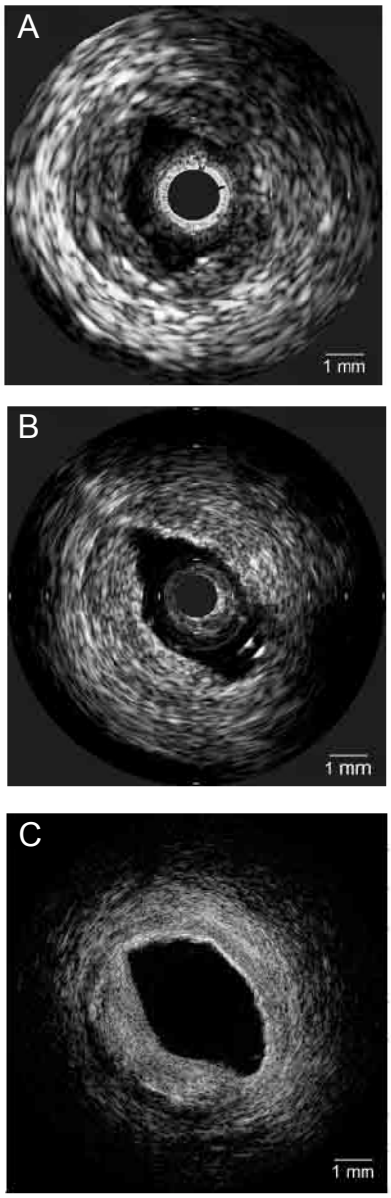

Figure 6.3.5-1: Comparison of human coronary artery images obtained using the commercial systems- (A) Volcano Eagle Eye™ *Gold* 20 MHz array catheter and (B) Volcano Revolution™ 45 MHz single element rotational catheter with (C) developed 1 mm aperture PVDF TrFE focused transducer. For the image from PVDF TrFE transducer, ringdown artifacts were eliminated during data processing. The PVDF TrFE transducer shows improved quality image with better contrast between the media and adventitia.

6.4 Conclusions

In this chapter, high-resolution focused broadband PVDF TrFE transducers suitable for harmonic IVUS were presented. The transducers exhibited broad bandwidth (~ 120% at -6 dB) and produced axial resolutions (<19 μm). The feasibility of harmonic IVUS using these transducers was shown. A method for ultrasonic multimodality imaging was developed where a single transducer produced five different imaging modes (standard 40 MHz, fundamental 20 MHz, harmonic 40 MHz, fundamental 40 MHz and harmonic 80 MHz). Harmonic signals demonstrated better lateral resolution compared to the fundamental signals. The 1mm PVDF TrFE transducers showed better quality tissue images when compared with the commercial IVUS systems. Such promising results suggest that single element focused broadband PVDF TrFE ultrasonic transducers with multimodality imaging capabilities have the potential to improve the functionality of IVUS imaging and thus, clinical use of IVUS.

CHAPTER VII

DISCUSSION AND CONCLUSIONS

7.1 General discussion

Intravascular ultrasound (IVUS) has become an important clinical tool for the detection and evaluation of atherosclerotic lesions, for therapeutic interventions and for clinical research. This catheter based imaging technique produces coronary images with sufficient penetration depth with no necessity for saline flushing or balloon occlusion. The spatial resolutions of the current IVUS systems are not sufficient enough to aid in detecting vulnerable plaques. The work presented in this Thesis shows the development of a focused ultrasound transducer with improved lateral and axial resolutions.

Harmonic ultrasound imaging which has been shown to suppress image artifacts and enhance image quality has become a standard imaging mode in the conventional diagnostic range (1-10 MHz). However, little work has been done to see if the advantages with harmonic imaging can be seen in

the high frequency ultrasound applications like IVUS. This work shows the feasibility of harmonic IVUS using focused polymer transducers and demonstrates its inherent benefits that show significant clinical potential.

The following section summarizes the most important findings of the study.

7.2 Summary and key contributions

The objective of this thesis is to develop an ultrasonic transducer for IVUS that shows superior lateral and axial resolutions and that has the capability to obtain harmonic IVUS images.

Various tasks were performed to pursue the objective of this study; 1) development of a focused broad bandwidth PVDF TrFE transducer for obtaining high resolutions, 2) improvement in the performance of such a transducer by eliminating the parasitic components, 3) application of these transducers to harmonic imaging techniques to show the feasibility of harmonic IVUS, 4) demonstrating the ultrasonic multi modality imaging capabilities using a single transducer.

Focused, broad bandwidth, high-resolution ultrasonic transducers were developed for high frequency applications using custom membrane deflection technique and MEMS compatible protocols. The transducers exhibited minimal ringing and showed broad bandwidth (120% at -6 dB). The transducers also demonstrated focused radiation patterns with diffraction limited lateral resolutions and axial resolutions less than 19 μm. The transducer development techniques presented in this study are compatible with the final MEMS fabrication process and are capable of being manufactured on silicon wafers after the completion of CMOS electronics to

create a monolithic transducer chip. The insertion loss of these transducers were improved by eliminating the parasitic capacitance resulting in a new transducer model with minimal parasitic capacitance. The new 1 mm aperture transducers showed an improved insertion loss of about 21 dB compared to the previous model.

The feasibility and potential benefits of harmonic IVUS using the focused transducers were investigated. It was shown that focused transducers build the harmonic field faster that lead to enhanced SNR of harmonic acquisitions and also improved lateral resolution at the focus. The other benefit of using focused transducers is that harmonic information from different regions of interest can be extracted by designing the focused transducers.

A method was developed where a single broad bandwidth transducer was used to produce ultrasonic multimodality images (fundamental 20 MHz, harmonic 40 MHz, fundamental 40 MHz, harmonic 80 MHz, standard 40 MHz) using a single transducer. Multimodality images provide complementary information about the tissue that could be used for better tissue/plaque characterization and thereby improve the diagnostic accuracy.

This dissertation makes vital contributions specifically to the field of IVUS which could be extrapolated to high frequency medical ultrasound. The innovations are –

1. Development of an ultrasonic transducer that has resolutions superior to the ones reported in the literature so far.
2. Feasibility and benefits of harmonic IVUS using focused transducers.
3. Demonstration of multimodality ultrasonic images using a single ultrasonic transducer

7.3 Future work

It has been shown that the development of a high resolution transducer suitable for harmonic imaging capabilities do not have to go through narrow-band excitation pulses and analog filtering. This work has shown the implementation of excitation pulse sequences in combination with signal processing techniques in laboratory based research. Translation of this work into high frequency clinical settings may not be an issue, since similar processing is available in conventional diagnostic ultrasound. However, high frequency systems have to be equipped with necessary hardware to implement pulse inversion based harmonic IVUS and need some level of optimization and tuning.

It has been indicated in chapter VII that different biological tissues have different nonlinearity coefficients. Although this study provides non linear information at different frequencies, further studies are necessary to extract the nonlinear information from the image to estimate tissue properties. Such studies could provide complementary information to the existing plaque characterization techniques [123] [124] to provide better diagnosis.

Harmonic IVUS benefits from small transducers with good sensitivity over a large bandwidth. Apart from piezoelectric polymer materials studied in this dissertation, such advantages are offered by relatively new and developing capacitive micro-machined ultrasonic transducer (CMUT) technology. This technology offers great advantages as very wide bandwidth, potential integration of electronics and ease of fabrication of arrays. However, concerns over limited output [13] and excitation of harmonics in transmission [14] need to be overcome.

A multi-disciplinary approach with collaboration between clinicians, engineers, scientists and pharmacists should play a key role in developing new technologies for harmonic IVUS.

REFERENCES

[1] F. Foster, C. Pavlin, K. Harasiewicz, D. Christopher, And D. Turnbull, "Advances In Ultrasound Biomicroscopy," *Ultrasound In Medicine And Biology,* Vol. 26, Pp. 1-27, Jan 2000.

[2] G. Lockwood, D. Turnbull, D. Christopher, And F. Foster, "Beyond 30 Mhz - Applications Of High-Frequency Ultrasound Imaging," *IEEE Engineering In Medicine And Biology Magazine,* Vol. 15, Pp. 60-71, Nov-Dec 1996.

[3] Y. Sajjo And A. F. W. Van Der Steen, "Vascular Ultrasound," *Springer Verlag, Tokyo* 2003.

[4] A. Nair, D. Calvetti, B. Kuban, And D. Vince, "Novel Technique For Normalization Of Intravascular Ultrasound Backscatter Data: Toward Automated And Real-Time Plaque Characterization.," *American Journal Of Cardiology,* Vol. 94, Pp. 123e-123e, Sep 30 2004.

[5] F. D. Kolodgie, A. P. Burke, A. Farb, H. K. Gold, J. Yuan, J. Narula, A. V. Finn, And R. Virmani, "The Thin-Cap Fibroatheroma: A Type Of Vulnerable Plaque: The Major Precursor Lesion To Acute Coronary Syndromes," *Curr Opin Cardiol,* Vol. 16, Pp. 285-92, Sep 2001.

[6] F. Foster, E. Harasiewicz, And M. Sherar, "A History Of Medical And Biological Imaging With Polyvinylidene Fluoride (Pvdf) Transducers," *IEEE Transactions On Ultrasonics Ferroelectrics And Frequency Control,* Vol. 47, Pp. 1363-1371, Nov 2000.

[7] L. F. Brown, "Ferroelectric Polymers: Current And Future Ultrasound Applications," *Proceedings Of IEEE Ultrasonics Symposim.,* Pp. 539-550, 1992.

[8] F. S. Foster, L. K. Ryan, And D. H. Turnbull, "Characterization Of Lead Zirconate Titanate Ceramics For Use In Miniature High-Frequency (20-80 Mhz) Transducers," *IEEE Trans Ultrason Ferroelectr Freq Control,* Vol. 38, Pp. 446-53, 1991.

[9] G. R. Lockwood And C. R. Hazard, "Miniature Polymer Transducers For High Frequency Medical Imaging," *Spie International Symposium On Medical Imaging* Vol. 3341, Pp. 228-236, 1998.

[10] A. Fleischman, C. Chandrana, F. Jin, J. Talman, S. Garverick, G. Lockwood, And S. Roy, "Components For Focused Integrated Pmuts For High-Resolution Medical Imaging," *IEEE Ultrason Sympos,* Vol. 2, Pp. 787-791, 18-21 Sept. 2005 2005.

[11] J. Johnson, O. Oralkan, U. Demirci, S. Ergun, M. Karaman, And P. Khuri-Yakub, "Medical Imaging Using Capacitive Micromachined Ultrasonic Transducer Arrays," *Ultrasonics,* Vol. 40, Pp. 471-6, May 2002.

[12] Yeh Dt, Oralkan Ö, Wygant Io, O. D. M, And K.-Y. Bt, "3d Ultrasound Imaging Using A Forward-Looking Cmut Ring Array For Intravascular/Intracardiac Applications," *Ultrasonics, Ferroelectrics And Frequency Control, IEEE Transactions On,* Vol. 53, Pp. 1202-1211, 2006.

[13] B. Bayram, O. Oralkan, A. Ergun, And E. Haeggstrom, "Capacitive Micromachined Ultrasonic Transducer Design For High Power Transmission," *IEEE Transactions On Ultrasonics Ferroelectrics And Frequency Control,* Vol. 52, Pp. 326-339, Feb 2005.

[14] S. Zhou, P. Reynolds, And J. Hossack, "Precompensated Excitation Waveforms To Suppress Harmonic Generation In MEMS Electrostatic

Transducers," *IEEE Transactions On Ultrasonics Ferroelectrics And Frequency Control,* Vol. 51, Pp. 1564-1574, Nov 2004.

[15] C. Chandrana, N. A. Kharin, A. Nair, K. R. Waters, D. G. Vince, B. Kuban, G. R. Lockwood, S. Roy, And A. J. Fleischman, "High Resolution Fundamental And Harmonic Imaging Using A MEMS Fabricated Ultrasonic Transduce," *Proceeding Of The 2007 Ultrasonics Symposium,* Pp. 1183-1187, Oct 2007 2007.

[16] C. Chandrana, N. A. Kharin, G. D. Vince, S. Roy, And A. J. Fleischman, "Micro-Electro-Mechanical Systems (MEMS) Based Focused Ultrasound Transducers For High Resolution Second Harmonic Imaging Applications " *IEEE Ultrasonic Symposium,* Pp. 693-697, 2006.

[17] *S. Kinlay*, *P. Libby*, And *P. Ganz*, "Endothelial Function And Coronary Artery Disease," *Current Opinion In Lipidology,* Vol. 12, Pp. 383-389, August 2001.

[18] :, " American Heart Association: Heart Disease And Stroke Statistics - 2008 Update," In *American Heart Association*. Vol. 2008 Dallas, Texas.

[19] P. Libby, "Inflammation In Atherosclerosis," *Nature,* Vol. 420, Pp. 868-874, Dec 26 2002.

[20] R. Ross, "Atherosclerosis: A Problem Of The Biology Of Artery Wall Cells And Their Interactions With Blood Components," *Atherosclerosis,* Vol. 1, Pp. 293-311, 1981.

[21] R. Ross, "Pathogenesis Of Atherosclerosis - An Update," *New England Journal Of Medicine,* Pp. 488-500, 1986.

[22] S. Glagov And C. Zarins, "Compensatory Enlargement Of Human Atherosclerotic Coronary-Arteries - Reply," *New England Journal Of Medicine,* Vol. 317, Pp. 1604-1604, Dec 17 1987.

[23] J. E. Muller And P. R. Moreno, *Definition Of Vulnerable Plaque. Handbook Of Vulnerable Plaque*. Serruys: Eds. Waksman, 2005.

[24] R. Virmani, "Pathology Of Vulnerable Plaque," *International Journal Of Cardiology,* Vol. 122, Pp. 8-8, Dec 1 2007.

[25] E. Arnett, J. Isner, D. Redwood, K. Kent, W. Baker, H. Ackerstein, And W. Roberts, "Coronary Artery Narrowing In Coronary Heart Disease: Comparison Of Cineangiographic And Necropsy Findings," *Ann Intern Med,* Vol. 91, Pp. 350-356, 1979.

[26] R. Goldberg, N. Kleiman, S. Minor, J. Abukhalil, And A. Raizner, "Comparison Of Quantitative Coronary Angiography To Visual Estimates Of Lesion Severity Pre And Post Ptca," *American Heart Journal,* Vol. 119, Pp. 178-184, Jan 1990.

[27] D. Franzen, U. Sechtem, And W. Hopp, "Comparison Of Angioscopic, Intravascular Ultrasonic, And Angiographic Detection Of Thrombus In Coronary Stenosis," *American Journal Of Cardiology,* Vol. 82, Pp. 1273-+, Nov 15 1998.

[28] J. Tobis, J. Mallery, D. Mahon, K. Lehmann, P. Zalesky, J. Griffith, J. Gessert, M. Moriuchi, M. Mcrae, M. Dwyer, N. Greep, And W. Henry, "Intravascular Ultrasound Imaging Of Human Coronary-Arteries Invivo - Analysis Of Tissue Characterizations With Comparison To Invitro Histological Specimens," *Circulation,* Vol. 83, Pp. 913-926, Mar 1991.

[29] A. Macisaac, J. Thomas, And E. Topol, "Toward The Quiescent Coronary Plaque," *Journal Of The American College Of Cardiology,* Vol. 22, Pp. 1228-1241, Oct 1993.

[30] E. N. Arnett, J. M. Isner, D. R. Redwood, K. M. Kent, W. P. Baker, H. Ackerstein, And W. C. Roberts, "Coronary Artery Narrowing In Coronary Heart Disease: Comparison Of Cineangiographic And Necropsy Findings," *Ann Intern Med,* Vol. 91, Pp. 350-356, 1979.

[31] J. Honye, D. Mahon, A. Jain, C. White, S. Ramee, J. Wallis, A. Alzarka, And J. Tobis, "Morphological Effects Of Coronary Balloon Angioplasty Invivo Assessed By Intravascular Ultrasound Imaging," *Circulation,* Vol. 85, Pp. 1012-1025, Mar 1992.

[32] D. Keane, J. Haase, C. Slager, E. Vanswijndregt, K. Lehmann, Y. Ozaki, C. Dimario, R. Kirkeeide, And P. Serruys, "Comparative Validation Of Quantitative Coronary Angiography Systems - Results And Implications From A Multicenter Study Using A Standardized Approach," *Circulation,* Vol. 91, Pp. 2174-2183, Apr 15 1995.

[33] E. Falk, P. Shah, And V. Fuster, "Coronary Plaque Disruption," *Circulation,* Vol. 92, Pp. 657-671, Aug 1 1995.

[34] C. Yuan And W. Kerwin, "Mri Of Atherosclerosis," *Journal Of Magnetic Resonance Imaging,* Vol. 19, Pp. 710-719, Jun 2004.

[35] P. De Feyter And K. Nieman, "New Coronary Imaging Techniques: What To Expect?," *Heart,* Vol. 87, Pp. 195-197, Mar 2002.

[36] Z. Fayad, V. Fuster, J. Fallon, T. Jayasundera, S. Worthley, G. Helft, J. Aguinaldo, J. Badimon, And S. Sharma, "Noninvasive In Vivo Human Coronary Artery Lumen And Wall Imaging Using Black-Blood Magnetic Resonance Imaging," *Circulation,* Vol. 102, Pp. 506-510, Aug 1 2000.

[37] W. Kim, M. Stuber, P. Bornert, K. Kissinger, W. Manning, And R. Botnar, "Three-Dimensional Black-Blood Cardiac Magnetic Resonance Coronary

Vessel Wall Imaging Detects Positive Arterial Remodeling In Patients With Nonsignificant Coronary Artery Disease," *Circulation,* Vol. 106, Pp. 296-299, Jul 16 2002.

[38] B. Qiu, P. Karmarkar, C. Brushett, F. Gao, R. Kon, S. Kar, E. Atalar, And X. Yang, "Development Of A 0.014-Inch Magnetic Resonance Imaging Guidewire," *Magnetic Resonance In Medicine,* Vol. 53, Pp. 986-990, Apr 2005.

[39] J. Schneiderman, R. Wilensky, A. Weiss, E. Samouha, L. Muchnik, M. Chen-Zion, M. Ilovitch, E. Golan, A. Blank, M. Flugelman, Y. Rozenman, And R. Virmani, "Diagnosis Of Thin-Cap Fibroatheromas By A Self-Contained Intravascular Magnetic Resonance Imaging Probe In Ex Vivo Human Aortas And In Situ Coronary Arteries," *Journal Of The American College Of Cardiology,* Vol. 45, Pp. 1961-1969, Jun 21 2005.

[40] N. Mollet, F. Cademartiri, G. Krestin, E. Mcfadden, C. Arampatzis, T. Baks, And P. De Feyter, "Non-Invasive Multislice Computer Tomography Coronary Angiography," *European Heart Journal,* Vol. 25, Pp. 472-472, Aug-Sep 2004.

[41] M. Garcia, J. Lessick, M. Hoffmann, C. S. Investigators, And "Accuracy Of 16-Row Multidetector Computed Tomography For The Assessment Of Coronary Artery Stenosis," *Jama-Journal Of The American Medical Association,* Vol. 296, Pp. 403-411, Jul 26 2006.

[42] J. H. C. Reiber And P. W. Serruys, "Quantitaive Coronary Arteriography," *Developments In Cardiovascular Medicine,* Vol. 117, 1991.

[43] M. Brezinski, "Optical Coherence Tomography For Identifying Unstable Coronary Plaque," *International Journal Of Cardiology,* Vol. 107, Pp. 154-165, Feb 15 2006.

[44] M. Brezinski, G. Tearney, N. Weissman, S. Boppart, B. Bouma, M. Hee, A. Weyman, E. Swanson, J. Southern, And J. Fujimoto, "Assessing Atherosclerotic Plaque Morphology: Comparison Of Optical Coherence Tomography And High Frequency Intravascular Ultrasound," *Heart,* Vol. 77, Pp. 397-403, May 1997.

[45] G. Gorge, J. Ge, M. Haude, D. Baumgart, G. Caspari, R. Leischik, F. Liu, And R. Erbel, "Intravascular Ultrasound: A Guide For Management Of Complications During Intervention?," *European Heart Journal,* Vol. 16, Pp. 86-92, Nov 1995.

[46] R. Siegel, M. Ariani, M. Fishbein, J. Chae, J. Park, G. Maurer, And J. Forrester, "Histopathologic Validation Of Angioscopy And Intravascular Ultrasound," *Circulation,* Vol. 84, Pp. 109-117, Jul 1991.

[47] T. Romer, J. Brennan, T. Schut, R. Wolthuis, R. Van Den Hoogen, J. Emeis, A. Van Der Laarse, A. Bruschke, And G. Puppels, "Raman Spectroscopy For Quantifying Cholesterol In Intact Coronary Artery Wall," *Atherosclerosis,* Vol. 141, Pp. 117-124, Nov 1998.

[48] W. Casscells, B. Hathorn, M. David, T. Krabach, W. Vaughn, H. Mcallister, G. Bearman, And J. Willerson, "Thermal Detection Of Cellular Infiltrates In Living Atherosclerotic Plaques: Possible Implications For Plaque Rupture And Thrombosis," *Lancet,* Vol. 347, Pp. 1447-1449, May 25 1996.

[49] M. Madjid, M. Naghavi, B. Malik, S. Litovsky, J. Willerson, And W. Casscells, "Thermal Detection Of Vulnerable Plaque," *American Journal Of Cardiology,* Vol. 90, Pp. 36l-39l, Nov 21 2002.

[50] C. De Korte, A. Van Der Steen, E. Cespedes, And G. Pasterkamp, "Intravascular Ultrasound Elastography In Human Arteries: Initial Experience

In Vitro," *Ultrasound In Medicine And Biology,* Vol. 24, Pp. 401-408, Mar 1998.

[51] C. De Korte, M. Sierevogel, F. Mastik, C. Strijder, J. Schaar, E. Velema, G. Pasterkamp, P. Serruys, And A. Van Der Steen, "Identification Of Atherosclerotic Plaque Components With Intravascular Ultrasound Elastography In Vivo A Yucatan Pig Study," *Circulation,* Vol. 105, Pp. 1627-1630, Apr 9 2002.

[52] M. Doyley, F. Mastik, C. De Korte, S. Carlier, E. Cespedes, P. Serruys, N. Bom, And A. Van Der Steen, "Advancing Intravascular Ultrasonic Palpation Toward Clinical Applications," *Ultrasound In Medicine And Biology,* Vol. 27, Pp. 1471-1480, Nov 2001.

[53] J. Schaar, C. De Korte, F. Mastik, L. Van Damme, R. Krams, P. Serruys, And A. Van Der Steen, "Three-Dimensional Palpography Of Human Coronary Arteries - Ex Vivo Validation And In-Patient Evaluation," *Herz,* Vol. 30, Pp. 125-133, Mar 2005.

[54] B. Kimura, V. Bhargava, And A. Demaria, "Value And Limitations Sf Intravascular Ultrasound Imaging In Characterizing Coronary Atherosclerotic Plaque," *American Heart Journal,* Vol. 130, Pp. 386-396, Aug 1995.

[55] A. Nair, J. D. Klingensmith, And D. G. Vince, "Real-Time Plaque Characterization And Visualization With Spectral Analysis Of Intravascular Ultrasound Data," *Plaque Imaging: Pixel To Molecular Level,* Pp. 300-320, 2005.

[56] M. Sonka, X. Zhang, M. Siebes, M. Bissing, S. Dejong, S. Collins, And C. Mckay, "Segmentation Of Intravascular Ultrasound Images: A Knowledge-

Based Approach," *IEEE Transactions On Medical Imaging,* Vol. 14, Pp. 719-732, Dec 1995.

[57] C. Vonbirgelen, C. Dimario, W. Li, J. Schuurbiers, C. Slager, P. Defeyter, J. Roelandt, And P. Serruys, "Morphometric Analysis In Three-Dimensional Intracoronary Ultrasound: An In Vitro And In Vivo Study Performed With A Novel System For The Contour Detection Of Lumen And Plaque," *American Heart Journal,* Vol. 132, Pp. 516-527, Sep 1996.

[58] R. Shekhar, R. Cothren, D. Vince, S. Chandra, J. Thomas, And J. Cornhill, "Three-Dimensional Segmentation Of Luminal And Adventitial Borders In Serial Intravascular Ultrasound Images," *Computerized Medical Imaging And Graphics,* Vol. 23, Pp. 299-309, Nov-Dec 1999.

[59] X. Zhang, C. Mckay, And M. Sonka, "Tissue Characterization In Intravascular Ultrasound Images," *IEEE Transactions On Medical Imaging,* Vol. 17, Pp. 889-899, Dec 1998.

[60] C. Vonbirgelen, C. Dimario, B. Reimers, F. Prati, N. Bruining, R. Gil, P. Serruys, And J. Roelandt, "Three-Dimensional Intracoronary Ultrasound Imaging - Methodology And Clinical Relevance For The Assessment Of Coronary Arteries And Bypass Grafts," *Journal Of Cardiovascular Surgery,* Vol. 37, Pp. 129-139, Apr 1996.

[61] J. M. Gessert, K. C, And J. Mallery, "Display Considerations For Intravascular Ultrasonic Imagng," *Spie: Catheter-Based Sensing And Imaging Technology,* Vol. 1068, Pp. 180-184, 1989.

[62] R. W. Martin And C. C. Johnson, "Engineering Considerations Of Catheters For Intravascular Ultrasonic Measurtements," *Spie: Catheter-Based Sensing And Imaging Technology,* Vol. 1068, Pp. 198-206, 1989.

[63] R. W. Martin, F. Silverstien, And M. Kimmey, "Mode Imaging And Doppler Ultrasonic Catheters For Use With Fiber Optic Endoscopes," *Spie: Microsensors And Catheter-Based Imaging Technology,* Vol. 904, Pp. 121-126, 1988.

[64] J. Griffith, M. Maciel, And P. Zalesky, "Factors Influencing Ultrasound Echoes From Arterial Walls," *Spie: Microsensors And Catheter-Based Imaging Technology,* Vol. 904, Pp. 100-104, 1988.

[65] B. Potkin, A. Bartorelli, J. Gessert, R. Neville, Y. Almagor, W. Roberts, And M. Leon, "Coronary-Artery Imaging With Intravascular High-Frequency Ultrasound," *Circulation,* Vol. 81, Pp. 1575-1585, May 1990.

[66] S. Nissen, C. Grines, J. Gurley, K. Sublett, D. Haynie, C. Diaz, D. Booth, And A. Demaria, "Application Of A New Phased-Array Ultrasound Imaging Catheter In The Assessment Of Vascular Dimensions - Invivo Comparison To Cineangiography," *Circulation,* Vol. 81, Pp. 660-666, Feb 1990.

[67] J. Wikstrand And O. Wiklund, "Frontiers In Cardiovascular Science - Quantitative Measurements Of Atherosclerotic Manifestations In Humans," *Arteriosclerosis And Thrombosis,* Vol. 12, Pp. 114-119, Jan 1992.

[68] P. Stahr, H. Rupprecht, T. Voigtlander, P. Kearney, R. Erbel, L. Koch, S. Krass, R. Brennecke, And J. Meyer, "Importance Of Calibration For Diameter And Area Determination By Intravascular Ultrasound," *International Journal Of Cardiac Imaging,* Vol. 12, Pp. 221-229, Dec 1996.

[69] G. Finet, E. Maurincomme, A. Tabib, R. Crowley, I. Magnin, R. Roriz, J. Beaune, And M. Amiel, "Artifacts In Intravascular Ultrasound Imaging - Analyses And Implications," *Ultrasound In Medicine And Biology,* Vol. 19, Pp. 533-547, 1993.

[70] R. Thompson And L. Wilson, "The Effect Of Variations In Transducer Position And Sound Speed In Intravascular Ultrasound: A Theoretical Study," *Ultrasound In Medicine And Biology,* Vol. 22, Pp. 719-734, 1996.

[71] C. R. Meyer, E. H. Chiang, And D. W. Fitting, "Feasibility And Diagnostic Value Of Catheter-Based Ultrasonic Systems For Intravascular Imaging: In Vitro Comparisions With Mri," *IEEE Ultrasonics Symposium,* Pp. 805-808, 1988.

[72] D. Vince, J. Klingensmith, A. Nair, B. Kuban, E. Tuzcu, R. Erbel, And W. Wijns, "Determination Of Plaque Composition In Human Coronary Arteries Using Intravascular Ultrasound Virtual Histology," *European Heart Journal,* Vol. 24, Pp. 418-418, Aug-Sep 2003.

[73] M. Sherar And F. Foster, "The Design And Fabrication Of High-Frequency Poly(Vinylidene Fluoride) Transducers," *Ultrasonic Imaging,* Vol. 11, Pp. 75-94, Apr 1989.

[74] F. S. Foster, D. A. Knapnik, J. C. Machado, L. K. Ryan, And S. E. Nissen, "High-Frequency Intracoronary Ultrasound Imaging," In *Seminars In Interventional Cardiology*. Vol. 2, 1997, Pp. 23-31.

[75] G. R. Lockwood And C. R. Hazard, "Development Of Small Aperture Polymer Transducers For High Frequency Imaging," *Proceeding Of The 1997 Ultrasonics Symposium* 1997.

[76] T. G. Muir And E. L. Cartensen, "Prediction Of Nonlinear Acoustic Effects At Biomedical Frequencies And Intensities," In *Ultrasound Med Biol* 1980, Pp. 345-357.

[77] E. L. Carstensen, W. K. Law, N. D. Mckay, And T. G. Muir, "Demonstration Of Nonlinear Acoustical Effects At Biological Frequencies And Intensities," *Ultrasound Med Biol* Vol. 6, Pp. 359-368, 1982.

[78] F. A. Duck, "Nonlinear Acoustics In Diagnostic Ultrasound," *Ultrasound Med Biol,* Vol. 28, Pp. 1-18, 2002.

[79] M. Hamilton And D. Blackstock, "On The Coefficient Of Nonlinearity-Beta In Nonlinear Acoustics," *Journal Of The Acoustical Society Of America,* Vol. 83, Pp. 74-77, Jan 1988.

[80] A. C. Baker, "Nonlinear Acoustics In Medical Ultrasound," *Proc Insititute Of Acoustics,* Vol. 14, Pp. 115-128, 1992.

[81] B. Ward, A. Baker, And V. Humphrey, "Nonlinear Propagation Applied To The Improvement Of Resolution In Diagnostic Medical Ultrasound," *Journal Of The Acoustical Society Of America,* Vol. 101, Pp. 143-154, Jan 1997.

[82] J. M. G. Borsboom, C. T. Chin, And N. De Jong, "Nonlinear Coded Excitation Method For Ultrasound Contrast Imaging," *Ultrasound Med Biol,* Vol. 29, Pp. 277-284, 2003.

[83] S. Tanaka, O. Oshikawa, T. Sasaki, T. Ioka, And H. Tsukuma, "Evaluation Of Tissue Harmonic Imaging For The Diagnosis Of Focal Liver Lesions.," *Ultrasound Med Biol* Vol. 26, Pp. 183-187, 2000.

[84] F. Tranquart, N. Grenier, V. Eder, And L. Pourcelot, "Clinical Use Of Ultrasound Tissue Harmonic Imaging," *Ultrasound Med Biol* Vol. 6, Pp. 889-894, 1999.

[85] T. Szabo, *Diagnostic Ultrasound Imaging: Inside Out*: Acadameic Press, 2004.

[86] A. F. W. Van Der Steen, J. K. Poulsen, E. W. Cherin, And F. S. Foster, "Harmonic Imaging At High Frequencies For Ivus," *IEEE Ultrason Sympos,* Vol. 2, Pp. 1537-1540, 1999.

[87] E. W. Cherin, J. K. Poulsen, A. F. W. Van Der Steen, P. Lum, And F. S. Foster, "Experimental Characterization Of Fundamental And Second Harmonic Beams For A High-Frequency Ultrasound Transducer," *Ultrasound Med Biol* Vol. 28, Pp. 635-646, 2002.

[88] M. Frijlink, D. Goertz, L. Van Damme, R. Krams, And A. Van Der Steen, "Intravascular Ultrasound Tissue Harmonic Imaging In Vivo," *IEEE Transactions On Ultrasonics Ferroelectrics And Frequency Control,* Vol. 53, Pp. 1844-1852, Oct 2006.

[89] A. Fiorillo, J. Vanderspiegel, P. Bloomfield, And D. Esmailzandi, "A P(Vdf-Trfe)-Based Integrated Ultrasonic Transducer," *Sensors And Actuators A-Physical,* Vol. 22, Pp. 719-725, Mar 1990.

[90] J. Mo, A. Robinson, D. Fitting, F. Terry, And P. Carson, "Micromachining For Improvement Of Integrated Ultrasonic Transducer Sensitivity," *IEEE Transactions On Electron Devices,* Vol. 37, Pp. 134-140, Jan 1990.

[91] A. Fleischman, R. Modi, A. Nair, J. Talman, G. Lockwood, And S. Roy, "Miniature High Frequency Focused Ultrasonic Transducers For Minimally Invasive Imaging Procedures," *Sensors And Actuators A-Physical,* Vol. 103, Pp. 76-82, Jan 15 2003.

[92] F. S. Foster, P. C. J, L. G. R, L. K. Ryan, K. A. Harasiewicz, L. Berube, And R. A. M, "Principles And Applications Of Ultrasound Backscatter Microscopy," *IEEE Transactions On Ultrasonics, Ferroelectrics And Frequency Control,* Vol. 40, Pp. 608-617, 1993.

[93] G. Lockwood And C. R. Hazard, "Miniature Polymer Transducers For High Frequency Medical Imaging," *Spie International Symposium On Medical Imaging,* Vol. 3341, Pp. 228-236, 1998.

[94] R. Swartz And J. Plummer, "Integrated Silicon-Pvf2 Acoustic Transducer Arrays," *IEEE Transactions On Electron Devices,* Vol. 26, Pp. 1921-1931, 1979.

[95] C. H. Han And E. S. Kim, "Fabrication Of Dome-Shaped Diaphragm With Circular Clamped Boundary On Silicon Substrate," *Twelfth IEEE International Conference On MEMS (Mem S'99),* Pp. 505-510, 1999.

[96] A. Fleischman, R. Modi, A. Nair, J. Talman, G. Lockwood, And S. Roy, "Miniature High Frequency Focused Ultrasonic Transducers For Minimally Invasive Imaging Procedures," *Sensors And Actuators,* Vol. 103 Pp. 76-82, January 15, 2003 2003.

[97] S. Timoshenko And S. Woinowsky-Krieger, *Theory Of Plates And Shells* Vol. 1: Mcgraw-Hill, 1987.

[98] D. K. Marker And C. H. Jenkins, "Surface Precision Of Optical Membranes With Curvature," *Optics Express,* Vol. 1, Pp. 324-331, 1997.

[99] W. P. Eaton, F. Bitsie, J. H. Smith, And D. W. Plummer, "A New Analytical Solution For Diaphragm Deflection And Its Application To A Surface-Micromachined Pressure Sensor," In *Conference On Modeling And Simulation Of Microsystems,* San Juan, Puerto Rico, Usa, 1999.

[100] J. Y. Pan, "A Study Of Suspended-Membrane And Acoustic Techniques For The Determination Of The Mechanical Properties Of Thin Polymer Films," In *Department Of Elelctrical Engineering*. Vol. Thesis Cambridge, Ma, Usa: Massachussets Institute Of Technology, 1991.

[101] M. Arditi, F. Foster, And J. Hunt, "Transient Fields Of Concave Annular Arrays," *Ultrasonic Imaging,* Vol. 3, Pp. 37-61, 1981.

[102] H. T. O'neil, "Theory Of Focusing Radiators," *JASA,* Vol. 21, Pp. 516-526, 1949.

[103] F. Duck, "Nonlinear Acoustics In Diagnostic Ultrasound," *Ultrasound In Medicine And Biology,* Vol. 28, Pp. 1-18, Jan 2002.

[104] A. Bouakaz And N. De Jong, "Native Tissue Imaging At Super-Harmonic Frequencies," *IEEE Trans Ultrason Ferroelec Freq Contr* Vol. 44, Pp. 125-139, 2003.

[105] X. Gong, D. Zhang, J. Liu, H. Wang, Y. Yan, And X. Xu, "Study Of Acoustic Nonlinearity Parameter Imaging Methods In Reflection Mode For Biological Tissues," *J Acoust Soc Am* Vol. 116, Pp. 1819-1825, 2004.

[106] I. Solodov, K. Pfleiderer, H. Gerhard, And G. Busse, "Nonlinear Acoustic Approach To Material Characterization Of Polymers And Composites In Tensile Tests," *Ultrasonics* Vol. 42, P. 1011–1015, 2004.

[107] D. Zhang And X. F. Gong, "Acoustic Nonlinearity Parameter Tomography; Pathological Tissues; Tissue Characterization," *Ultrasound In Medicine & Biology,* Pp. 593-599, May, 1999 1999.

[108] P. Burns, D. Simpson, And M. Averkiou, "Nonlinear Imaging," *Ultrasound In Medicine And Biology,* Vol. 26, Pp. S19-S22, 2000.

[109] A. Nair, Vince, D.G. Calvetti, D., " *'Blind' Data Calibration Of Intravascular Ultrasound Data For Automated Tissue Characterization*., Vol 2: P 1126-1129.," In *IEEE Ultrasonics. Symposium 2004.* Vol. 2, 2004, Pp. 1126-1129.

[110] M. E. Frijlink, D. E. Goertz, And A. F. Vandersteen, "*Reduction Of Stent Artifacts Using High- Frequency Harmonic Ultrasound Imaging.*," *Ultrasound In Medicine And Biology,* Vol. 31, Pp. 1335-1342, 2005.

[111] N. A. Kharin And D. G. Vince, "Moderately Nonlinear Ultrasound Propagation In Blood-Mimicking Fluid," *Ultrasound In Medicine And Biology,* Vol. 30, Pp. 501-509, April, 2004 2004.

[112] N. A. Kharin, "Development Of Ultrasound Transducer Diffractive Field Theory For Nonlinear Tissues," *Ultrasonic Imaging And Signal Processing; Proceedings Of Spie,* Vol. 3982, Pp. 122-131, 2000.

[113] M. F. Hamilton And D. T. Blackstock, *Nonlinear Acoustics*. San Diego: Academic Press, 1998.

[114] M. F. Hamilton And D. T. Blackstock, *Nonlinear Acoustics.* San Diego: Academic Press., 1998.

[115] G. Lockwood, J. Hunt, And F. Foster, "The Design Of Protection Circuitry For High-Frequency Ultrasound Imaging-Systems," *IEEE Transactions On Ultrasonics Ferroelectrics And Frequency Control,* Vol. 38, Pp. 48-55, Jan 1991.

[116] D. Rugar, "Resolution Beyond The Diffraction Limit In The Acoustic Microscope - A Nonlinear Effect," *Journal Of Applied Physics,* Vol. 56, Pp. 1338-1346, 1984.

[117] W. Law, L. Frizzell, And F. Dunn, "Ultrasonic Determination Of The Nonlinearity Parameter B-A For Biological Media," *Journal Of The Acoustical Society Of America,* Vol. 69, Pp. 1210-1212, 1981.

[118] D. Simpson, C. Chin, And P. Burns, "Pulse Inversion Doppler: A New Method For Detecting Nonlinear Echoes From Microbubble Contrast Agents,"

IEEE Transactions On Ultrasonics Ferroelectrics And Frequency Control, Vol. 46, Pp. 372-382, Mar 1999.

[119] J. E. Powers, P. N. Burns, And J. Souquet, *Imaging Instrumentation For Ultrasound Contrast Agents*, 2 Ed. Norwell, Ma: Kluwer, 1997.

[120] P. N. Burns, D. H. Simpson, And M. A. Averkiou, "Nonlinear Imaging," *Ultrasound Med Biol,* Vol. 26, Pp. S19-S22, 2000.

[121] P. Jiang, Z. Mao, And J. Lazenby, "A New Tissue Harmonic Imaging Scheme With Better Fundamental Frequency Cancellation And Higher Signal To-Noise Ratio," *Proceedings Of IEEE Ultrasonics Symposium,* Vol. 2, 1998.

[122] C. Sehgal, G. Brown, R. Bahn, And J. Greenleaf, "Measurement And Use Of Acoustic Nonlinearity And Sound Speed To Estimate Composition Of Excised Livers," *Ultrasound In Medicine And Biology,* Vol. 12, Pp. 865-874, Nov 1986.

[123] T. Baldeweck, P. Laugier, A. Herment, And G. Berger, "Application Of Autoregressive Spectral-Analysis For Ultrasound Attenuation Estimation - Interest In Highly Attenuating Medium," *IEEE Transactions On Ultrasonics Ferroelectrics And Frequency Control,* Vol. 42, Pp. 99-110, Jan 1995.

[124] A. Nair, B. Kuban, E. Tuzcu, P. Schoenhagen, S. Nissen, And D. Vince, "Coronary Plaque Classification With Intravascular Ultrasound Radiofrequency Data Analysis," *Circulation,* Vol. 106, Pp. 2200-2206, Oct 22 2002.